View metadata, citation and similar papers at core.ac.uk
brought to you by CORE
provided by Illinois Digital Environment for Access to Learning and Scholarship Repository

INACTIVATION KINETICS AND MECHANISMS OF ROTAVIRUS: THE ROLES OF SUNLIGHT, TEMPERATURE, AND SENSITIZERS

BY

OFELIA CAMPOS ROMERO-MARACCINI

DISSERTATION

Submitted in partial fulfillment of the requirements
for the degree of Doctor of Philosophy in Environmental Engineering in Civil Engineering
in the Graduate College of the
University of Illinois at Urbana-Champaign, 2014

Urbana, Illinois

Doctoral Committee:

Associate Professor Thanh Huong Nguyen, Chair
Professor Wen-Tso Liu
Professor Benito Jose Mariñas
Professor Joanna L. Shisler

ABSTRACT

Rotavirus is the leading cause of diarrhea hospitalizations and deaths among young children worldwide, responsible for an estimated 453,000 deaths each year. The only proven route of rotavirus transmission is via the fecal–oral route, yet all documented rotavirus waterborne outbreaks have been associated with direct fecal contamination of a water supply or improper water treatment. Rotaviruses can remain infectious after undergoing typical wastewater treatment, and thus can contaminate drinking water sources, such as rivers. The transmission route and resilience of rotaviruses strengthen the importance of effective potable water treatment technologies against rotaviruses in developing countries.

Solar disinfection is a cost-effective and promising alternative for water and wastewater treatment in less-developed countries lacking reliable water treatment technologies. However, the solar inactivation mechanisms of rotaviruses have not been investigated. Improved knowledge of the photochemical and molecular mechanisms leading to rotavirus inactivation by solar and thermal treatments will help in the development and design of new technologies to detect and control rotaviruses in water. The objectives for this study were: 1) to investigate the natural sunlight conditions that induced rotavirus inactivation such as the effects of sunlight fractions, organic matter, temperature; 2) to determine how different types of organic matter influenced rotavirus inactivation by their photochemical contributions; and 3) to determine the molecular determinants causing inactivation of rotavirus upon heat and solar irradiation treatments.

Our results showed that rotaviruses were inactivated upon solar irradiation, especially with full spectrum irradiation that contains UVB light. When the UVB fraction of sunlight was blocked, rotavirus inactivation greatly decreased when compared to full spectrum irradiation.

However, independent of the sunlight fraction used, irradiation of natural organic matter triggered a photochemical production of radicals that indirectly inactivated rotavirus. These photo-chemically produced radicals were likely hydroxyl radicals and excited triplet state species. Our molecular work showed that rotavirus inactivation was linked to genome damage by solar irradiation, regardless of the sunlight fraction, while thermal treatment caused primarily protein damage. The presence of organic matter augmented rotavirus inactivation by causing protein damage, likely targeted by the indirectly-produced radicals.

This dissertation is dedicated to my Mom, Dad, Brothers, Sisters and Peter for their love and support always

ACKNOWLEDGEMENTS

Getting to the end of the PhD journal is no journey for a single person. A few key characters during this journal have accompanied me and made completion of this journey now a reality. First, I want to thank my adviser and mentor, Prof. Helen Nguyen, who saw and continues to see a potential in me that I am beginning to embrace. Her guidance, patience, and persistent support throughout these past 6 years have helped me transform into a better researcher and also a better person. I also want to thank my husband, Peter Maraccini, without his unconditional support and love I would not have gotten here.

I would like to thank those involved in getting my graduate studies started or who have helped me a project started. I want to thank Tamar Kohn for her initial research training, advice during the first 3 years, and support throughout this journey. I want to thank Kara Nelson for taking me in as undergraduate and encouraging me to pursue graduate studies. Special thanks to Prof. Vern Snoeyink for helping me overcome public speaking terror, now I just get nervous not terrified. I want to thank Shaoying Qi for helping me build the solar simulator setup and for his continuous help throughout these years. I also want to thank Mark and Theresa Kuhlenschmidt for getting me started with rotavirus work and for their extremely insightful advice. I thank Joanna Shisler for her enormous contribution in getting the last thesis chapter done. Finally, I could not have completed this work without my awesome assistants: Nora Sadik, Jesse Lopez, Alicia Chuchro, and Charlie Pugh.

Special thanks to those who made home away from home possible. I am extremely grateful to have worked with superstars throughout the world and to be able to call them family. These individuals who encouraged and challenged me are (in alphabetical order): Ana Martinez,

Annia Vargas, Anthony Straub, Arezoo Khodayari, Daniel Castaneda, Dao Janjaroen, Franscisco Mena, Hanting Wang, Ian Bradley, Leonardo Gutierrez, Nanxi Lv, Raul Tenorio, Sahid Rosado, Susana Kimura, Yuanyuan Liu. Very special thanks to my family who have encouraged me to pursue this unknown journey. I want acknowledge my two younger sisters who have accompanied me in this educational journey.

There are also others that are involved in the completion of my Ph.D. I would like to thank and acknowledge my other PhD committee members: Prof. Benito Marinas, Prof. Wen-Tso, and Prof. Joanna Shisler. Thanks to my CEE professors for preparing me. I would like to thank Marvis Orzek, Mary Pearson, and Joan Christian for their help coordinating the many exams and events needed for the PhD.

I also would like to acknowledge the Graduate College, College of Engineering, SURGE fellowship, GAANN fellowship, and the NSF Graduate Student Fellowship Program for financially supporting my graduate studies.

TABLE OF CONTENTS

CHAPTER 1

INTRODUCTION

1.1 Background on solar inactivation and its existing applications

Solar disinfection is one of the oldest recorded methods of water purification. However, only in more recent times our scientific understanding and acceptance of this process for water treatment have been fully recognized (Reed, 2004). The first systematic solar disinfection studies by Downes and Blunt (1877) reported that the development of bacteria in nutrient broth and urine was inhibited by exposure to sunlight (Downes & Blunt, 1877). Later, they demonstrated that the spores of mycelial fungi were more resistant than bacterial cells to sunlight, and that short-wavelength solar radiation has the greatest antimicrobial effect (Downes & Blunt, 1878). More than a century later, Acra and co-workers (1980) proposed, for the first time, the practical application of sunlight for water disinfection and showed systematic disinfection kinetic data of bacteria (Acra, Karahagopian, Raffoul, & Dajani, 1980). Soon after, Acra and co-workers demonstrated in laboratory and field studies that solar radiation could inactivate a wide range of microorganisms including *Escherichia coli*, *Salmonella typhi*, *Shigella flexneri*, and various yeasts and molds (Acra, A., Raffoul, Z., and Karahagopian, 1984). These initial studies paved the way for recent solar disinfection applications and cutting-edge research studies.

The first application of solar disinfection was initiated as a means to provide low-cost, sustainable, and simple drinking water treatment in developing countries with consistently sunny climates. Solar disinfection for drinking water (SODIS), consists of filling a transparent glass or plastic bottle with contaminated water and exposing it to full-strength sunlight for several hours to inactivate pathogenic microorganisms. Apart from SODIS, other engineered water treatment

technologies that harness light and heat energy from sunlight to inactivate pathogens in drinking water or wastewaters have recently emerged (Byrne, Fernandez-Ibañez, Dunlop, Alrousan, & Hamilton, 2011; Caslake & Connolly, 2004; Mara, 2004; WHO, 2006). Within the past 25 years, solar disinfection studies have greatly augmented, and sunlight disinfection of pathogens has been reported in fresh water, sea water, and wastewaters (Reed, 2004). Below, we briefly summarize the most recent applications of sunlight disinfection at different scales and note the public health impacts.

In later sections of this chapter we discuss the inactivation mechanisms and known factors affecting these. We conclude the chapter with the role of solar inactivation as a potential solution to battle diarrhea, an outcome of poor sanitation and lack of safe access to drinking water. We specifically draw attention to the importance of studying the solar inactivation mechanisms of rotaviruses, the leading cause of life-threatening diarrhea in children under five year of age.

1.1.1 SODIS for drinking water treatment

Contaminated water is responsible for an estimated 6 to 60 billion cases of gastrointestinal illness annually (Caslake & Connolly, 2004). Most of these cases occur in developing countries where inadequate sanitation is unavailable and consequently, water becomes polluted with pathogens. Several methods (e.g. boiling, chlorination, filtration and SODIS) are recommended for the disinfection of drinking water at the household level. Though, the selection of the most appropriate, cost-effective and sustainable option is highly dependent on local conditions (Graf et al., 2010). In places with ample sunlight year-round, and where a continuous supply of wood for burning, chlorine tablets, and filtration units is not available, SODIS is a recommended technology as it only requires direct sunlight and polyethylene

terephthalate (PET) bottles. PET bottles with low-turbidity water are placed on a roof or rack for six hours (if sunny) or two days (if cloudy) before drinking (Graf et al., 2010). The sun's ultraviolet radiation and infrared heat synergistically lead to pathogen inactivation (Graf et al., 2010). This method has been proven to inactivate microorganisms responsible for diarrheal illness including bacteria, viruses, protozoa cryptosporidium and giardia (Byrne et al., 2011; Lantagne, Quick, & Mintz, 2006).

SODIS is presently promoted in dissemination projects in at least 33 countries (Lantagne et al., 2006) with an estimated 4.5 million regular users worldwide, predominately in Africa, Latin America, and Asia. SODIS is also promoted by the World Health Organization to treat drinking water (Byrne et al., 2011). Households fully complying with the intervention in randomized controlled studies in developing countries including Cameroon, India, Kenya, and Cambodia have showed a reduced diarrheal disease incidence ranging between 9-86 percent (Graf et al., 2010; Lantagne et al., 2006; K G McGuigan, Joyce, & Conroy, 1999; Kevin G McGuigan, Samaiyar, du Preez, & Conroy, 2011; Rose et al., 2006).

Despite the advantages of SODIS in developing countries, its use is not recommended over other treatment options such as chlorination (Byrne et al., 2011). Two of the major challenges with SODIS use are: the use of PET bottles allows for only small volumes to be treated (2-3 L) and the process efficiency is highly dependent on a range of environmental parameters. Some of these parameters include solar irradiance, initial water quality parameters such as organic loading, dissolved organic matter, and pathogens to be disinfected, as some pathogens are more resistant to sunlight disinfection than others (Byrne et al., 2011).

1.1.2 Engineered sunlight treatment systems

Apart from SODIS, other engineered water treatment improvements and technologies that rely on sunlight to inactivate pathogens in drinking water or wastewaters were developed or are currently under development (Byrne et al., 2011; Caslake & Connolly, 2004; Mara, 2004; WHO, 2006). In a recent review, Byrne, et al. (2011) summarized the latest SODIS enhancements. To circumvent the low sunlight irradiation challenges, SODIS bags were designed where the solar dose per volume is increased. Additionally, a solar disinfection unit that maximized the irradiation time by elongating the exposure surface was shown to inactivate more than 4_{log10} units of total coliforms within 30 min in midday summer sunlight (Caslake & Connolly, 2004). The use of semiconductor photocatalysis for enhanced treatment efficacy has been widely tested, but not yet implemented. In lab studies, semiconductor photocatalysis has been shown to be effective against a wide range of microorganisms under environmental conditions for both small-scale and large-scale applications (Byrne et al., 2011).

The use of sunlight in wastewater treatment is widespread. Lagoons or waste stabilization ponds (WSP) are a wastewater treatment technology developed to solely utilize sunlight as its only source of energy. WSP are suitable for places where construction, operation and maintenance costs exceed land costs and where sunlight is plentiful (Mara, 2004). Sunlight in WSP is capable of achieving significant inactivation of indicator organisms (T. P. Curtis, Mara, & Silva, 1992; Davies-Colley, Donnison, Speed, Ross, & Nagels, 1999) and pathogens, including the recalcitrant *Cryptosporidium parvum* oocysts (Reinoso & Bécares, 2008). Most of the pathogen inactivation in WSP has been observed in the tertiary ponds, where most of the BOD and suspended solids have been removed. In tertiary ponds, light penetration, pH, and temperature have a more dominant role on pathogen fate than in the primary or secondary ponds (T. P. Curtis et al., 1992). Other versions of WSP that enable greater exposure of wastewater to

sunlight than in conventional WSP have been designed. Shallow depth and mixing in ecologically engineered high rate ponds have shown fast inactivation of *E.coli* and attribute 75 percent of the total *E. coli* inactivation to sunlight action (Craggs, Zwart, Nagels, & Davies-Colley, 2004). Due to their proven efficiency and low-maintenance, WSP and other versions of these ponds have been built throughout the world including central America (Oakley, Pocasangre, Flores, Monge, & Estrada, 2000), Africa, the Middle East, north America, and Europe (Maynard, Ouki, & Williams, 1999). WSP have been shown to provide high quality effluent of domestic wastewaters able to meet the World Health Organization guidelines for safe use of wastewaters (Mara DD, 2007; WHO, 2006). Thus, WSP treated wastewater can be reused for irrigation and thus help to reduce potable water demand (Hamilton et al., 2007) or it be safely discharged into bodies of water to reduce pathogen contamination (15).

1.1.3 Sunlight effects on environmental surface waters

Although, not designed or intended for water treatment, solar inactivation has been observed in natural sunlit surface waters. This natural phenomenon is important to public health because surface water is an important source for drinking water, irrigation, and recreation. Often, sewage effluents, storm water overflows, and diffuse sources like agriculture run-off are sources of microbe contamination for surface waters (Schultz-Fademrecht, Wichern, & Horn, 2008). Indicator organisms are routinely used to measure levels of pathogen contamination in waters and their survival during the summer season points to the importance of sunlight disinfection. In a study by Burkhardt et al. (2000), *in situ* experiments were performed in estuarine waters of Alabama and Rhode Island in the summer and winter. Fecal coliforms, *E.coli*, *Clostridium perfringens*, and male-specific bacteriophage were monitored, and among the parameters examined, sunlight and/or temperature most significantly affected the microorganisms' decay

rates. However, inactivation effects were not the same for all, fecal coliforms were inactivated much faster than the bacteriophages and *C. perfringens* (Burkhardt, Calci, Watkins, Rippey, & Chirtel, 2000). Environmental monitoring studies of bacterial pathogens in coastal streams have shown that sunlight inactivation is important for their occurrence, but not for all bacterial pathogens. Viau et al. (2011) reported that of five bacterial pathogens (*Salmonella*, *Campylobacter*, *Staphylococcus aureus*, *Vibrio vulnificus*, and *V. Parahaemolyticus*) monitored in Hawaiian coastal streams, only *Campylobacter* and *enterococci* appeared to be sensitive to sunlight (Viau et al., 2011). During a 72 h period study, Boehm, et al. (2009) found that lower concentrations of all microbes tested (*E. coli* and *enterococci*, F+(DNA and RNA), somatic coliphages, *Bacteroidales*, human enterovirus, and human adenovirus) excluding the HF and enterovirus markers, were observed during sunlit as opposed to dark hours, suggesting that photoinactivation was significant (Boehm et al., 2009). A year-round monitoring study showed that rotavirus infectivity in a wastewater-impacted river significantly decreased in the summer months when compared to winter months (Li et al., 2011). The authors concluded that stronger UV sunlight and higher temperatures were the main factors responsible for decreased rotavirus infectivity (Li et al., 2011).

Although sunlight has been proven effective for the disinfection of microbes, detailed knowledge on effects of sunlight on the wide range of other human pathogens commonly found in environmental waters is still lacking. A better understanding of the pathogen inactivation mechanisms in sunlit surface water could aid in the assessment of natural sunlight disinfection and its implication on public health.

1.2 Solar disinfection mechanisms of microorganisms

Three mechanisms have been proposed in the solar disinfection of microorganisms: direct, indirect endogenous, and indirect exogenous (Davies-Colley et al., 1999). The direct and

indirect endogenous mechanisms require absorption of photons by microbe components (e.g., nucleic acid, riboflavins, porphyrin), while the indirect exogenous mechanism involves the absorption of photons by exogenous photosensitizers (i.e., dissolved organic matter, algae). For the direct mechanism, light-absorbing components (proteins or nucleic acids), called chromophores, undergo chemical changes as a direct consequence of absorbing photons (Zafiriou, Joussot-Dubien, Zepp, & Zika, 1984). In contrast, the indirect endogenous mechanism occurs when photons are absorbed by one part of the microorganism, but other microorganism components are damaged through electron or energy transfer reactions (Michael J. Davies, 2003). The exogenous mechanism results when external photosensitizers, compounds that absorb photons and transfer this energy to other compounds, produce transient radicals as a direct consequence of photon absorption and cause oxidative damage to microorganisms (T. P. Curtis et al., 1992). More details on the three mechanisms are provided in the Bio-Chemical Properties and Physical Aspect sections that follow.

In the Chemical Aspects section, the known chemical pathways, the radicals produced by light irradiation, and the usual suspects responsible for microorganism damage are presented. In the Physical Aspects section we discussed the extent to which known parameters: pH, temperature, light intensity, ionic strength and dissolved organic matter affect solar disinfection mechanisms.

1.2.1 Solar inactivation mechanisms

All three inactivation mechanisms involve photochemical reactions that lead to protein damage, nucleic acid damage or both. Direct damage of microorganism's components is primarily driven by UVB irradiation and is an outcome of the microorganism's chromophores (i.e., nucleic acid and proteins) that become chemically altered as a result of absorbing photons

(Zafiriou et al., 1984). Direct damage of the genome is largely a result of the formation of pyrimidine dimer lesions in genomic nucleic acid (Schuch & Menck, 2010). If these UVB-induced nucleic acid lesions are not repaired, they can interfere with processes such as transcription, replication, and therefore can lead to mutations and/or death (Schuch & Menck, 2010). Direct damage to protein chromophores arises from the formation of excited state species that in turn cause damage to the same protein chromophores (Michael J. Davies, 2003). Briefly, upon photon absorption by the chromophoric protein structure, the protein structure enters into the short-lived first excited singlet state (lifetime in the range of nano-seconds) that rapidly transfers to the longer-lived excited triplet state (lifetimes in the range of micro-seconds). Triplets can undergo electron transfer with some internal molecules that can lead to protein cleavage (M J Davies & Truscott, 2001). The major chromophoric amino acids present in proteins are tryptophan (Trp), tyrosine (Tyr), phenylalanine (Phe), histidine (His), cysteine (Cys) and cystine (M J Davies & Truscott, 2001). Of these amino acids, the most environmentally relevant are Phe, Tyr, and Trp because these show broad fluorescence spectra with emission maxima at 280 nm (Phe), 300 nm (Tyr) and 350 nm (Trp), and fluorescence quantum yields of ca. 0.04, 0.14 and 0.2, respectively (M J Davies & Truscott, 2001). Trp is the most significant chromophore in many proteins because it has the longest wavelength ground state absorption spectrum and a significantly greater molar absorption coefficient for each of its major absorption bands than the other amino acids (M J Davies & Truscott, 2001).

The indirect endogenous and exogenous mechanisms involve the indirect oxidation of microorganism's components after photons absorbed by one part of the microorganism or external components in the water column, trigger the formation of transient radicals that cause damage to microorganism entities. This process is similar to the direct protein damage

mechanism: upon photon absorption by the chromophoric microorganism entity, such entity enters into the first excited singlet state followed by the excited triplet state. Triplets can undergo electron or energy transfer with some internal molecules and also oxygen, which can result in the production of reactive oxygen species including singlet oxygen, hydrogen peroxide, superoxide, and hydroxyl radical (M J Davies & Truscott, 2001). These short-lived radicals lead to photo-oxidative damage, which is caused by the action of light (T. P. Curtis et al., 1992). Below is a schematic of the indirect photolysis pathways and the most common reactive species in the environment (Figure 1).

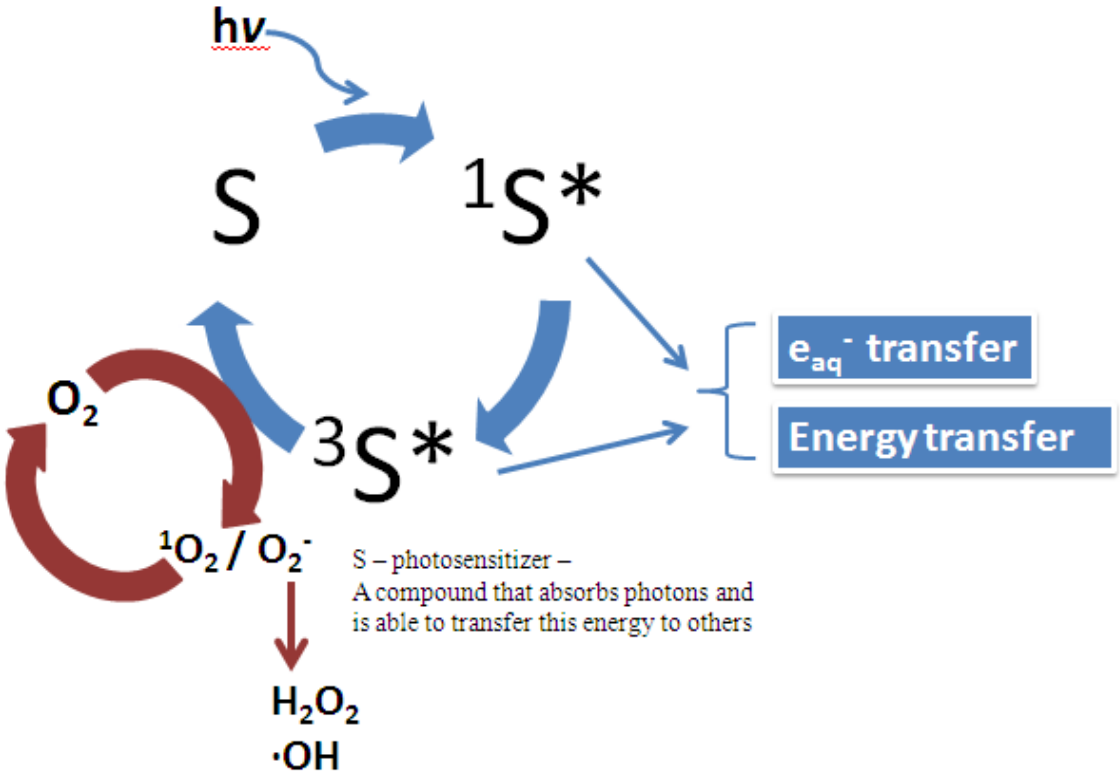

Figure 1: Pathways of indirect photolysis

A range of chemical alterations have been reported in photo-oxidized proteins, including: an increase in susceptibility of the oxidized protein to proteolytic enzymes; an increased extent,

or susceptibility to, unfolding; changes in conformation; an increase in hydrophobicity; changes in binding of co-factors and metal ions (M J Davies & Truscott, 2001). Because of the immense diversity of microbe proteins, structures, and other complexities, microorganisms have varied responses to solar inactivation. Some microorganisms become readily inactivated by sunlight irradiation, while others are more resistant and require higher light doses. Some microorganisms are highly susceptible to the exogenous mechanism, while the direct and endogenous mechanism have little effect (Davies-Colley et al., 1999; Silverman, Peterson, Boehm, McNeill, & Nelson, 2013). For example, in a recent study by Silverman, et al. (2013) human adenovirus type 2 was inactivated around three times faster in a solution containing natural photosensitizers than in the sensitizer-free buffer control under full spectrum irradiation. In another study, bacterial indicators were found to be more susceptible to sunlight irradiation than virus indicators in water samples from a waste stabilization pond (Davies-Colley et al., 1999). Thus, the composition and biochemical properties of microorganism components highly influence their susceptibility/resistance to solar inactivation.

1.2.2 Physical Aspects

Numerous physical factors have been found to affect solar disinfection mechanisms. Most of the physical parameters have been studied for the exogenous mechanism as this is highly influenced by the external components in a water column. The direct and endogenous mechanisms are largely driven by the biochemical properties of the organism itself, UVB light, and other parameters that affect light penetration such as dissolved organic matter. As a result, except for light fractions and dissolved organic matter, the following parameters will be described for the exogenous mechanism. In this section we discuss the most widely studied parameters: pH, sunlight intensity, ionic strength, dissolved oxygen concentrations, dissolved

organic matter, and type and concentrations of photosensitizers present in the water column (M J Davies & Truscott, 2001; Pigault & Gerard, 1984; Romero, Straub, Kohn, & Nguyen, 2011; Romero-Maraccini et al., 2013; Silverman et al., 2013).

- *pH*: The pH of seawater is 8 ± 0.5 and that of freshwater is 7 ± 3 (Zafiriou et al., 1984). Consequently, in fresh waters, pH has been found to be a key variable in solar inactivation studies (T. P. Curtis et al., 1992). pH levels of 8.5 and higher have been shown to increase inactivation kinetic rates of several microorganisms vulnerable to the exogenous mechanism (T. P. Curtis et al., 1992; Davies-Colley et al., 1999). The high pH effects may be attributable to lower resistance of the organism to the effects of light or increased production of reactive oxygen species (T. P. Curtis et al., 1992). Low pH values (pH 4) have also been linked to increased microbe inactivation (Kohn, Grandbois, McNeill, & Nelson, 2007). When the iso-electric point of both photosensitizer and microbe is low (< 4), low pH results in lower electrostatic repulsion between the charged entities through protonation of the negatively charged functional groups. This lower repulsion between the microbe and photosenstizer increases their association, which may result in higher exposure to transient radicals produced by the photosensitizer (Kohn et al., 2007).

- *Ionic strength*: Similar to the pH effect, high ionic strength can help neutralize the negative charge by compressing the electric double layer surrounding charged particles or it can complex the negatively charged functional groups thus leading to lower electrostatic repulsion. The decrease in lower electrostatic repulsion can favor the association between the microorganism and photosenstizer to allow for exposure to higher levels of radicals, and thus lead to faster inactivation (Kohn et al., 2007).

- *Dissolved organic matter (DOM)*: Dissolved organic substances are ubiquitous in the environment, thus these determine the spectral attenuation properties of natural waters. DOM functions as both a light attenuator and as a photosensitizer. The photosensitizer properties of organic matter will be discussed in the Photosensitizer section. DOM determines light attenuation, particularly UVB attenuation, in environmental waters including wetlands, lakes, and waste stabilization ponds (Arts et al., 2000; T. Curtis, Mara, Dixo, & Silva, 1994). Attenuation of UV photons obstructs inactivation by reducing the photons that could otherwise induce direct damage or indirect photo-oxidative damage. In contrast to UVB light, UVA and visible light are less attenuated and therefore reach deeper depths in the water column (Arts et al., 2000; T. Curtis et al., 1994). Therefore, DOM determines the overall light penetration in a water column. In water systems with high concentrations of DOM, UVA and visible light are likely the governing solar players.

- *Light fraction and intensity*: Sunlight consists of the infrared, visible, and UV light. Infrared light is absorbed by water and therefore contributes to increased water temperature. Some photosensitizers absorb light in the visible spectrum and therefore, contribute to photo-oxidative damage. Yet, UV wavelengths are the most lethal to microorganisms. UVB wavelengths (280-320 nm) can initiate all three inactivation mechanisms, principally the direct and endogenous mechanisms (Davies-Colley et al., 1999; Romero et al., 2011). UVA wavelengths (320-400 nm) can set off the indirect inactivation mechanisms, especially the exogenous mechanism that depends on the nature of external photosensitizers (see Photosensitizers below). The higher the light intensity, the higher the photons emitted, therefore, more opportunities for photolysis.

- *Dissolved oxygen*: In environmental waters, dissolved oxygen is major acceptor of energy or electrons arising from photosensitizers and is also involved in secondary reactions of radical species (Zafiriou et al., 1984). The strong oxygen dependence of the inactivation kinetics of microorganisms suggests that a photo-oxidative process is involved. For several organisms, including *E.coli*, F-RNA pages, *E. faecalis* the presence of oxygen greatly increased their photo inactivation rates (T. P. Curtis et al., 1992; Davies-Colley et al., 1999; Kadir & Nelson, 2013).

- *Temperature*: The lowest pasteurizing temperature is 63°C for 30 min. Therefore, temperature alone can cause damage to microorganisms. In the natural environment, temperatures fluctuate between 14 and 35°C (Gu, Luck, & Stefan, 1996). In SODIS studies involving 2-L bottles exposed to sunlight, temperatures > 45°C have been measured (Kevin G McGuigan et al., 2011). Though, these temperatures alone will likely have little effect on the inactivation of microorganisms. Instead, the synergism between light and temperature has been shown to increase inactivation. For example, the exogenous inactivation of rotavirus and MS2 was significantly increased for temperatures > 33°C when compared to the inactivation measured at 25°C (Romero et al., 2011). On the other hand, direct inactivation was shown not to be significantly influenced by temperature in the range of 14-40°C (Romero et al., 2011).

- *Photosensitizers*: Photosensitizers vary in source, type, and role, which depends on the light source. Common environmentally relevant photosensitizers include microorganism components, organic matter, algae, trace metals, nitrate and nitrite. The photolytic potential of these photosensitizers is significantly dependent on their absorption spectra, quantum yields, concentration in the water column, light penetration, temperature, and

dissolved oxygen (T. Curtis et al., 1994; T. P. Curtis et al., 1992; M J Davies & Truscott, 2001; Romero et al., 2011). Photosensitizers also vary in the radicals they produce upon light irradiation. For example, nitrate/nitrite generate hydroxyl radicals (Zepp, Hoigne, & Bader, 1987), while organic matter generates hydroxyl radical, singlet oxygen, superoxide, and hydrogen peroxide among others (Kohn & Nelson, 2007; Romero-Maraccini et al., 2013). High abundance of photosensitizers, light penetration, and oxygen are likely ideal parameters for exogenous solar inactivation.

1.3 Safe water access and sanitation challenges: the role of solar inactivation as a potential sustainable solution

About 884 millions of people worldwide lack access to clean water, while 2.5 billion people lack access to improved sanitation facilities (UN, 2010). This lack of access to safe water and sanitation has extensive human and economic costs. Lack of clean drinking water is responsible for major health issues that result in 14,000 to 30,000 preventable deaths each day (Scanlon, Cassar, & Nemes, 2004), while costs due to lack of access to sanitation have been estimated at US$ 260 billion each year (WB, 2013). Most of these cases happen in developing countries, where the economical and technological means to properly treat contaminated wastewater or drinking water are not available. Poor sanitation, lack of or minimal collection, treatment and disposal or re-use of excreta and wastewater, is critical because it strongly influences the quality of drinking water sources, and it is one of the strongest determinants of child survival (COHRE, WaterAid, SDC, & UN-HABITAT, 2008). Despite the improvements and efforts of numerous entities to increase access to safe water and sanitation in impoverished communities, the rapid increase in population and social and environmental challenges including accelerating urbanization, climate change, increasing pollution, and depletion of water resources

in these regions make access a persistent challenge (UN, 2010). For example, In Sub-Saharan Africa, clean water access has significantly increased since 1990, jumping from 49 percent to 60 percent; however, population growth has exceeded the progress to the extent that the actual number of people without access was greater in 2008 than it was in 1990 (WHO/UNICEF, 2011).

The human and economic costs of poor sanitation and safe access to drinking water result from the widespread transmission of diseases. Among these diseases, diarrhea is the leading cause of preventable death, especially in children under five, and is responsible for about 800,000 fatalities each year worldwide (Kotloff et al., 2013). Diarrhea is caused by infectious organisms, including viruses, bacteria, protozoa, and helminthes that can spread by feces-contaminated water. However, the list of the chief diarrhea-causing agents is short. Recently, Kotloff, et al. (2013) published their findings on a case-control study of the burden and etiology of diarrheal disease in infants and young children in developing countries (the Global Enteric Multicenter Study, GEMS). After adjusting for population attributable fractions, the most attributable cases of moderate-to-severe diarrhea were due to four pathogens: rotavirus, *Cryptosporidium*, enterotoxigenic *E. coli* producing heat-stable toxin (ST-ETEC), and *Shigella* (Kotloff et al., 2013). To substantially reduce the burden of moderate-to-severe diarrhea, the authors recommended interventions targeting five pathogens (rotavirus, *Shigella*, ST-ETEC, *Cryptosporidium*, typical entero-pathogenic *E coli*).

It is highly unlike that a single intervention will be the silver bullet for all diarrheal troubles in developing countries. For example the distribution of chlorine tablets or the use of other chemical disinfectants is highly effective and rapidly provide safe water, but their use is not sustainable. The need for a constant supply of these chemicals over long periods of time is

unfeasible due to the continuous costs and supply uncertainties. Hence, water treatment technologies that are low-cost, effective, sustainable, resilient and easy to use will be needed to circumvent diarrhea, a major outcome of poor sanitation and safe water shortages.

1.3.1 The role of solar disinfection as a potential sustainable solution

Solar disinfection technologies have been designed, and can be vastly improved for efficient drinking water treatment (i.e., SODIS) and improved sanitation through wastewater treatment (i.e., WSP and ecologically engineered high rate ponds). The use of solar disinfection in technology development is ideal for water treatment because solar energy is a free, sustainable, and highly effective against pathogens. Technological improvements and innovations can be designed to be both resilient and easy to use. To better develop these technologies, it is imperative to understand the basic solar disinfection mechanisms of the most detrimental human pathogens. A strong understanding of the mechanisms involved in pathogen inactivation would also enable predicting the susceptibility of new and non-culturable pathogen strains to solar disinfection.

While our main objective is to augment the current understanding of the fate of rotavirus and its treatment with sunlight, our goal is to also provide the foundation for approaching the much needed research in the inactivation of other harmful pathogens by solar disinfection or other newly developed sustainable technologies.

1.3.2 Rotavirus: the model for sunlight disinfection studies

In this project, solar disinfection studies were carried out with rotavirus. Despite the availability of two efficacious rotavirus vaccines (Rotarix™ and RotaTeq™), rotavirus remains the leading cause of life-threatening diarrheal disease in children and is responsible for an estimated 440,000 annual deaths in children under five years of age worldwide (Parashar,

Gibson, Bresee, & Glass, 2006). According to the recent publication by Kotloff, et al. (2013), rotavirus is one the four pathogens that cause most of the moderate-to-severe diarrhea incidences in children in developing countries and preventive strategies targeting rotavirus could have a significant impact during the first 2 years of life (Kotloff et al., 2013). To date, the only proven route of rotavirus transmission is via the faecal–oral route, either by environmental contact with contaminated surfaces, persons, or by ingestion of contaminated water and food (Li et al., 2011). Yet, all documented rotavirus waterborne outbreaks have been associated with direct fecal contamination of a water supply or improper water treatment (Gerba, Rose, Haas, & Crabtree, 1996). Therefore, preventative measures such as improving sanitation, to prevent fecal contamination of drinking water sources, and treating drinking water will greatly reduce rotavirus transmission, thus reducing the prevalence of diarrhea.

Rotavirus characteristics influence its persistence in the environment. Rotavirus is highly infectious and it is shed in high concentrations ranging between 10^{10} and 10^{11} particles per gram of feces for up to two weeks (Marshall, 2009). Rotavirus infectivity can be retained for several days in water environments at temperatures up to 40°C and for ≥ 1 h in the pH range of 3-10 (Estes, Graham, & Estes, Mary K; Graham, 1979; Wood & Adams, 1992). In year-round monitoring study, the presence of infectious rotaviruses in effluents from wastewater treatment plants and receiving bodies of water in Beijing, China, were evaluated (Li et al., 2011). The results showed that the secondary treatment processes such as active sludge can inactive/remove most of infectious rotaviruses, and the tertiary treatments were able to further remove rotaviruses. However, even after tertiary treatment, which included sand filtration and coagulative precipitation, or membrane ultrafiltration, infectious rotaviruses were detected in the tertiary effluents (Li et al., 2011). This study demonstrated the resilience of rotavirus and its

potential transmission into potable water sources through treated wastewater discharge. Rotavirus resilience and transmission route strengthen the importance to improve sanitation and especially drinking water treatment technologies against rotavirus.

Apart from being a current public health burden, rotavirus is an excellent pathogen model for having a number of hosts and for its ability to reassort. The hosts of rotavirus are not limited to humans, but also include mice, cattle, bovine, monkeys, horses, dogs, rabbits and birds (Martella, Bányai, Matthijnssens, Buonavoglia, & Ciarlet, 2010). Rotavirus strains of different hosts have been shown to reassort, and the genetic diversity and evolution of rotavirus group A has been recently reviewed in Matthijssens and van Ranst (2012) (Matthijnssens & Van Ranst, 2012). To date, genome sequencing studies have shown evidence for reassortment of bovine and human rotaviruses (Afrad et al., 2013; Matsushima et al., 2012), and porcine and human rotavirus (Kim et al., 2012). More recently, through genome characterization colleagues demonstrated a porcine-human-like constellation in four children with diarrhea (My et al., 2013). Reassortant rotavirus strains containing mixed genome constellations (dsRNA segments derived from both human and animal viruses) appear to be quicker to spread and more persistent in human populations than completely heterologous rotavirus strains (with all the genome segments derived from animal viruses), likely as a result of improved adaptation to the new host and lack of preexisting population immunity against the new strain (Martella et al., 2010). Because of reassortment, positive accumulation of single point mutations, inter-segmental recombination, and segment rearrangement (Martella et al., 2010), the potential of rotavirus to continue changing over time as human and animal populations grow, climate and other environmental changes occur is critical. Rotavirus level of resistance to disinfectants will be of central

importance to public health as well as rotavirus whole genome sequencing for sustained strain surveillance.

1.4 Research objectives

The objectives of this study were to shed light into the inactivation mechanisms of rotavirus by solar inactivation by taking into account the environmentally relevant parameters: fractions of light, temperature, and photosensitizers. These parameters were chosen among others parameters known to affect solar inactivation because these are the most directly linked to the effects of sunlight in a water column. Additionally, these parameters were the least investigated and/or the most likely to vary in a water column. We chose to work at a pH of 8 and 1 mM ionic strength because these parameters are environmentally relevant and help maintain rotavirus stability. We chose not to study the dissolved oxygen concentrations because most open water systems are aerated. Our objects were:

1. Identify the roles of different fractions of light and temperature on the inactivation of rotaviruses
2. Elucidate the role of photosensitizers and the photo-oxidative radicals inducing rotavirus inactivation
3. Determine the inactivation mechanism of rotaviruses at the molecular level

Chapters 2 and 3 of this dissertation document the inactivation kinetics of these two rotavirus strains under varying conditions: temperatures from 14-57 °C, in the presence of different photosensitizers, and different fractions of light. Chapter 4 provides insight into the molecular mechanisms that govern inactivation of rotavirus by solar and thermal treatments. Chapter 5 concludes the contributions of this project.

1.5 References

Acra, A., Karahagopian, Y., Raffoul, Z., & Dajani, R. (1980). Disinfection of oral rehydration solutions by sunlight. *The Lancet, ii*, 1257–1258.

Acra, A., Raffoul, Z., and Karahagopian, Y. (1984). (1984). *Solar disinfection of drinking water and oral rehydration solutions: guidelines for household application in developing countries. UNICEF*.

Afrad, M. H., Matthijnssens, J., Moni, S., Kabir, F., Ashrafi, A., Rahman, M. Z., … Rahman, M. (2013). Genetic characterization of a rare bovine-like human VP4 mono-reassortant G6P[8] rotavirus strain detected from an infant in Bangladesh. *Infect. Genet. Evol.*, *19*, 120–126. doi:10.1016/j.meegid.2013.06.030

Arts, M. T., Robarts, R. D., Kasai, F., Waiser, M. J., Tumber, V. P., Plante, A. J., … de Lange, H. J. (2000). The attenuation of ultraviolet radiation in high dissolved organic carbon waters of wetlands and lakes on the northern Great Plains. *Limnol. Oceanogr.*, *45*(2), 292–299. doi:10.4319/lo.2000.45.2.0292

Boehm, A. B., Yamahara, K. M., Love, D. C., Peterson, B. M., McNeill, K., & Nelson, K. L. (2009). Covariation and photoinactivation of traditional and novel indicator organisms and human viruses at a sewage-impacted marine beach. *Environ. Sci. Technol.*, *43*(21), 8046–8052. doi:10.1021/es9015124

Burkhardt, W. I., Calci, K. R., Watkins, W. D., Rippey, S. R., & Chirtel, S. J. (2000). Inactivation of indicator microorganisms in estuarine waters. *Water Research*, *34*(8), 2207–2214. Retrieved from http://www.sciencedirect.com/science/article/pii/S0043135499003991

Byrne, J. A., Fernandez-Ibañez, P. a., Dunlop, P. S. M., Alrousan, D. M. a., & Hamilton, J. W. J. (2011). Photocatalytic Enhancement for Solar Disinfection of Water: A Review. *International Journal of Photoenergy*, *2011*, 1–12. doi:10.1155/2011/798051

Caslake, L., & Connolly, D. (2004). Disinfection of contaminated water by using solar irradiation. *Appl. Environ. Microbiol.*, *70*(2), 1145–1150. doi:10.1128/AEM.70.2.1145

COHRE, WaterAid, SDC, & UN-HABITAT. (2008). *Sanitation: A human rights imperative* (p. 50). Geneva, Switzerland.

Craggs, R. J., Zwart, A., Nagels, J. W., & Davies-Colley, R. J. (2004). Modelling sunlight disinfection in a high rate pond. *Ecological Engineering*, *22*(2), 113–122. doi:10.1016/j.ecoleng.2004.03.001

Curtis, T., Mara, D., Dixo, N., & Silva, S. (1994). Light penetration in waste stabilization ponds. *Water Research*, *28*(5), 1031–1038. Retrieved from http://www.sciencedirect.com/science/article/pii/0043135494901880

Curtis, T. P., Mara, D. D., & Silva, S. a. (1992). Influence of pH, Oxygen, and Humic Substances on Ability of Sunlight To Damage Fecal Coliforms in Waste Stabilization Pond Water. *Applied and Environmental Microbiology*, *58*(4), 1335–43. Retrieved from http://www.pubmedcentral.nih.gov/articlerender.fcgi?artid=195595&tool=pmcentrez&rendertype=abstract

Davies, M. J. (2003). Singlet oxygen-mediated damage to proteins and its consequences. *Biochemical and Biophysical Research Communications*, *305*(3), 761–770. doi:10.1016/S0006-291X(03)00817-9

Davies, M. J., & Truscott, R. J. (2001). Photo-oxidation of proteins and its role in cataractogenesis. *Journal of Photochemistry and Photobiology. B, Biology*, *63*(1-3), 114–25. Retrieved from http://www.ncbi.nlm.nih.gov/pubmed/11684458

Davies-Colley, R. ., Donnison, A. ., Speed, D. ., Ross, C. ., & Nagels, J. . (1999). Inactivation of faecal indicator micro-organisms in waste stabilisation ponds: interactions of environmental factors with sunlight. *Water Res.*, *33*(5), 1220–1230. doi:10.1016/S0043-1354(98)00321-2

Downes, A., & Blunt, T. (1877). Researches on the effect of light upon bacteria and other organisms. *Proceedings of the Royal …*, *26*(1877), 488–500. Retrieved from http://rspl.royalsocietypublishing.org/content/26/179-184/488.full.pdf

Downes, A., & Blunt, T. (1878). On the influence of light upon protoplasm. *Proceedings of the Royal …*, *28*, 199–212. Retrieved from http://rspl.royalsocietypublishing.org/content/28/190-195/199.full.pdf

Estes, M., Graham, D., & Estes, Mary K; Graham, D. Y. . (1979). Rotavirus Stability and Inactivation. *J. Gen. Virol.*, *43*(2), 403–409. Retrieved from http://www.ncbi.nlm.nih.gov/pubmed/39115

Gerba, C. P., Rose, J. B., Haas, C. N., & Crabtree, K. D. (1996). Waterborne rotavirus: A risk assessment. *Water Res.*, *30*(12), 2929–2940. doi:10.1016/S0043-1354(96)00187-X

Graf, J., Zebaze Togouet, S., Kemka, N., Niyitegeka, D., Meierhofer, R., & Gangoue Pieboji, J. (2010). Health gains from solar water disinfection (SODIS): evaluation of a water quality intervention in Yaoundé, Cameroon. *J. Water Health*, *8*(4), 779–96. doi:10.2166/wh.2010.003

Gu, R., Luck, F. N., & Stefan, H. G. (1996). Water Quality Stratification in Shallow Wastewater Stabilization Ponds. *Water Resources Bulletin*, *32*(4), 831–844.

Hamilton, A. J., Stagnitti, F., Xiong, X., Kreidl, S. L., Benke, K. K., & Maher, P. (2007). Wastewater Irrigation: The State of Play. *Vadose Zone Journal*, *6*(4), 823. doi:10.2136/vzj2007.0026

Kadir, K., & Nelson, K. L. (2013). Sunlight mediated inactivation mechanisms of Enterococcus faecalis and Escherichia coli in clear water versus waste stabilization pond water. *Water Research*, 1–11. doi:10.1016/j.watres.2013.10.046

Kim, H.-H., Matthijnssens, J., Kim, H.-J., Kwon, H.-J., Park, J.-G., Son, K.-Y., … Cho, K.-O. (2012). Full-length genomic analysis of porcine G9P[23] and G9P[7] rotavirus strains isolated from pigs with diarrhea in South Korea. *Infect. Genet. Evol.*, *12*(7), 1427–1435. doi:10.1016/j.meegid.2012.04.028

Kohn, T., Grandbois, M., McNeill, K., & Nelson, K. L. (2007). Association with natural organic matter enhances the sunlight-mediated inactivation of MS2 coliphage by singlet oxygen. *Environ. Sci. Technol.*, *41*(13), 4626–4632. Retrieved from http://www.ncbi.nlm.nih.gov/pubmed/17695907

Kohn, T., & Nelson, K. L. (2007). Sunlight-mediated inactivation of MS2 coliphage via exogenous singlet oxygen produced by sensitizers in natural waters. *Environ. Sci. Technol.*, *41*(1), 192–197. Retrieved from http://www.ncbi.nlm.nih.gov/pubmed/17265947

Kotloff, K. L., Nataro, J. P., Blackwelder, W. C., Nasrin, D., Farag, T. H., Panchalingam, S., … Levine, M. M. (2013). Burden and aetiology of diarrhoeal disease in infants and young children in developing countries (the Global Enteric Multicenter Study, GEMS): a prospective, case-control study. *Lancet*, *382*(9888), 209–22. doi:10.1016/S0140-6736(13)60844-2

Lantagne, D., Quick, R., & Mintz, E. (2006). Household water treatment and safe storage options in developing countries: a review of current implementation practices. *U.S. Centers for Disease Control and Prevention*. Retrieved from http://josiah.berkeley.edu/2007Fall/ER275/Readings/DP1-2/Lantagne et al 2006.pdf

Li, D., Gu, a Z., Zeng, S.-Y., Yang, W., He, M., & Shi, H.-C. (2011). Monitoring and evaluation of infectious rotaviruses in various wastewater effluents and receiving waters revealed correlation and seasonal pattern of occurrences. *J. Appl. Microbiol.*, *110*(5), 1129–37. doi:10.1111/j.1365-2672.2011.04954.x

Mara, D. (2004). *Domestic Wastewater Treatment in Developing Countries* (1st ed.). London: Earthscan Publications.

Mara DD, J. M. (2007). Waste stabilization ponds and rock filters: solutions for small communities. *Water Sci. Technol.*, *55*(7), 103–107.

Marshall, G. S. (2009). Rotavirus disease and prevention through vaccination. *Pediatr. Infect. Dis. J.*, *28*(4), 351–362. doi:10.1097/INF.0b013e318199494a

Martella, V., Bányai, K., Matthijnssens, J., Buonavoglia, C., & Ciarlet, M. (2010). Zoonotic aspects of rotaviruses. *Veterinary Microbiology*, *140*(3-4), 246–55. doi:10.1016/j.vetmic.2009.08.028

Matsushima, Y., Nakajima, E., Nguyen, T. A., Shimizu, H., Kano, A., Ishimaru, Y., … Ushijima, H. (2012). Genome Sequence of an Unusual Human G10P[8] Rotavirus Detected in Vietnam. *J. Virol.*, *86*(18), 10236–7. doi:10.1128/JVI.01588-12

Matthijnssens, J., & Van Ranst, M. (2012). Genotype constellation and evolution of group A rotaviruses infecting humans. *Curr. Opin. Virol.*, *2*(4), 426–433. doi:10.1016/j.coviro.2012.04.007

Maynard, H., Ouki, S., & Williams, S. (1999). Tertiary lagoons: a review of removal mecnisms and performance. *Water Research*, *33*(1), 1–13. Retrieved from http://www.sciencedirect.com/science/article/pii/S0043135498001985

McGuigan, K. G., Joyce, T. M., & Conroy, R. M. (1999). Solar disinfection: use of sunlight to decontaminate drinking water in developing countries. *Journal of Medical Microbiology*, *48*(9), 785–7. Retrieved from http://www.ncbi.nlm.nih.gov/pubmed/10482288

McGuigan, K. G., Samaiyar, P., du Preez, M., & Conroy, R. M. (2011). High compliance randomized controlled field trial of solar disinfection of drinking water and its impact on

childhood diarrhea in rural Cambodia. *Environ. Sci. Technol.*, *45*(18), 7862–7. doi:10.1021/es201313x

My, P. V. T., Donato, C., Rabaa, M. A., Cowley, D., Phat, V. V., Kirkwood, C., & Baker, S. (2013). Novel porcine-related G26P[19] rotavirus in pediatric diarrheal patients in Vietnam. *Submitted*.

Oakley, S., Pocasangre, A., Flores, C., Monge, J., & Estrada, M. (2000). Waste stabilization pond use in Central America: the experiences of El Salvador, Guatemala, Honduras and Nicaragua. *Water Science & …*, *42*(10), 51–58. Retrieved from http://www.bvsde.paho.org/bvsaidis/guatemala21/7wastestab.pdf

Parashar, U. D., Gibson, C. J., Bresee, J. S., & Glass, R. I. (2006). Rotavirus and severe childhood diarrhea. *Emerging Infectious Diseases*, *12*(2), 304–307.

Pigault, C., & Gerard, D. (1984). Influence of the location of tryptophanyl residues in proteins on their photosensitivity. *Photochemistry and Photobiology*, *40*(3), 291–7. Retrieved from http://www.ncbi.nlm.nih.gov/pubmed/6484000

Reed, R. H. (2004). The inactivation of microbes by sunlight: solar disinfection as a water treatment process. *Advances in Applied Microbiology*, *54*, 333–65. doi:10.1016/S0065-2164(04)54012-1

Reinoso, R., & Bécares, E. (2008). Environmental inactivation of Cryptosporidium parvum oocysts in waste stabilization ponds. *Microbial Ecology*, *56*(4), 585–92. doi:10.1007/s00248-008-9378-7

Romero, O. C., Straub, A. P., Kohn, T., & Nguyen, T. H. (2011). Role of temperature and Suwannee River natural organic matter on inactivation kinetics of rotavirus and bacteriophage MS2 by solar irradiation. *Environmental Science & Technology*, *45*(24), 10385–10393. doi:10.1021/es202067f

Romero-Maraccini, O. C., Sadik, J., Rosado-Lausell, S. L., Pugh, C. R., Niu, X.-Z., Croue, J.-P., & Nguyen, T. H. (2013). Sunlight-Induced Inactivation of Human Wa and Porcine OSU Rotaviruses in the Presence of Exogenous Photosensitizers. *Environmental Science & Technology*, *47*(19), 11004–11012. Retrieved from http://pubs.acs.org/doi/abs/10.1021/es402285u

Rose, a, Roy, S., Abraham, V., Holmgren, G., George, K., Balraj, V., … Kang, G. (2006). Solar disinfection of water for diarrhoeal prevention in southern India. *Archives of Disease in Childhood*, *91*(2), 139–41. doi:10.1136/adc.2005.077867

Scanlon, J., Cassar, A., & Nemes, N. (2004). *Water as a Human Right? IUCN* (p. +53). Gland, Switzerland and Cambridge, UK.

Schuch, A. P., & Menck, C. F. M. (2010). The genotoxic effects of DNA lesions induced by artificial UV-radiation and sunlight. *J. Photochem. Photobiol., B*, *99*(3), 111–116. doi:10.1016/j.jphotobiol.2010.03.004

Schultz-Fademrecht, C., Wichern, M., & Horn, H. (2008). The impact of sunlight on inactivation of indicator microorganisms both in river water and benthic biofilms. *Water Research*, *42*(19), 4771–9. doi:10.1016/j.watres.2008.08.022

Silverman, A. I., Peterson, B. M., Boehm, A. B., McNeill, K., & Nelson, K. L. (2013). Sunlight inactivation of human viruses and bacteriophages in coastal waters containing natural photosensitizers. *Environ. Sci. Technol.*, *47*(4), 1870–1878. doi:10.1021/es3036913

UN. (2010). *Human Rights Fact Sheet No. 35: The Right to Water. United Nations High Commissioner for Human Rights*. Geneva, Switzerland.

Viau, E. J., Goodwin, K. D., Yamahara, K. M., Layton, B. A., Sassoubre, L. M., Burns, S. L., … Boehm, A. B. (2011). Bacterial pathogens in Hawaiian coastal streams—Associations with fecal indicators, land cover, and water quality. *Water Res.*, *45*(11), 3279–3290. Retrieved from http://www.sciencedirect.com/science/article/pii/S0043135411001448

WB. (2013). WB confronts US$260 billion a year in global economic losses from lack of sanitation. *The Wold Bank,* (July). Retrieved from http://www.worldbank.org/en/news/press-release/2013/04/19/wb-confronts-us-260-billion-a-year-in-global-economic-losses-from-lack-of-sanitation

WHO. (2006). *Guidelines for the Safe Use of Wastewater, Excreta and Greywater: Volume 2, Wastewater Use in Agriculture*.

WHO/UNICEF. (2011). *Drinking Water: Equity, Safety and Sustainability. JMP* (pp. 1–62). Geneva, Switzerland and New York, USA. Retrieved from http://www.unicef.org/media/media_61057.html

Wood, G. W. ., & Adams, M. R. (1992). Effects of Acidification, Bacterial Fermentation, and Temperature on the Survival of Rotavirus in a Model Weaning Food. *J. Food Prot., 55*(1), 52–55.

Zafiriou, O., Joussot-Dubien, J., Zepp, R., & Zika, R. (1984). Photochemistry of natural waters. *Environ. Sci. Technol., 18*(12), 358A–371A. Retrieved from http://pubs.acs.org/doi/abs/10.1021/es00130a711

Zepp, R., Hoigne, J., & Bader, H. (1987). Nitrate-induced photooxidation of trace organic chemicals in water. *Environ. Sci. Technol., 21*(5), 443–450. Retrieved from http://pubs.acs.org/doi/abs/10.1021/es00159a004

CHAPTER 2

ROLE OF TEMPERATURE AND SUWANNEE RIVER NATURAL ORGANIC MATTER ON INACTIVATION KINETICS OF ROTAVIRUS AND BACTERIOPHAGE MS2 BY SOLAR IRRADIATION[1]

2.1 Abstract

Although the sunlight mediated inactivation of viruses has been recognized as an important process that controls surface water quality, the mechanisms of virus inactivation by sunlight are not yet clearly understood. We investigated the synergistic role of temperature and Suwannee River natural organic matter (SRNOM), an exogenous sensitizer, for sunlight-mediated inactivation of porcine rotavirus and MS2 bacteriophage. Upon irradiation by a full spectrum of simulated sunlight in the absence of SRNOM and in the temperature range of 14-42°C, high inactivation rate constants, k_{obs}, of MS2 ($k_{obs} \leq 3.8$ hr-1 or 1-$\log_{10}$ over 0.6 hr) and rotavirus ($k_{obs} \leq 11.8$ hr-1 or ~1-$\log_{10}$ over 0.2 hr) were measured. A weak temperature (14 – 42°C) dependence of k_{obs} values was observed for both viruses irradiated by the full sunlight spectrum. Under the same irradiation condition, the presence of SRNOM reduced the inactivation of both viruses due to attenuation of lower wavelengths of the simulated sunlight. For rotavirus and MS2 solutions irradiated by only UVA and visible light in the absence of SRNOM, inactivation kinetics were slow ($k_{obs} < 0.3$ hr-1 or < 1-$\log_{10}$ unit reduction over 7 hr) and temperature-independent for the range considered. Conversely, under UVA and visible light irradiation and in the presence of SRNOM, temperature- dependent inactivation of MS2 was

[1] Adapted with permission from (Romero, O. C.; Straub, A. P.; Kohn, T.; Nguyen, T. H. Role of temperature and Suwannee River natural organic matter on inactivation kinetics of rotavirus and bacteriophage MS2 by solar irradiation. *Environ. Sci. Technol.* **2011**, *45*, 10385–10393.). Copyright (2011) American Chemical Society.

observed. For rotavirus, the SRNOM-mediated exogenous inactivation was only important at temperatures > 33°C, with low rotavirus k_{obs} values (k_{obs} ~ 0.2 hr-1; 1-$\log_{10}$ unit reduction over 12 hr) for the temperature range of 14-33ºC. These k_{obs} values increased to 0.5 hr-1 at 43°C and 1.5 hr-1 (1-$\log_{10}$ reduction over 1.6 hr) at 50°C. While SRNOM-mediated exogenous inactivation of MS2 was triggered by singlet oxygen, the presence of hydrogen peroxide was important for rotavirus inactivation in the 40-50°C range.

2.2 Introduction

Surface water is an important resource for irrigation, drinking water, and recreation. Runoff from both agricultural and urban land can lead to surface water contamination by bacterial and viral pathogens (Aw & Gin, 2011; Aw, Gin, Oon, Chen, & Woo, 2009; Boehm et al., 2009; Jiang, Noble, & Chui, 2001; Viau et al., 2011). In California, surface water contaminated by storm water runoff has been linked to an increased health risk for swimmers (Haile et al., 1999). A nine-year study of water quality in the Great Lakes found culturable pathogenic viruses present in wastewater discharged to Lake Michigan and the influent water of nearby drinking water treatment plants (Sedmak, Bina, MacDonald, & Couillard, 2005). Viral nucleic acids of norovirus, adenovirus, and astrovirus have been found in urban water catchments, which are used as drinking water sources for millions of people in Singapore (Aw & Gin, 2011; Aw et al., 2009). The presence of viruses in drinking water sources is notably troublesome because compared to bacteria, viruses are more difficult to remove and inactivate by conventional water treatment technologies (Mi et al., 2005; Sirikanchana, Shisler, & Marinas, 2008a, 2008b). In places without centralized water treatment facilities, surface and rainwater may be used for drinking after treatment by sunlight or heat (Davies, Roser, Feitz, & Ashbolt, 2009). Furthermore, wastewater may be treated by a system of stabilization ponds, which is

powered by solar energy, and then used for irrigation (Curtis, Mara, Dixo, & Silva, 1994; Curtis, Mara, & Silva, 1992; Da Silva et al., 2008). Despite the importance of microbial surface water quality, a clear understanding of pathogen inactivation mechanisms in surface water is not yet available, particularly for enteric viruses. Field studies have linked the persistence of pathogens, including enteric viruses, in coastal water with sunlight irradiation (Boehm et al., 2009; Viau et al., 2011). Other studies have shown that sunlight disinfection is important in sunlit surface waters. Under various conditions tested, solar disinfection studies have reported higher inactivation rates for bacterial indicators than for virus indicators (R. J. Davies-Colley, Donnison, & Speed, 2000; Sinton, Hall, Lynch, & Davies-Colley, 2002). These findings stress the need for a better understanding of solar disinfection mechanisms of viruses.

Three different mechanisms have been identified in the solar disinfection of microorganisms: direct, indirect endogenous, and indirect exogenous inactivation (R. J. Davies-Colley et al., 2000; R. J. Davies-Colley, Donnison, Speed, Ross, & Nagels, 1999). The first mechanism involves direct damage of the genome by light in the UVB (280 – 320 nm) range and the formation of photoproducts that block genome replication (Schuch & Menck; Sutherland, 1981). In addition, direct UVB damage to the proteins of adenovirus has also been reported (Eischeid & Linden, 2011). Indirect endogenous inactivation is initiated by light absorption via sensitizers associated with the microorganisms themselves (e.g. riboflavins, porphyrin) (He & Häder, 2002; Joshi & Keane; Lesser & Shick, 1989; Strakhovskaya, Shumarina, Fraikin, & Rubin, 1999; vanderMeulen et al., 1997). Electron or energy transfer from the excited sensitizers to dissolved oxygen leads to the formation of reactive oxygen species (ROS) that damage internal targets (i.e., nucleic acids, proteins) (Schuch & Menck, 2010). Indirect exogenous inactivation causes photo-oxidative damage of microorganisms by ROS formed by the external

sensitizers such as natural organic matter (NOM) in solution (Kohn, Grandbois, McNeill, & Nelson, 2007; Kohn & Nelson, 2007). Both endogenous and exogenous inactivation can be initiated by light in the UVB range as well as by higher wavelength light.

UVB radiation is indisputably effective for disinfection of viruses, including enteric viruses and bacteriophages used as pathogen indicators (Kohn & Nelson, 2007; Love, Silverman, & Nelson, 2010). Some F-RNA, F-DNA, and somatic phages were shown to only be inactivated by the UVB portion of the sunlight spectrum (R. J. Davies-Colley et al., 1999; Sinton et al., 2002). However, a number of RNA phages are also effectively inactivated by the indirect exogenous mechanism (R. J. Davies-Colley et al., 1999; Kohn & Nelson, 2007; Love et al., 2010; Sinton et al., 2002). NOM and trace metals have been found to serve as exogenous sensitizers facilitating inactivation of bacteriophages (Kohn et al., 2007; Kohn & Nelson, 2007; Nieto-Juarez, Pierzchla, Sienkiewicz, & Kohn, 2010). Specifically, among the ROS produced by the irradiation of NOM, singlet oxygen ($^1O_2$) was the most significant species causing the inactivation of MS2 bacteriophage (Kohn et al., 2007; Kohn & Nelson, 2007). In the presence of trace metals, such as iron colloids, and hydrogen peroxide (H_2O_2) photo-Fenton-like processes efficiently formed hydroxyl radicals (·OH) capable of inactivating MS2 (Nieto-Juarez et al., 2010). Thus, exogenous inactivation mediated by the ubiquitous sensitizers NOM or iron could serve as an important disinfection process of viruses in surface waters.

Rotavirus has been recognized as the most common cause of acute infectious gastroenteritis in children (Marshall, 2009); nevertheless all age groups are affected worldwide (Gerba, Rose, Haas, & Crabtree, 1996). Besides infecting humans, rotavirus also infects the agriculturally important swine and calves among others (Rolsma, Gelberg, & Kuhlenschmidt, 1994). Among seven infectious serogroups of rotavirus, labeled A-G, only groups A-C are

human pathogens, with group A being the primary pathogenic type for humans worldwide and responsible for the majority of outbreaks (Marshall, 2009). These serogroups are distinguished by antigenic differences within the virus core and by migration of ds RNA segments (Marshall, 2009); however, each serogroup may share the same cellular receptor (Rolsma, Kuhlenschmidt, Gelberg, & Kuhlenschmidt, 1998). Rotavirus is highly infectious and spreads via the fecal-oral route. Infected individuals shed rotavirus at high concentrations (10^{10}-10^{11} virions per gram of feces) for up to two weeks (Marshall, 2009). Rotavirus infectivity can be retained for several days in water environments at temperatures up to 40°C and for ≥ 1-hr in the pH range of 3 to 10 (Estes, Graham, Smith, & Gerba, 1979; Marshall, 2009; Shamim A. Ansari, 1991; Ward & Ashley, 1980; Wood & Adams, 1992). The rotavirus minimal infective dose has been reported to be as little as one cell culture-infective unit (Graham, Dufour, & Estes, 1987), but higher infective doses have also been reported (Payment & Morin, 1990). While the main route of rotavirus transmission is person-to-person contact, all documented rotavirus waterborne outbreaks have been associated with direct fecal contamination of a water supply or improper water treatment (Gerba et al., 1996). Due to its resilient characteristics and prevalence, particularly in the developing world (Parashar, Gibson, Bresee, & Glass, 2006), rotavirus transmission via water has been recognized as a potentially significant public health problem (Graham et al., 1987). The objectives of this study are to investigate the synergistic roles of temperature, sunlight, and SRNOM on inactivation mechanisms of group A porcine rotavirus, and to compare its inactivation to that of the commonly used viral surrogate MS2.

2.3 Materials and methods

Virus inactivation experiments were conducted in solutions irradiated by either full spectrum simulated sunlight or partial spectrum without UVB. The investigated temperature

range was 14-35^{o}C, which covered the range of surface water temperatures under sunlight conditions (Gu, Luck, & Stefan, 1996). We further increased the temperature to 60^{o}C, at which a previous study found complete inactivation of rotavirus by heat (Wood & Adams, 1992). Suwannee River NOM (SRNOM) was used for a model sensitizer because it is well-characterized and has been used previously in photolysis studies (Kanan, Kanan, Austin, & Patterson, 2003; Page, Arnold, & McNeill, 2011). Inactivation experiments with quenchers, which selectively remove ROS, and experiments with D_2O, which reduce singlet oxygen quenching compared to H_2O, were also conducted to determine the radicals responsible for rotavirus inactivation. Concentrations of singlet oxygen and OH radicals and accumulation rates of hydrogen peroxide were also determined.

2.3.1 Model viruses

MS2 bacteriophage (ATCC 15597-B1) was obtained from the American Type Culture Collection and was replicated and purified as described elsewhere (Gutierrez et al., 2009). Briefly, MS2 was propagated in *Escherichia coli* (ATCC 15597) and further purified by sequential centrifugation (Eppendorf centrifuge 5416) at 5000 rpm ($g \times 100$) for 15 min at 20°C and microfiltered to remove *E. coli* cell debris. Subsequently, the filtered MS2 stock was concentrated on a Millipore 100-kDa membrane (Koch Membranes, USA) and rinsed with sterilized 1 mM NaCl (Fisher) solution in an ultrafiltration unit (Whatman Nucleopore, USA). The final MS2 stock, with a concentration of ~10^{11} plaque forming units (PFU) per mL, was stored at 4^{o}C in sterilized 1 mM NaCl solution. MS2 enumeration was performed following the double agar layer procedure (Adams, 1959). Group A porcine rotavirus OSU strain (ATCC # VR-892) was propagated in embryonic African green monkey kidney cells (MA-104 cells) and was extracted from the cell culture as described elsewhere (Rolsma et al., 1994). Rotavirus was

purified following the same protocol as for MS2, except the microfiltration through the 0.2-µm membrane was not performed. To prevent outer capsid protein denaturation (Ruiz et al., 1996), solution of 1 mM NaCl and 0.5 mM $CaCl_2$ (Fisher) was used for concentrating rotavirus with 100 kDa membrane. The final purified rotavirus stock concentration of ~10^6 focus forming units (FFU) per mL was stored in the dark at 4°C. Samples were enumerated by infectivity assay (Rolsma et al., 1998) with concentrations of rotavirus reported as focus forming units per mL (FFU/mL).

2.3.2 Rotavirus infectivity assay, enumeration, and uncertainties

The rotavirus focus forming assay and enumeration procedures were described in more detail elsewhere (Rolsma, Gelberg, & Kuhlenschmidt, 1994).

2.3.2.1 Focus forming infectivity (FFU) method

The rotavirus samples were treated with 10 ug/mL crystallized trypsin (Sigma). Appropriate dilutions of the trypsinized virus sample were made in serum-free Eagle's minimum essential medium (MEM; GIBCO). Confluent monolayers of MA-104 cells in 24-well plates were rinsed twice with 1mL phosphate-buffered saline (PBS). Two wells were inoculated with 100 µL of each virus dilution for 30 min and later aspirated. Each well was rinsed once with serum-free MEM and incubated with 1 mL serum-free MEM in a 5% CO_2 incubator set to 37°C for 16-18 hr prior to quantification of infected cells by immunocytochemical detection of virus infected cells (FFU assay).

2.3.2.2 FFU method enumeration

After 16-18 hr incubation, the infected monolayers were rinsed twice with 1mL PBS, fixed 1 mL of with 9:1 methanol (Sigma) – glacial acidic acid (Fisher) for 2 min and rehydrated with 0.5 mL of 70 and 50% ethanol (Sigma) for 5 min. Monolayers were then treated for 10 min with 150 µL of 3% H_2O_2 (30%; Fisher) and diluted in wash buffer. The wash buffer (WB) consisted of 125 mM Tris (Fisher), 350 mM NaCl (Fisher), and 0.25% Triton X-100 (Sigma) at pH 7.6. The monolayers were then washed with 1 mL WB for 10 min. A 150 µL volume of 5% normal goat serum (Vector Laboratories) was used (20 min) for each monolayer to inhibit nonspecific primary antibody binding. The normal goat serum solution was replaced by 150 µL the primary antibody (Dako; catalog no. B218) diluted 1:100 in WB and incubated for 1 hr at 37°C. The monolayers were then rinsed twice with 0.5 mL of WB. After, 150 µL of the secondary antibody (biotinylated goat anti-rabbit immuno-globulin G; Vector Elite Kit; Vector Labs) diluted 1:200 in WB was replaced and incubated for 20 min. Two 10-min 0.5 mL WB rinses followed. The ABC reagent (Vector Elite Kit) was made 30 min prior to use and contained 1:50 dilutions of reagents A and B in WB. After washing, 150 µL of the ABC reagent was added to the monolayers for 20 min. Two more 10-min 0.5 mL WB rinses were performed on the monolayers. The peroxidase chromogen (Kirkegaard & Perry) was prepared as directed by the kit instructions and added to promote color development. The peroxidase chromogen was stopped before nonspecific cell staining occurred (< 9 min). Finally, 0.5 mL of deionized water was added to each well. The number of brown-stained (viral-antigen-positive) cells was quantified under an inverted microscope equipped with contrast enhancement and a mechanical stage.

2.3.2.3 Uncertainties associated with the FFU method

The rotavirus enumeration method is similar to a PFU method, where each individual brown-stained cell represents an infected cell by a single infectious rotavirus particle. The color change is due to viral-antigen-positive, recognized by the primary antibody. Some of the possible errors associated with the FFU method include: infection of a single MA-104 cell by a multiple rotavirus particles and not a single rotavirus, primary antibody binding to other non-specific antigens that may result in false-positives, and MA-104 infected cells inability to express viral-antigens resulting in false-negatives. To reduce single cell infectivity by multiple rotavirus, rotavirus solutions should be kept monodispersed throughout the experiment, which is the longest length of time the rotavirus solutions were stirred. We have measured any possible aggregation of rotavirus in different conditions as explained in the methods section: Detection of Aggregation by Dynamic Light Scattering and have not observed any aggregation. As for the non-specific binding of the primary antibody, an inhibitor (normal goat serum) for nonspecific binding was added each time during the FFU assay. Nonetheless, for every 24 well-plate, at least one well was used as control, where only the serum-free MEM solution was added. To counteract error from a cell's inability to express the antigens, samples from the same experiment were plated on the same 24 well-plate. Because all cells in each plate were inoculated at the same time with the same cell concentration, there should not be significant differences between cells of the same plate and the number of false-negatives should be equally distributed. Therefore, when calculating the inactivation kinetics ($\ln C/C_0$) vs. time, any differences in cells would be included in the calculation.

Any errors might affect the trends between different conditions due to differences in MA104 cells batches, but should not affect the data from a single condition, as samples for the

same experiment were plated on the same batch of cells. We have conducted experiments for a single condition at least twice and have found the trends to be consistent. See Table A1

2.3.3 Model aquatic natural organic matter (NOM)

Suwannee River NOM (SRNOM) was obtained from the International Humic Substances Society. The procedure for NOM solution preparation was described elsewhere (Nguyen & Chen, 2007). Briefly, SRNOM was dissolved in a solution containing 1 mM NaCl and 2 mM $NaHCO_3$ (Fisher). The final SRNOM solution at pH 7.2 was filtered through a 0.22 μm acetate membrane and stored at 4°C. The total organic carbon concentration of 230 mg/L (reported as mg C/L) for the final SRNOM stock solution was measured at the Illinois Sustainable Technology Center.

2.3.4 Experimental setup for virus inactivation

Solar disinfection experiments were conducted using an Atlas Suntest(r) XLS+ photosimulator (Chicago, IL) equipped with a Xenon arc lamp, which irradiates light with wavelength from 280 nm and above. The solar simulator was also fitted with a filter (Atlas MTS, Cat. 56052372), which cuts off most, but not all, of the irradiance below 320 nm. This Atlas filter was in place throughout all irradiation experiments conducted and it was the only filter used in the full spectrum (280-700 nm) irradiation experiments. Due to the UVB bleeding of the Atlas filter, a second UVB filter (Newport, FSQ-WG320) with a 320-nm cutoff was placed atop each reactor testing UVA and visible light (320 – 700 nm) effects. A calibrated StellarNet Inc. spectrometer was used to measure the irradiance of the solar simulator from 280-700 nm. The solar simulator intensity was set to 400 $W.m^{-2}$. The fraction of the UVB (280-320 nm) irradiance measured with and without the Newport 320 nm cut-off filter was 4.71 and 6.24%, respectively.

For comparison, the fraction of the UVB irradiance of natural sunlight measured at noon on March 5, 2010 during a clear day in Urbana, IL was 5.86%. The measured irradiance did not change with or without the Newport 320 nm cut-off filter.

All reactors were painted black to avoid light reflection and immersed in a circulating water bath. All solutions were stirred by a Variomag electronic stirrer set to 130 rpm. For MS2 inactivation, 50-mL pyrex beakers with 40-mL containing 1 mM sodium bicarbonate buffer, SRNOM (0-20 mg C/L), and an initial MS2 concentration of 10^8 plaque forming units (PFU) per mL were used. One-mL sample aliquots were collected in 1.7-mL centrifuge tubes at regular intervals and stored in the dark until enumeration (normally 2-12 hrs from sample collection).

For rotavirus inactivation experiments, a similar protocol was used. A 0.5-1-mL aliquot of the rotavirus stock solution was added to each 10-mL pyrex beaker, achieving a 10^4-10^5 FFU/mL concentration in each reactor. A 200-µL sample aliquot was collected in 1.5-mL centrifuge tubes at regular intervals and stored in the dark until the samples were enumerated (within 2-12 hrs). pH readings of each reactor were taken immediately before and after irradiation. The pH remained stable (7.6 - 8.0 ± 0.2) for all conditions tested. A duplicate reactor without the virus spike was included with each experiment to take temperature readings during each sample acquisition. The same sample volume was also withdrawn from the duplicate reactor, so that all reactors had the same volume throughout the experiment.

2.3.5 Singlet oxygen and hydroxyl radical measurements

Concentrations of singlet oxygen ($^1O_2$) and hydroxyl radicals (·OH) produced by the irradiated SRNOM solution were measured by using furfuryl alcohol (FAA; 98%, Acros Organics) and phenol (99%, Acros Organics), respectively, as probes described in previous

publications (Alexieva, Yemendzhiev, & Zlateva; Gottfried & Kimel, 1991; Haag & Hoigne, 1986; Haag, Hoigne, Gassman, & Braun, 1984). Briefly, concentrations of $^1O_2$ and HO· were measured in separate irradiated solutions (40-mL) containing 1 mM sodium bicarbonate buffer and SRNOM (0-20 mg C/L), and initial concentrations of 40 µM of FFA or 10 µM of phenol. The samples were analyzed by reverse-phase HPLC 1200 Series and an Eclipse XDB- C18 column. For FFA detection, the HPLC isocratic mobile phase containing 40% acetonitrile (HPLC grade, Acros Organic), 60% Nanopure water, and 0.1% acetic acid (~98% LC-MS grade, Fluka) was pumped at flow rate of 0.41 mL/min and detected by diode array detector (DAD) at 216 nm with a retention time of 5.11 ± .05 minutes. The concentration of singlet oxygen was calculated as:

$$[1O2]_{apparent} = k_{exp}/k_2 \qquad \text{(eq. S1)}$$

where $[1O2]_{apparent}$ is the apparent steady state concentration of singlet oxygen (M) in the bulk solution, k_{exp} is the experimentally determined pseudo-first order reaction rate constant (s^{-1}), k_2 (1.2 x 108 M-1s-1at 25°C) is the second order reaction rate constant of the reaction between singlet oxygen and FFA (Alexieva, Yemendzhiev & Zlateva, 2010; Gottfried & Kimel, 1991; Haag & Hoigne, 1986; Haag, Hoigne, Gassman, & Braun, 1984). Previous studies have reported activation energies of 0.5-8 kJ/mol for [1O2]ss oxidation reactions (Gottfried & Kimel, 1991). Consequently, the temperature dependence of k_{exp} is too low to significantly affect the $[1O2]_{measured}$ calculated by eq. S1. However, the quenching rate of FFA is temperature-dependent (activation energy of 22 kJ/mol), and the reported $[1O2]_{measured}$ reflect this dependence (Gottfried & Kimel, 1991). In the absence of SRNOM, no FFA decay was observed in the temperature range considered.

For phenol detection, the HPLC isocratic mobile phase containing 70% methanol (HPLC grade), 27.5% Nanopure water, and 2.5% acetic acid (~98% LC-MS grade, Fluka) was pumped at flow rate of 0.35 mL/min and detected by DAD at 260 nm with a retention time of 6.5 ± .05 minutes. The decay of phenol concentrations were calculated using eq. S1, where k_2 (1.4×10^{10} $M^{-1}s^{-1}$ at ambient temperature and pH 7.4-7.7) is the second order reaction rate constant of the reaction between ·OH and phenol (Alexieva, Yemendzhiev & Zlateva, 2010). For phenol, the k_{exp} and k_2 rates were not adjusted for temperature effects. Instead, we accounted for the decay of phenol due to increased temperature and irradiation in water only (without SRNOM). The data collected from the irradiation experiments without SRNOM at each temperature were subtracted from the data collected in the presence of 20 mg C/L of SRNOM.

2.3.6 Hydrogen peroxide measurement

The concentration of hydrogen peroxide (H_2O_2) produced by the irradiated SRNOM solution was measured by using a 0.1 M potassium iodide (PI; 99+%, Fisher) and 0.01 M ammonium heptamolybdate tetrahydrate ($H_{24}MO_7N_6O_{24}·4H_2O$, Acros Organics) mixture as shown in Kormann et *al*. (Kormann, Bahnemann, & Hoffmann, 1988). Briefly, to quantify the H_2O_2 concentration, 1000-µL of the PI solution and 20-µL of the molybdate solution were added to a 2-mL cuvette (Petribrand) and rapidly mixed with 200-µL of sample. The absorbance was recorded at 350 nm after ~30-60 seconds, when the reading stabilized. The concentration of H_2O_2 was calculated by Lambert-Beer's Law: $A = \varepsilon\ b\ d\ [H_2O_2]$, where A is the absorbance determined at 350 nm, ε is H_2O_2's molar extinction coefficient (26400 $M^{-1}cm^{-1}$), b is the path length of optic cell (e.g. 1 cm), d is the sample dilution factor, and $[H_2O_2]$ is the molar concentration of hydrogen peroxide in molar. In the absence of SRNOM, no H_2O_2 accumulation was observed for the temperature range considered.

2.3.7 Quenching experiments

The quenchers and respective concentrations used were 50 mM of sodium formate (MP Biomedicals) for ·OH, 20 mM of L-Histidine (Acros Organics) for $^1O_2$, and 200 U/mL of catalase (Aldrich) for H_2O_2. Additionally, commercially available H_2O_2 (30%, Fisher) and D_2O (99.8%, Acros) were used.

2.3.8 Detection of aggregation by dynamic light scattering

A ZS90 Zetasizer instrument (Malvern, UK) was used to measure the size distribution of the two viruses at 25 and 50°C (42°C for MS2). With the known hydrodynamic diameters of MS2 and rotavirus (Gutierrez et al., 2009), it was possible to determine the monodispersivity or aggregation of the desired solutions. The detection limit for MS2 and rotavirus in solution was ~10^{10} PFU/mL and ~10^4 FFU/mL, respectively. A minimum of two measurements per sample were recorded. No aggregation for any virus was observed in the time frame considered.

2.3.9 Measuring trace metal concentrations in SRNOM and buffer solutions

Trace metal concentrations were determined using inductively coupled plasma mass spectrometry with an ELAN Dynamic Reaction Cell instrument (PerkinElmer, Norwalk, USA) at the Microanalysis Laboratory at the University of Illinois at Urbana-Champaign. Samples were diluted to a total dissolved solid concentration of 0.25% and the light wavelength intensity from excited atom species was used to determine analyte concentrations.

2.3.10 Correction for light screening

To account for light attenuation by SRNOM in solution, k_{obs} was adjusted by a light screening correction factor. For inactivation by full spectrum irradiation (direct inactivation), the correction factor was based on the concept that different wavelengths differ in their efficiency to inactivate viruses. The most important wavelengths are those that are both irradiated at significant intensities (data obtained from the spectra of the lamp), and those that are lethal to the

microorganism. Direct inactivation is only possible for wavelengths which are absorbed (predominantly wavelengths < 300 nm) by viral genomes and/or proteins (Eischeid & Linden; Hijnen, Beerendonk, & Medema, 2006; Schuch & Menck). The lethality of each wavelength was therefore estimated from the absorbance spectra of the studied microorganisms (protein and nucleic acid). The higher the absorbance measured for the microorganism, the greater the assumed propensity for photolysis at that wavelength. The product of the lamp irradiance and the absorbance of the microorganism (protein and nucleic acid) was used to determine the most important wavelength (280 nm) in the inactivation of MS2 and rotavirus (see Figure A1 in the Appendix). For rotavirus, the absorbance spectrum for double-stranded RNA from 280-300 nm normalized by the absorbance at 260 nm was extracted from the normalized spectrum published in Ref. (Bockstahler, 1967). The absorbance spectrum for single-stranded RNA from 280-300 nm normalized by the absorbance at 260 nm was extracted from the normalized spectrum published in Ref. (Porterfield & Zlotnick, 2010). Stocks of MS2 and rotavirus were used to determine the normalized absorbance spectra of the total virus including the protein capsids. The light screening correction factors for indirect inactivation were briefly described below and have also been detailed in previous publications (Grandbois, Latch, & McNeill, 2008; Schwarzenbach, Gschwend, & Imboden, 2002).

In contrast to direct inactivation, indirect inactivation can be promoted by a broader range of light since the SRNOM sensitizer absorbs light and thus produces ROS. Therefore, the light screening correction factor for k_{obs} values, as well as ROS production, by UVA and visible light (indirect inactivation included a wider range of wavelengths (280-400 nm). We chose to only correct for the 280-400 nm range because this is the range where light attenutation by SRNOM was the highest (97.4 % of the total absorption spectrum from 280-700 nm). The spectra of

SRNOM containing solutions were measured using a UV-Vis spectrophotometer (UV 2450, Shimadzu) in 1 cm cuvettes (Plastibrand).

2.3.11 Calculations for light screening correction

The light screening correction factor was derived from the comparison of light intensity at the surface of the solution and the mean light intensity over a given solution thickness. At the optically thin surface layer, the rate of light absorption is given by the sum of the light absorbed over the light spectrum (eq. S1).

$$k_{obs,thin} = 2.303\sum_{\lambda}\alpha_{\lambda} I_{\lambda,0} \qquad \text{(eq. S1)}$$

Where α_λ is the light attenuation at a given wavelength and $I_{\lambda,0}$ is the light irradiance at a given wavelength at the surface (or as measured by the spectrophotometer). Outside the optically thin regime, the mean light intensity, $\langle I_\lambda \rangle_z$, is used due to the significant absorption within solutions (eq. S2).

$$k_{obs,thick} = 2.303\sum_{\lambda}\alpha_{\lambda} \left\langle I_{\lambda} \right\rangle_z \qquad \text{(eq. S2)}$$

The average light irradiance at total depth z is the irradiance at the surface multiplied by the light screening correction factor, S_λ, as shown in eq. S3.

$$\left\langle I_{\lambda} \right\rangle_z = I_{\lambda,0} \frac{\left(1-10^{\alpha_{\lambda} z}\right)}{2.303\alpha_{\lambda} z} = I_{\lambda,0} S_{\lambda} \qquad \text{(eq. S3)}$$

The correction factor (CF) is then defined as the ratio of light absorbed at optically thin conditions over the light absorbed at optically thick conditions (eq. S4).

$$CF = \frac{k_{obs,thin}}{k_{obs,thick}} = \frac{\sum_{\lambda} \alpha_{\lambda} I_{\lambda,0}}{\sum_{\lambda} \alpha_{\lambda} \langle I_{\lambda} \rangle_z} = \frac{\sum_{\lambda} \alpha_{\lambda} I_{\lambda,0}}{\sum_{\lambda} \alpha_{\lambda} I_{\lambda,0} S_{\lambda}} \qquad \text{(eq. S4)}$$

The CF was applied to data acquired for all experiments containing SRNOM. For the UVA-induced experiments, the correction factor was calculated for wavelengths ranging from 280-400 nm, as explained previously. For the full spectrum experiments, the correction factor was estimated using a single wavelength (280 nm), as explained above. When a single wavelength was used, eq. S5 simplified to $CF_{280nm} = \frac{1}{S_{280nm}}$.

2.4 Kinetic data analysis

The pseudo-first order inactivation rate, k_{obs} (hr^{-1}), was obtained by determining the slope of ln(PFU or FFU/mL) vs. time (hr) plots. Linear regression analysis was used to calculate the k_{obs} value and the corresponding 95% confidence interval for a single condition. Linear regression analysis was also used to determine whether the slopes of the lines in the inactivation kinetic and k_{obs} vs. temperature plots were significantly different from a slope of zero ($p < 0.05$). A multiple linear regression analysis (Neter, Wasserman, & Kutner, 1990) was used to compare if the slopes of the inactivation kinetic and k_{obs} vs. temperature plots for different conditions were significantly different ($p < 0.05$) from each other. From each reactor a single sample was collected at a given time. For each sample, appropriate dilutions were made and each dilution was plated twice on either wells (for rotavirus) or petri dishes (for MS2). Counts in duplicate were averaged and used for further analysis. Most conditions were tested multiple times in separate experiments, with similar trends (see Table A1 in the Appendix).

2.5 Results

2.5.1 Full sunlight spectrum inactivation at 23-26°C

UVB has been reported to be the most lethal portion of the solar spectrum for most indicators of waterborne pathogens (Sinton et al., 2002; Williamson, Neale, Grad, De Lange, & Hargreaves, 2001); accordingly, rapid inactivation of both rotavirus and MS2 was observed in bicarbonate-buffered solutions irradiated by the full sunlight spectrum (Figure 2). UVB, however, is rapidly screened if NOM is present, and much slower inactivation kinetics were observed in solutions containing 20 mg C/L. When the inactivation rate constants were corrected for UVB light screening, statistically similar inactivation kinetics were observed in the presence and absence of SRNOM for both MS2 ($p = 0.37$) and rotavirus ($p = 0.83$) at 23 and 26°C, respectively (Figure 2). This observation suggests that the SRNOM-mediated, indirect exogenous effects were negligible for MS2 and rotavirus inactivation by the full sunlight spectrum.

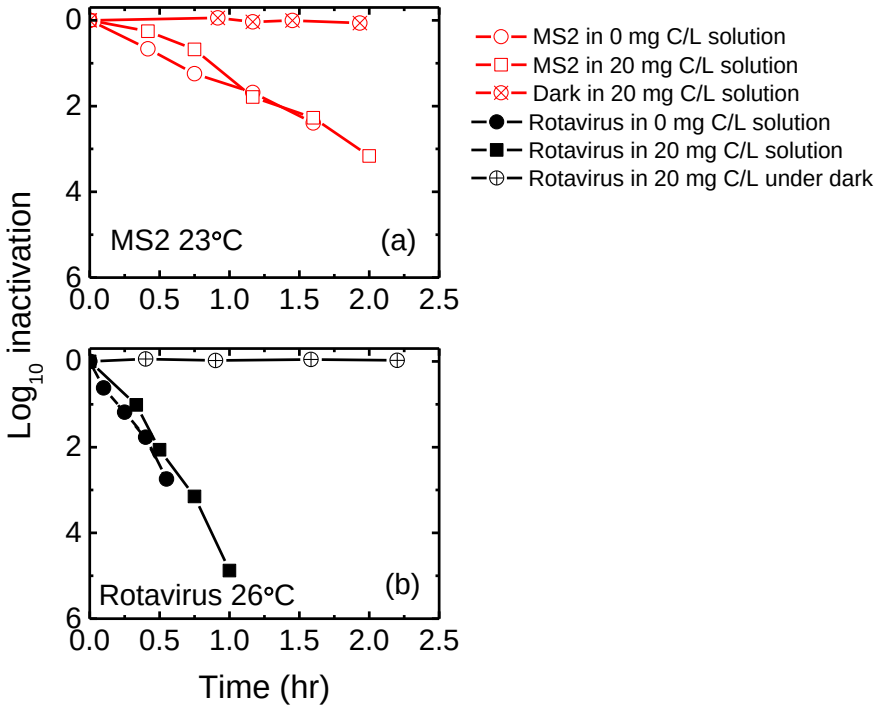

Figure 2: Full sunlight spectrum inactivation of MS2 (**a**) and rotavirus (**b**) at 23 and 26°C, respectively, as a function of time in the presence and absence of SRNOM in 1 mM sodium bicarbonate buffer. The plots were corrected for light screening.

2.5.2 Dark and endogenous inactivation of MS2 and rotavirus at 23-26°C

The contribution of endogenous inactivation was investigated by irradiating virus solutions with the UVB portion removed from the full sunlight spectrum. This condition avoids the confounding effects of direct inactivation. In the absence of SRNOM and exposed only to light in the UVA/visible range, MS2 and rotavirus showed slow and statistically similar ($p = 0.86$) endogenous inactivation kinetics ($k_{obs} \sim 0.16 \pm 0.03$ hr^{-1}; ~0.5-log unit reduction over 7 hrs; see Figures 3a and b). This observed slow inactivation for MS2 and rotavirus irradiated with UVA and visible light are consistent with other previously reported studies with RNA viruses (R. J. Davies-Colley et al., 1999; Kohn & Nelson, 2007), which appear to be resistant to endogenous

inactivation. In the dark, neither MS2 nor rotavirus inactivation kinetics showed significant ($p = 0.70$-0.62) deviation from a slope of zero in the presence or absence of SRNOM over 10 hrs.

2.5.3 SRNOM-mediated exogenous inactivation of MS2 and rotavirus at 22-23°C

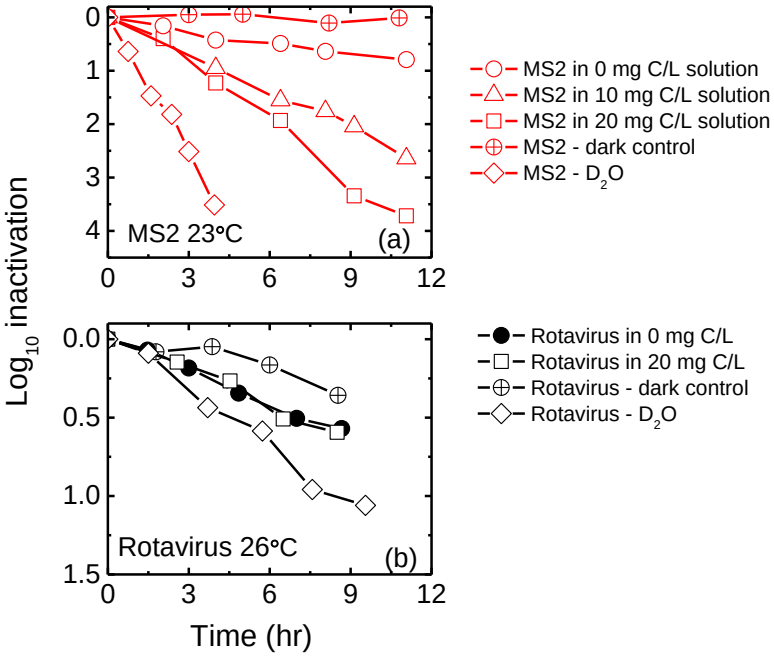

Figure 3: Inactivation kinetics for MS2 (a) and rotavirus (b) under UVA and visible light irradiation at 23 and 26°C, respectively. All experiments were conducted in 1 mM sodium bicarbonate buffer. Except for the dark conditions, samples were irradiated with UVA and visible light. The plots have been corrected for light screening.

As discussed above, the contribution of exogenous inactivation was insignificant in experiments using the full sunlight spectrum. However, as light in the UVB range is rapidly screened by NOM in solution, exogenous inactivation may become relevant at lower depths in a water column. For this reason, irradiation by UVA and visible light was also investigated. The inactivation kinetics of MS2 in solutions containing different concentrations of organic matter irradiated with light in the UVA/visible range is illustrated in Fig. 3a. The SRNOM-mediated exogenous inactivation rate constants, k_{obs}, for MS2 increased with SRNOM concentrations

(expressed as DOC) after light screening correction. Specifically, the MS2 k_{obs} values at [DOC] of 0, 10, and 20 mg C/L were 0.16 ± 0.03, 0.53 ± 0.5, and 0.91 ± 0.1 hr^{-1}, respectively. Inactivation kinetics for these conditions showed a significantly difference with p values < 0.01.

Previous studies have shown that among the ROS formed by irradiated humic acid, $^1O_2$ was the most important disinfectant for MS2 (Kohn & Nelson, 2007). The increased k_{obs} values for MS2 can be explained by the increased $^1O_2$ formation as a function of SRNOM concentration (Figure 2S in Supporting Information). Evidence of the importance of $^1O_2$ for MS2 inactivation by SRNOM is given by experiments conducted in D_2O (Fig. 2a). Water is a more efficient $^1O_2$ quencher than D_2O. Specifically the quenching rates of $^1O_2$ in D_2O and H_2O are 1.6×10^4 s^{-1} and 2.5×10^5 s^{-1}, respectively (Haag & Hoigne, 1986). Therefore, the $^1O_2$ concentration in D_2O should be higher than in water. Indeed in solution containing 20 mg C/L, the measured $^1O_2$ concentrations were $(24.5 \pm 3.4) \times 10^{-14}$ M in water to $(120 \pm 5) \times 10^{-14}$ M in D_2O. This five-time increase in $^1O_2$ concentration resulted in an MS2 k_{obs} value 2.4-times higher in D_2O than in H_2O. The lower than the expected five-time increase in k_{obs} suggests that $^1O_2$ may only account for a part of the total inactivation of MS2. In the absence of SRNOM, no significant ($p = 0.57$) difference in inactivation kinetics was observed between the D_2O and H_2O conditions. Thus, the increase in k_{obs} value with increasing concentrations of $^1O_2$ formed by SRNOM is consistent with previous studies suggesting its important role (Sutherland, 1981).

No significant difference ($p = 0.61$) in rotavirus inactivation kinetics was observed in the presence or absence of SRNOM over 9 hrs. To confirm the lack of $^1O_2$-induced rotavirus inactivation, additional experiments were conducted in D_2O. In the presence of 20 mg C/L, the rotavirus k_{obs} value was 1.6 times higher in D_2O than in H_2O ($p = 0.006$ for comparison of kinetic data). This small increase in rotavirus k_{obs} value suggests that $^1O_2$ only minimally

inactivates rotavirus at 23˚C and in the presence of 20 mg C/L SRNOM. Our results suggest that $^1O_2$ formed by NOM in sunlit surface waters at ambient temperatures is not expected to inactivate rotavirus since $^1O_2$ is present only at low steady-state concentrations ($< 10^{-12}$ M) (Cooper, Zika, Petasne, & Fischer, 1988).

2.5.4 Role of temperature on inactivation of MS2 and rotavirus

The temperature dependence of MS2 and rotavirus inactivation in the dark is plotted in Figures 4a and 4b, respectively. We performed linear regression analysis to determine if the slope of the k_{obs} values plotted against temperature differed from a slope of zero ($p < 0.05$). Because the slopes for temperature (14-42 °C) and dark inactivation rate constants for MS2 ($p = 0.38$) and rotavirus ($p = 0.19$) did not differ from a slope of zero, we concluded that there was no significant trend between temperature and k_{obs} values for both viruses in the dark. The inactivation rate constants remained low for both viruses ($k_{obs} \sim 0.05$ hr^{-1} or 0.25 $\log_{10}$ unit reductions in 10 hr) from 14-42°C. However, at 50°C the k_{obs} values for both MS2 and rotavirus increased to 0.76 ± 0.2 hr^{-1} (~1-$\log_{10}$ reduction over 3 hr) and 0.5 ± 0.2 hr^{-1} (~1-$\log_{10}$ reduction over 5 hr), respectively. At 60°C, the MS2 k_{obs} values obtained for the dark and for the condition without SRNOM increased to ~6 hr^{-1} (~1-$\log_{10}$ reduction over 0.36 hr; data not shown) with no statistically different inactivation kinetics ($p = 0.14$). For rotavirus, when the temperature reached 60°C, no infectious virus was detected from an initial sample of $10^{3.5}$ FFU/mL after 6 min of heat exposure (data not plotted) for any condition tested, including irradiation by the full sunlight spectrum and under dark conditions. Thus, the log reduction for this case was estimated to be 3.5 or k_{obs} of 30 hr^{-1}. At a temperature equal to or above 60°C, heat is expected to be the main factor for rotavirus inactivation. The rotavirus data presented here is in agreement with a previous study, wherein rotavirus was found to remain stable at 30 and 40°C for at least 24 hr in

viral growth media. A 1.5-log unit reduction at 50°C in 1 hr (estimated k_{obs} of ~3.5 hr^{-1}) and 3.25-log unit reduction at 60°C in 5 min (est. k_{obs} of ~90 hr^{-1}) were reported (Wood & Adams, 1992).

For the full solar spectrum irradiation, MS2 solutions containing 0 mg C/L and 20 mg C/L were investigated in the temperature range of 14–42°C. For these conditions, k_{obs} values were weakly but linearly correlated with temperature. Specifically, for solutions containing 0 mg C/L and 20 mg C/L, the slopes of the regression lines for k_{obs} values and temperature were 0.02 ($p = 0.0009$) and 0.06 ($p = 0.03$), respectively (Figure 4a). For rotavirus irradiated by the full sunlight spectrum (Figure 4b) in solutions containing 0 and 20 mg C/L of SRNOM, the slopes of the regression lines for k_{obs} vs. temperature (14-42°C) were ~ 0.15 ($p < 0.05$). The inactivation kinetic plots for the two conditions aforementioned were not statistically different from each other ($p = 0.85$).

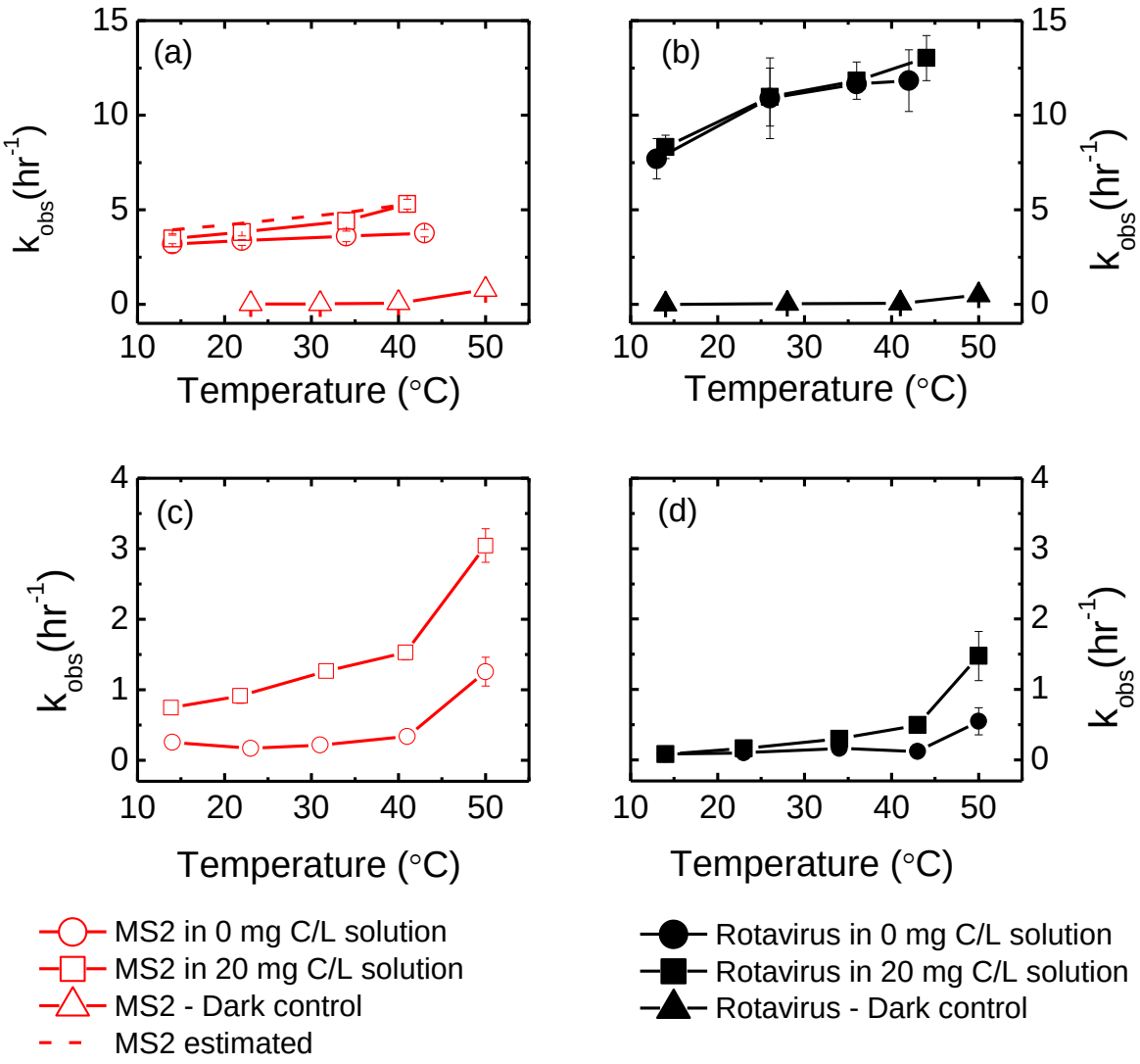

Figure 4: Inactivation rate constants as a function of temperature for MS2 irradiated with the full sunlight spectrum (**a**), rotavirus irradiated with the full sunlight spectrum (**b**), MS2 irradiated with UVA and visible light (**c**), and rotavirus irradiated with UVA and visible light (**d**). The plots have been corrected for light screening and the error bars correspond to 95% confidence intervals. Only one set of the dark inactivation is shown for clarity.

When MS2 was irradiated by only UVA and visible light (Figures 4c), the slope of the regression line for endogenous (i.e. without SRNOM) k_{obs} values and temperature (14-42°C) did not significantly differ from a slope of zero ($p = 0.46$). The k_{obs} values obtained for MS2 solutions without SRNOM were < 0.33 hr^{-1} (< 1-log_{10} unit reduction over ~7 hrs) in the temperature range of 14-42°C. At 50°C, the MS2 k_{obs} value increased to 1.26 ± 0.2 hr^{-1} (~1-log_{10} unit reduction in 1 hr).

For rotavirus, the UVA and visible light induced endogenous k_{obs} values (Figure 4d) remained low (k_{obs} < 0.2 hr^{-1}; ~1 log_{10} unit reduction in 12 hr) for the temperature range of 14-42°C. The linear plots for the endogenous and dark k_{obs} values vs. temperature (14-42°C) were not statistically different from each other ($p = 0.81$). Under the same irradiation condition at 50°C, the endogenous and dark kinetic plots were not statistically different from each other ($p = 0.73$) and measured a k_{obs} value of ~0.5 hr^{-1}.

In the absence of UVB, the SRNOM-mediated exogenous (i.e., with 20 mg C/L of SRNOM) k_{obs} values for MS2 and rotavirus increased with temperatures from 14 to 50°C (Figure 4c and d). For MS2, there was a linear relationship between temperatures from 14 to 42 °C and the SRNOM-mediated exogenous k_{obs} values (slope = 0.03; $p = 0.004$). The k_{obs} values due to SRNOM-mediated exogenous inactivation of MS2 increased from 1.5 ± 0.1 hr^{-1} at 42°C to 3 ± 0.2 hr^{-1}at 50°C and to 18.9 ± 1 hr^{-1} (~1-log_{10} unit reduction in 0.13 hr) at 60°C.

For rotavirus under UVA and visible light irradiation, the linear plots obtained by plotting the endogenous and SRNOM-mediated exogenous k_{obs} values against temperature from 14-33°C were not statistically different from each other ($p = 0.29$). For rotavirus, the k_{obs} values due to SRNOM-mediated exogenous inactivation increased from 0.3 ± 0.06 hr^{-1} at 34°C to 0.5 ± 0.05

hr^{-1} at 42°C and 1.5 ± 0.3 hr^{-1} (~1-log_{10} unit reduction in 1.5 hr) at 50°C. Comparing the k_{obs} values obtained from solutions irradiated by UVA and visible light with and without SRNOM at 50°C, the SRNOM-mediated exogenous conditions resulted in higher inactivation rates (1.5 vs. 0.5 hr^{-1}). Thus, this increased inactivation of rotavirus at 50°C in the presence of SRNOM is due to the synergistic effects of heat, sunlight irradiation, and NOM. To our knowledge, this is the first study to report the importance of high temperature (i.e. > 25°C) for sunlight-mediated inactivation of rotavirus.

2.5.5 Quenching experiments at 50°C for rotavirus

Quenching tests were conducted at 50°C to identify which ROS was responsible for the inactivation of rotavirus by exogenous effects (see Table A1 found in the Appendix). Singlet oxygen was investigated first, as it has been shown to be responsible for MS2 inactivation. At 50°C and 20 mg C/L (Table A1), the inactivation kinetics obtained in solutions with and without 50 mM L-Histidine, a quencher for $^1O_2$, were not significantly different ($p = 0.58$). Also, for this same condition, the inactivation kinetics obtained in D_2O and H_2O were not statistically different ($p = 0.78$). Thus, the experimental results suggest that rotavirus inactivation at 50 °C is not primarily due to damage by $^1O_2$.

Quenching experiments with 200 U/mL catalase were conducted at 50°C to determine the role of H_2O_2 on exogenous rotavirus inactivation (Table A2 found in the Appendix). In the presence of catalase and 20 mg C/L, the rotavirus k_{obs} value decreased from 1.5 ± 0.3 hr^{-1} to 0.5 ± 0.3 hr^{-1}, which was the k_{obs} value determined for the 0 mg C/L condition. While the presence of H_2O_2 may be related to rotavirus inactivation, the quenching experiments did not provide direct evidence that rotavirus inactivation was due to oxidation by H_2O_2. We therefore conducted

another set of experiments, for which H_2O_2 was added at concentrations of 0, 6, 60, and 600 µM to rotavirus solutions kept in the dark at 50°C. Up to 60 µM, these experiments did not show statistically different (p value range 0.17 – 0.58) inactivation kinetics (k_{obs} ~ 0.45 hr^{-1}; or 1-log_{10} unit in 6 hr). The condition with 600 µM H_2O_2 showed significantly greater rotavirus inactivation, with a k_{obs} value of 5.5± 3.3 hr^{-1} (~1-log_{10} units in 0.5 hr). Although the H_2O_2 formation rate by SRNOM irradiation increased with temperature (see Figure A3 found in the Appendix), the maximum [H_2O_2] measured at 50°C did not exceed 6 µM over the 3-hr period of all rotavirus experiments at 50°C. This suggests that H_2O_2 produced by UVA and visible light irradiation of solutions containing 20 mg C/L of SRNOM was not directly responsible for the inactivation of rotavirus.

2.6 Discussion

Direct photolysis processes, such as those that cause direct damage to the genome by UVB light, are typically temperature-independent for non-cellular systems lacking self-repairing mechanisms such as extracellular biomolecules and viruses (Eischeid, Thurston, & Linden, 2011; Li, Paulsson, & Björn, 2002; Matallana-Surget, Douki, Meador, Cavicchioli, & Joux, 2010). In the absence of external sensitizers (SRNOM), the small slope of MS2 k_{obs} vs. temperature (i.e., slope =0.02 with p = 0.0009 for the temperature range of 14 - 42°C) suggested that direct photolysis was responsible for MS2 inactivation by the full solar spectrum. For rotavirus irradiated with full spectrum sunlight at this same temperature range, the slope of k_{obs} vs. temperature was greater (slope = 0.15; p = 0.017). This temperature dependence for rotavirus inactivation may stem from endogenous inactivation in the UVB range (R. J. Davies-Colley et al., 1999; He & Häder, 2002). After the absorption of UVB light by the internal sensitizers such as RNA and proteins, the excited sensitizers may react via bimolecular reactions with virus

constituents directly, or may react with dissolved oxygen to generate inactivating ROS (Schuch & Menck, 2010). Such internal bimolecular reactions are likely to be enhanced by temperature (Li et al., 2002) and may therefore be responsible for the observed increase in rotavirus k_{obs} values from 14 – 42°C in the absence of exogenous sensitizers. However, the insignificance kinetics difference ($p = 0.85$) between rotavirus k_{obs} values obtained from solutions with and without SRNOM vs. temperature (14-42°C) suggested that SRNOM-mediated exogenous inactivation did not contribute significantly to the overall inactivation caused by full spectrum irradiation. Thus, for full spectrum irradiation, direct photolysis played a dominant role for rotavirus inactivation in the presence or absence of SRNOM. A similar conclusion about the role of direct photolysis was reported for adenovirus and poliovirus (Love et al., 2010).

The contribution of SRNOM to MS2 inactivation by full spectrum or UVA and visible light was studied with solutions containing 20 mg C/L SRNOM in the temperature range of 14-42 °C. Under UVA and visible light only, exogenous inactivation from the addition of SRNOM constituted a majority of inactivation and increased temperature dependence of disinfection as compared to the reactor without SRNOM (slope difference of 0.03 from k_{obs} vs. temperature plots). Under full spectrum irradiation in the same temperature range, the addition of SRNOM-mediated exogenous inactivation also increased k_{obs} values and temperature dependence (slope difference of 0.04 from k_{obs} vs. temperature plots). To compare the contribution of exogenous effects between full spectrum and only UVA and visible light, estimated full spectrum kobs values in SRNOM were obtained by adding the k_{obs} value for the SRNOM-mediated exogenous inactivation measured under UVA and visible light (Fig. 4c) to the k_{obs} value obtained from full spectrum irradiation in the absence of SRNOM (Fig. 4a) at a given temperature. The plots (Fig. 4a) generated from the estimated kobs and the measured values for full spectrum irradiation in

20 mg C/L against temperature (14-42°C) were not statistically different from each other ($p = 0.18$). Agreement between observed and estimated k_{obs} suggests that for MS2, the SRNOM-mediated exogenous effects contributed similarly to inactivation and temperature dependence regardless of the magnitude of endogenous and direct inactivation in solution or the addition of UVB.

Formation of ROS, including $^1O_2$, $\cdot OH$, and H_2O_2 by SRNOM solution irradiated with UVA and visible light may be responsible for virus inactivation. We first discuss the temperature dependence of $^1O_2$ concentration on MS2 inactivation because $^1O_2$ is the oxidant responsible for MS2 inactivation in humic acid solutions (Kohn & Nelson, 2007). Concentrations of $^1O_2$ (Figure 3Sa-A in Appendix A), did not significantly differ from a slope of zero with temperature from 14 – 42°C ($p = 0.11$). Statistically faster exogenous inactivation of MS2 thus cannot be explained by increased $^1O_2$ concentration, but is likely due to an increased reaction rate between ROS formed exogenously with the viral particles. Additionally, the MS2 capsid could become more permeable to ROS at increased temperature as observed for the canine parvovirus capsid (Nelson et al., 2008), which would allow the penetration of $^1O_2$ and other ROS to damage the genome more readily.

As shown in the results, formation of H_2O_2 by SRNOM irradiated with UVA and visible light was essential for rotavirus inactivation at 50°C, but the presence of < 60 µM of H_2O_2 in the dark was not enough to explain the observed inactivation of rotavirus. Because H_2O_2 is thought to form as a secondary product of sunlight-induced reactions, the formation of H_2O_2 in SRNOM solutions exposed to sunlight is indicative of the formation of other reactive species potentially responsible for inactivating rotavirus (Cooper et al., 1988). For example, H_2O_2 is photochemically produced by the reaction between superoxide anion and triplet-excited state

NOM (Cooper & Zika, 1983; Garg, Rose, & Waite, 2011). H_2O_2 is also a promoter of ·OH formation in the presence of trace metals via the Fenton and Fenton-like processes, which may contribute to virus inactivation (Nieto-Juarez et al., 2010). A trace metal analysis found 1.33 µM of iron and 6 nM of copper in the SRNOM solutions containing 20 mg C/L. Fe (III) and Cu (II) concentrations of ~ 1µM at neutral pH have been shown to cause virus inactivation by (photo)-Fenton-like processes at 20°C (Nieto-Juarez et al., 2010). Though iron and copper are likely to be in complexation with NOM and, at pH levels of 7.6-8.1 for the inactivation experiments, reaction rates of these complexes with H_2O_2 should be slow (Miller, Rose, & Waite, 2009; Voelker, Morel, & Sulzberger, 1997). Besides photo-Fenton reactions, ·OH can also be produced by triplet state NOM (Cooper & Zika, 1983; Page et al., 2011). The increased concentration of ·OH measured as a function of temperature (23-50°C) time suggested faster reaction for ·OH formation (Fig A3 in the Appendix). Thus, rotavirus inactivation is likely related to triplet state NOM and ·OH formation in UVA and visible light irradiated solutions containing SRNOM.

MS2 and rotavirus are biologically different, which is potentially the primary characteristic influencing their unique responses to solar disinfection. Whereas MS2 bacteriophage is composed of a single protein capsid with a positive-sense RNA strand (Acheson, 2006), rotavirus consists of three concentric and complex protein capsids with 11 double-stranded RNA segments (Marshall, 2009). The structures of the protein capsids and the genomes of these two viruses may be responsible for the observed difference in their reactivity with individual ROS at temperature range of 14-42ºC. Currently, work is being done to investigate the molecular mechanisms of rotavirus inactivation by sunlight irradiation.

2.7 Environmental relevance

The data reported here showed that temperature plays an important role in the sunlight-mediated inactivation of rotavirus and MS2. Compared to indirect inactivation, direct UVB irradiation was indisputably the most effective for both viruses in the temperature range considered (14-42°), and it was also the least influenced by temperature. At ambient temperature of 20-25°C, rotavirus inactivation by full spectrum irradiation was dominant. Similar results have been observed for adenovirus type 2 and poliovirus type 3 (Love et al., 2010). SRNOM-mediated exogenous inactivation was temperature-dependent for both viruses. For rotavirus, SRNOM-mediated exogenous inactivation was observed to be significant only in the 33 – 50°C temperature range.

The temperatures of surface water bodies measured in the upper layers (4 – 30 cm depths) have been shown to range from 0 to 35°C depending on the season, with fluctuations of up to 14°C differentials between day and night (Gu et al., 1996). The results from this study suggest that inactivation of rotavirus in surface water may change significantly depending on sunlight intensity, cloud coverage, and UV index. The top layer of surface water is also important for virus disinfection because attenuation of UV irradiation by high NOM concentrations and/or suspended solids is minimized at shallow depths (0 – 20 cm) (Arts et al., 2000). Since UVB irradiation is more rapidly attenuated by high NOM systems rather than UVA irradiation *(68)*, UVB effects would only be significant at very short depths (0 – 10 cm) and the indirect exogenous effects would contribute to virus disinfection at lower depths, particularly at high temperatures (>33˚C). Besides the temperature and NOM concentration governing sunlight inactivation, other factors such as pH, type and origin of NOM, the presence of suspended solids, and biological activity should be considered for predicting inactivation of rotavirus.

2.8 Acknowledgement

We acknowledge the financial support of NSF CTS-0120978 and its supplements, USDA Grant No. 2008-35102-19143, and NSF CAREER grant to THN (0954501), and NSF GRF DGE 07-15088 FLW to OCR. This work is partially funded by the Academic Excellence Alliance (AEA) program at King Abdullah University of Science and Technology (KAUST).

2.9 Literature Cited

Acheson, N. H. (2006). *Fundamentals of Molecular Virology*: John Wiley & Sons, Inc.

Adams, M. (1959). *Bacteriophages*. New York: Interscience Publishers.

Alexieva, Z., Yemendzhiev, H., & Zlateva, P. (2010). Cresols utilization by Trametes versicolor and substrate interactions in the mixture with phenol. *Biodegradation, 21*(4), 625-635

Arts, M. T., Robarts, R. D., Kasai, F., Waiser, M. J., Tumber, V. P., Plante, A. J., . . . de Lange, H. J. (2000). The attenuation of ultraviolet radiation in high dissolved organic carbon waters of wetlands and lakes on the northern Great Plains. *Limnology and Oceanography, 45*(2), 292-299.

Aw, T. G., & Gin, K. Y. H. (2011). Prevalence and genetic diversity of waterborne pathogenic viruses in surface waters of tropical urban catchments. *Journal of Applied Microbiology, 110*(4), 903-914. doi: 10.1111/j.1365-2672.2011.04947.x

Aw, T. G., Gin, K. Y. H., Oon, L. L. E., Chen, E. X., & Woo, C. H. (2009). Prevalence and Genotypes of Human Noroviruses in Tropical Urban Surface Waters and Clinical Samples in Singapore. *Applied and Environmental Microbiology, 75*(15), 4984-4992. doi: 10.1128/aem.00489-09

Boehm, A. B., Yamahara, K. M., Love, D. C., Peterson, B. M., McNeill, K., & Nelson, K. L. (2009). Covariation and Photoinactivation of Traditional and Novel Indicator Organisms and Human Viruses at a Sewage-Impacted Marine Beach. *Environmental Science & Technology, 43*(21), 8046-8052. doi: 10.1021/es9015124

Cooper, W. J., & Zika, R. G. (1983). Photochemical formation of hydrogen-peroxide in surface and ground waters exposed to sunlight. *Science, 220*(4598), 711-712. doi: 10.1126/science.220.4598.711

Cooper, W. J., Zika, R. G., Petasne, R. G., & Fischer, A. M. (1988). Sunlight-Induced Photochemistry of Humic Substances in Natural Waters: Major Reactive Species. In Aquatic Humic Substances, (Vol. 219, pp. 333-362): American Chemical Society

Curtis, T. P., Mara, D. D., Dixo, N. G. H., & Silva, S. A. (1994). Light Penetration in Waste Stabilization Ponds. *Water Research, 28*(5), 1031-1038.

Curtis, T. P., Mara, D. D., & Silva, S. A. (1992). Influence of Ph, Oxygen, and Humic Substances on Ability of Sunlight to Damage Fecal-Coliforms in Waste Stabilization Pond Water. *Applied and Environmental Microbiology, 58*(4), 1335-1343.

Da Silva, A. K., Le Guyader, F. S., Le Saux, J. C., Pommepuy, M., Montgomery, M. A., & Elimelech, M. (2008). Norovirus Removal and Particle Association in a Waste Stabilization Pond. *Environmental Science & Technology, 42*(24), 9151-9157. doi: 10.1021/es802787v

Davies, C. M., Roser, D. J., Feitz, A. J., & Ashbolt, N. J. (2009). Solar radiation disinfection of drinking water at temperate latitudes: Inactivation rates for an optimised reactor configuration. *Water Research, 43*(3), 643-652. doi: 10.1016/j.watres.2008.11.016

Davies-Colley, R. J., Donnison, A. M., & Speed, D. J. (2000). Towards a mechanistic understanding of pond disinfection. *Water Science and Technology, 42*(10-11), 149-158.

Davies-Colley, R. J., Donnison, A. M., Speed, D. J., Ross, C. M., & Nagels, J. W. (1999). Inactivation of faecal indicator microorganisms in waste stabilisation ponds: Interactions of environmental factors with sunlight. *Water Research, 33*(5), 1220-1230.

Eischeid, A. C., & Linden, K. G. (2011). Molecular Indications of Protein Damage in Adenoviruses after UV Disinfection. *Applied and Environmental Microbiology, 77*(3), 1145-1147. doi: 10.1128/aem.00403-10

Eischeid, A. C., Thurston, J. A., & Linden, K. G. (2011). UV Disinfection of Adenovirus: Present State of the Research and Future Directions. *Critical Reviews in Environmental Science and Technology, 41*(15), 1375-1396. doi: 10.1080/10643381003608268

Estes, M. K., Graham, D. Y., Smith, E. M., & Gerba, C. P. (1979). Rotavirus Stability and Inactivation. *Journal of General Virology, 43*(MAY), 403-409.

Garg, S., Rose, A. L., & Waite, T. D. (2011). Photochemical production of superoxide and hydrogen peroxide from natural organic matter. *Geochimica Et Cosmochimica Acta, 75*(15), 4310-4320. doi: 10.1016/j.gca.2011.05.014

Gerba, C. P., Rose, J. B., Haas, C. N., & Crabtree, K. D. (1996). Waterborne rotavirus: A risk assessment. *Water Research, 30*(12), 2929-2940.

Graham, D. Y., Dufour, G. R., & Estes, M. K. (1987). Minimal Infective Dose of Rotavirus. *Archives of Virology, 92*(3-4), 261-271.

Gu, R., Luck, F. N., & Stefan, H. G. (1996). Water Quality Stratification in Shallow Wastewater Stabilization Ponds. *Journal of the American Water Resources Association, 32*(4), 831-844.

Gutierrez, L., Li, X., Wang, J., Nangmenyi, G., Economy, J., Kuhlenschmidt, T. B., Nguyen, T. H. (2009). Adsorption of rotavirus and bacteriophage MS2 using glass fiber coated with hematite nanoparticles. *Water Research, 43*(20), 5198-5208.

Haag, W. R., & Hoigne, J. (1986). Singlet Oxygen in Surface Waters .3. Photochemical Formation and Steady-State Concentrations in Various Types of Waters. *Environmental Science & Technology, 20*(4), 341-348.

Haag, W. R., Hoigne, J., Gassman, E., & Braun, A. M. (1984). Singlet Oxygen in Surface Waters .1. Furfuryl Alcohol as a Trapping Agent. *Chemosphere, 13*(5-6), 631-640

Haile, R. W., Witte, J. S., Gold, M., Cressey, R., McGee, C., Millikan, R. C., Wang, G. Y. (1999). The health effects of swimming in ocean water contaminated by storm drain runoff. *Epidemiology, 10*(4), 355-363. doi: 10.1097/00001648-199907000-00004

He, Y.-Y., & Häder, D.-P. (2002). Involvement of reactive oxygen species in the UV-B damage to the cyanobacterium Anabaena sp. *Journal of Photochemistry and Photobiology B-Biology, 66*(1), 73-80.

Jiang, S., Noble, R., & Chui, W. P. (2001). Human adenoviruses and coliphages in urban runoff-impacted coastal waters of Southern California. *Applied and Environmental Microbiology, 67*(1), 179-184. doi: 10.1128/aem.67.1.179-184.2001

Joshi, P. C., & Keane, T. C. (2010). Investigation of riboflavin sensitized degradation of purine and pyrimidine derivatives of DNA and RNA under UVA and UVB. *Biochemical and Biophysical Research Communications, 400*(4), 729-733. doi: 10.1016/j.bbrc.2010.08.138

Kanan, M. C., Kanan, S. M., Austin, R. N., & Patterson, H. H. (2003). Photodecomposition of carbaryl in the presence of silver-doped zeolite Y and Suwannee River natural organic matter. *Environmental Science & Technology, 37*(10), 2280-2285. doi: 10.1021/es026136+

Kohn, T., Grandbois, M., McNeill, K., & Nelson, K. L. (2007). Association with natural organic matter enhances the sunlight-mediated inactivation of MS2 coliphage by singlet oxygen. *Environmental Science & Technology, 41*(13), 4626-4632. doi: 10.1021/es070295h

Kohn, T., & Nelson, K. L. (2007). Sunlight-mediated inactivation of MS2 coliphage via exogenous singlet oxygen produced by sensitizers in natural waters. *Environmental Science & Technology, 41*(1), 192-197. doi: 10.1021/es061716i

Lesser, M. P., & Shick, J. M. (1989). Effects of irradiance and ultraviolet radiation on photoadaptation in the zooxanthellae of Aiptasia pallida: primary production, photoinhibition, and enzymic defenses against oxygen toxicity. *Marine Biology, 102*(2), 243-255.

Li, S., Paulsson, M., & Björn, L. O. (2002). Temperature-dependent formation and photorepair of DNA damage induced by UV-B radiation in suspension-cultured tobacco cells. *Journal of Photochemistry and Photobiology B-Biology, 66*(1), 67-72.

Love, D. C., Silverman, A., & Nelson, K. L. (2010). Human Virus and Bacteriophage Inactivation in Clear Water by Simulated Sunlight Compared to Bacteriophage Inactivation at a Southern California Beach. *Environmental Science & Technology, 44*(18), 6965-6970. doi: 10.1021/es1001924

Marshall, G. S. (2009). Rotavirus Disease and Prevention Through Vaccination. *Pediatric Infectious Disease Journal, 28*(4), 355-362. doi: 10.1097/INF.0b013e318199494a

Matallana-Surget, S., Douki, T., Meador, J. A., Cavicchioli, R., & Joux, F. (2010). Influence of growth temperature and starvation state on survival and DNA damage induction in the marine bacterium Sphingopyxis alaskensis exposed to UV radiation. *Journal of Photochemistry and Photobiology B-Biology, 100*(2), 51-56.

Mi, B. X., Marinas, B. J., Curl, J., Sethi, S., Crozes, G., & Hugaboom, D. (2005). Microbial passage in low pressure membrane elements with compromised integrity. *Environmental Science & Technology, 39*(11), 4270-4279. doi: 10.1021/es0484092

Miller, C. J., Rose, A. L., & Waite, T. D. (2009). Impact of natural organic matter on H_2O_2-mediated oxidation of Fe(II) in a simulated freshwater system. *Geochimica Et Cosmochimica Acta, 73*(10), 2758-2768. doi: 10.1016/j.gca.2009.02.027

Nelson, C. D. S., Minkkinen, E., Bergkvist, M., Hoelzer, K., Fisher, M., Bothner, B., & Parrish, C. R. (2008). Detecting Small Changes and Additional Peptides in the Canine Parvovirus Capsid Structure. *Journal of Virology, 82*(21), 10397-10407. doi: 10.1128/jvi.00972-08

Neter, J., Wasserman, W., & Kutner, M. H. (1990). *Applied Linear Statistical Models: Regression, Analysis of Variance, and Experimental Designs* (Third ed.). Boston, MA: CRC Press.

Nguyen, T. H., & Chen, K. L. (2007). Role of divalent cations in plasmid DNA adsorption to natural organic matter-coated silica surface. *Environmental Science & Technology, 41*(15), 5370-5375. doi: 10.1021/es070425m

Nieto-Juarez, J. I., Pierzchla, K., Sienkiewicz, A., & Kohn, T. (2010). Inactivation of MS2 coliphage in Fenton and Fenton-like systems: role of transition metals, hydrogen peroxide and sunlight. *Environmental Science & Technology, 44*(9), 3351-3356. doi: 10.1021/es903739f

Page, S. E., Arnold, W. A., & McNeill, K. (2011). Assessing the Contribution of Free Hydroxyl Radical in Organic Matter-Sensitized Photohydroxylation Reactions. *Environmental Science & Technology, 45*(7), 2818-2825. doi: 10.1021/es2000694

Parashar, U. D., Gibson, C. J., Bresee, J. S., & Glass, R. I. (2006). Rotavirus and severe childhood diarrhea. *Emerging Infectious Disease, 12*(2), 304-306.

Payment, P., & Morin, É. (1990). Minimal infective dose of the OSU strain of porcine rotavirus. *Archives of Virology, 112*(3), 277-282. doi: 10.1007/bf01323172

Rolsma, M. D., Gelberg, H. B., & Kuhlenschmidt, M. S. (1994). Assay for Evaluation of Rotavirus-Cell Interactions - Identification of an Enterocyte Ganglioside Fraction That Mediates Group-a Porcine Rotavirus Recognition. *Journal of Virology, 68*(1), 258-268.

Rolsma, M. D., Kuhlenschmidt, T. B., Gelberg, H. B., & Kuhlenschmidt, M. S. (1998). Structure and function of a ganglioside receptor for porcine rotavirus. *Journal of Virology, 72*(11), 9079-9091.

Ruiz, M., Charpilienne, A., Liprandi, F., Gajardo, R., Michelangeli, F., & Cohen, J. (1996). The concentration of Ca2+ that solubilizes outer capsid proteins from rotavirus particles is dependent on the strain. *Journal of Virology, 70*(8), 4877-4883.

Schuch, A. P., & Menck, C. F. M. (2010). The genotoxic effects of DNA lesions induced by artificial UV-radiation and sunlight. *Journal of Photochemistry and Photobiology B-Biology, 99*(3), 111-116. doi: 10.1016/j.jphotobiol.2010.03.004

Sedmak, G., Bina, D., MacDonald, J., & Couillard, L. (2005). Nine-year study of the occurrence of culturable viruses in source water for two drinking water treatment plants and the influent and effluent of a wastewater treatment plant in Milwaukee, Wisconsin (August 1994 through July 2003). *Applied and Environmental Microbiology, 71*(2), 1042-1050. doi: 10.1128/aem.71.2.1042-1050.2005

Shamim A. Ansari, V. S. S. a. S. A. S. (1991). Survival and Vehicular Spread of Human Rotaviruses: Possible Relation to Seasonality of Outbreaks. *Reviews of Infectious Diseases, 13*(3), 448-461

Sinton, L. W., Hall, C. H., Lynch, P. A., & Davies-Colley, R. J. (2002). Sunlight inactivation of fecal indicator bacteria and bacteriophages from waste stabilization pond effluent in fresh and saline waters. *Applied and Environmental Microbiology, 68*(3), 1122-1131. doi: 10.1128/aem.68.3.1122-1131.2002

Sirikanchana, K., Shisler, J. L., & Marinas, B. J. (2008a). Effect of exposure to UV-C irradiation and monochloramine on adenovirus serotype 2 early protein expression and DNA replication. *Applied and Environmental Microbiology, 74*(12), 3774-3782. doi: 10.1128/aem.02049-07

Sirikanchana, K., Shisler, J. L., & Marinas, B. J. (2008b). Inactivation kinetics of adenovirus serotype 2 with monochloramine. *Water Research, 42*(6-7), 1467-1474. doi: 10.1016/j.watres.2007.10.024

Strakhovskaya, M. G., Shumarina, A. O., Fraikin, G. Y., & Rubin, A. B. (1999). Endogenous porphyrin accumulation and photosensitization in the yeast Saccharomyces cerevisiae in the presence of 2,2 '-dipyridyl. *Journal of Photochemistry and Photobiology B-Biology, 49*(1), 18-22.

Sutherland, B. M. (1981). Photoreactivation. *BioScience, 31*(6), 439-444.

vanderMeulen, F. W., Ibrahim, K., Sterenborg, H., Alphen, L. V., Maikoe, A., & Dankert, J. (1997). Photodynamic destruction of Haemophilus parainfluenzae by endogenously

produced porphyrins. *Journal of Photochemistry and Photobiology B-Biology*, *40*(3), 204-208.

Viau, E. J., Goodwin, K. D., Yamahara, K. M., Layton, B. A., Sassoubre, L. M., Burns, S. L., . . . Boehm, A. B. (2011). Bacterial pathogens in Hawaiian coastal streams-Associations with fecal indicators, land cover, and water quality. *Water Research, 45*(11), 3279-3290. doi: 10.1016/j.watres.2011.03.033

Voelker, B. M., Morel, F. M. M., & Sulzberger, B. (1997). Iron redox cycling in surface waters: Effects of humic substances and light. *Environmental Science & Technology, 31*(4), 1004-1011. doi: 10.1021/es9604018

Ward, R. L., & Ashley, C. S. (1980). Effects of wastewater sludge and its detergents on the stability of rotavirus. *Applied and Environmental Microbiology, 39*(6), 1154-1158.

Williamson, C. E., Neale, P. J., Grad, G., De Lange, H. J., & Hargreaves, B. R. (2001). Beneficial and detrimental effects of UV on aquatic organisms: Implications of spectral variation. *Ecological Applications*, *11*(6), 1843-1857.

Wood, G. W., & Adams, M. R. (1992). Effects of Acidification, Bacterial Fermentation, and Temperature on the Survival of Rotavirus in a Model Weaning Food. *Journal of Food Protection, 55*(1), 52-55.

CHAPTER 3

SUNLIGHT-INDUCED INACTIVATION OF HUMAN WA AND PORCINE OSU ROTAVIRUSES IN THE PRESENCE OF EXOGENOUS PHOTOSENSITIZERS[2]

3.1 Abstract

Human rotavirus Wa and porcine rotavirus OSU solutions were irradiated with simulated solar UV and visible light in the presence of different photosensitizers dissolved in buffered solutions. For human rotavirus, the exogenous effects were greater than the endogenous effects under irradiation with full spectrum and UVA and visible light at 25°C. For porcine rotavirus, the exogenous effects with UVA and visible light irradiation were only observed at high temperatures, > 40°C. The results from dark experiments conducted at different temperatures suggest that porcine rotavirus has higher thermostability than human rotavirus. Concentrations of 3'-MAP excited triplet states of 1.76 fM and above resulted in significant human rotavirus inactivation. The measured excited triplet state concentrations of ≤ 0.45 fM produced by UVA and visible light irradiation of natural dissolved organic matter solutions were likely not directly responsible for rotavirus inactivation. Instead, the linear correlation for human rotavirus inactivation rate constant (k_{obs}) with the phenol degradation rate constant (k_{exp}) found in both 1 mM $NaHCO_3$ and 1 mM phosphate buffered solutions suggested that OH radical was a major reactive species for the exogenous inactivation of rotaviruses. Linear correlations between

[2] Adapted with permission from (Romero-Maraccini, O. C.; Sadik, J.; Rosado-Lausell, S. L.; Pugh, C. R.; Niu, X.-Z.; Croue, J.-P.; Nguyen, T. H. Sunlight-Induced Inactivation of Human Wa and Porcine OSU Rotaviruses in the Presence of Exogenous Photosensitizers. *Environ. Sci. Technol.* **2013**, *47*, 11004–11012.). Copyright (2013) American Chemical Society.

rotavirus k_{obs} and specific UV_{254nm} absorbance of two river dissolved organic matter and two effluent organic matter isolates indicated that organic matter aromaticity may help predict the formation of radicals responsible for rotavirus inactivation. The results from this study also suggested that the differences in rotavirus strains should be considered when predicting solar inactivation of rotavirus in sunlit surface waters.

3.2 Introduction

Rotavirus is recognized as the most common cause of acute infectious gastroenteritis in children under the age of five (Marshall, 2009). It is estimated in sub-Saharan Africa countries alone, a total of 300,000 children die of rotavirus infection each year (Sanchez-Padilla et al., 2009). Of the seven serogroups (A-G) used to classify rotaviruses, only groups A-C are human pathogens, with group A being the primary pathogenic type for humans worldwide and responsible for the majority of outbreaks (Marshall, 2009; Sanchez-Padilla et al., 2009). To date, all documented rotavirus waterborne outbreaks have been associated with direct fecal contamination of a water supply or improper water treatment (Gerba, Rose, Haas, & Crabtree, 1996; Griffin & Donaldson, 2003; Dan Li, Gu, He, Shi, & Yang, 2009). Rotaviruses have been detected in surface waters worldwide, including coastal waters (Griffin & Donaldson, 2003), rivers and even treated wastewater effluents (He et al., 2009; D Li et al., 2011; van Zyl, Page, Grabow, Steele, & Taylor, 2006), with the highest concentrations of rotaviruses found in surface waters receiving untreated wastewater effluent (Griffin & Donaldson, 2003). Group A rotavirus was also detected in drinking water samples in Beijing, China (He et al., 2009) and in Southern Africa (van Zyl et al., 2006), possibly as a result of contamination by wastewater intrusion into the drinking water distribution system (He et al., 2009).

Li, *et al.* (2011) demonstrated that wastewater discharges were a likely source of rotavirus contamination in receiving surface waters (D Li et al., 2011). The same authors noted that the absence of infectious rotaviruses in receiving surface water samples collected in summer were likely a result of higher temperature and stronger UV compared to winter (D Li et al., 2011). This observation by Li, *et al.* (2011) is in agreement with findings from field studies that have linked the occurrence of pathogens, including enteric viruses, in coastal water with sunlight irradiation (Boehm et al., 2009; Viau et al., 2011). Because surface waters are a major source for drinking and recreational waters, contamination by enteric viruses such as rotaviruses from any source, including wastewater discharge, presents a threat to public health. Together, the studies above point to the public health burden and persistence of rotaviruses in surface waters and the need to better understand solar disinfection for improving removal of infectious rotaviruses from surface waters. To date, few studies have focused on the solar inactivation mechanisms of viruses, especially human pathogenic viruses such as human rotavirus.

Three sunlight inactivation mechanisms have been proposed: direct, endogenous and exogenous inactivation (Davies-Colley, Donnison, Speed, Ross, & Nagels, 1999). However, the direct and endogenous mechanisms are experimentally difficult to separate (Silverman, Peterson, Boehm, McNeill, & Nelson, 2013). The endogenous mechanism, which is primarily triggered by the UVB wavelengths in full spectrum irradiation (Davies-Colley et al., 1999). was the most effective for porcine rotavirus OSU and polio virus type 3 (Romero, Straub, Kohn, & Nguyen, 2011; Silverman et al., 2013). The endogenous inactivation initiated by UVA and visible light irradiation of photosensitizers that are associated with the microorganism (Joshi & Keane, 2010; Strakhovskaya, Shumarina, Fraikin, & Rubin, 1999), was negligible for porcine rotavirus inactivation (Romero et al., 2011), The exogenous inactivation mechanism relies on the

formation of reactive oxygen species and other transient radicals, such as excited triplet states, during UV and visible light irradiation of external photosensitizers (i.e., dissolved organic matter (DOM)) (Kohn & Nelson, 2007; Romero et al., 2011). In the absence of UVB, the exogenous mechanism was significant for porcine rotavirus only at high temperatures > 40°C (Romero et al., 2011). However, the exogenous inactivation mechanism is important because, unlike the endogenous mechanism which is dominated by UVB irradiation, the exogenous mechanism is largely driven by UVA and visible light irradiation (Romero et al., 2011). UVA light has been shown to reach deeper water levels in surface waters because it is less attenuated than UVB by turbidity and DOM (Arts et al., 2000; Davies, Roser, Feitz, & Ashbolt, 2009). Therefore, UVA and visible light irradiation should be of significant interest in environmental systems with high attenuation levels (i.e. waste stabilization ponds).

To date, our understanding of the role of different photosensitizers, both natural and synthetic, for the exogenous inactivation of human pathogens is incomplete. Because the ubiquitous presence of natural organic matter in most freshwater systems will cause the attenuation of UVB (Arts et al., 2000), this study will especially focus on the UVA and visible light irradiation of pathogenic group A human rotavirus Wa. However, a selected set of experiments for human rotavirus was conducted to study the exogenous inactivation under full spectrum irradiation. While clear coastal water and rivers may have DOM at concentrations up to 10 mg C/L (Boehm et al., 2009; Rosado-Lausell et al., 2013a), freshwater lakes can have up to 60 mg C/L. In this study, we tested the following two hypotheses: 1) the exogenous inactivation of rotavirus, by UVA and visible light irradiation of pathogenic group A human rotavirus Wa, is influenced by sources and types of 20 mg C/L of DOM and other exogenous photosensitizers; 2) a difference in capsid amino acid composition affects exogenous inactivation of Group A human

rotavirus Wa and porcine rotavirus OSU. A schematic delineating the rationale for the experiments conducted in this study is provided in the Appendix (Figure A4).

3.3 Materials and methods

The chemicals and reagents used for this study can be found in the Appendix. The descriptions for propagation and concentrations of the model viruses, cell growth procedure, infectivity assay, quenching tests and dark hydrogen peroxide inactivation tests, and SUVA determination are found in the Appendix.

3.3.1 Selection of photosensitizers

Four DOM fractions isolated using the XAD-8/XAD-4 resins were used at a concentration of 20 mg C/L (Croué, 2004; Zheng & Croue, 2012): Suwannee River hydrophobic acid (SWRHPO, i.e., humic substances as mixture of humic and fulvic acids), Jeddah treated wastewater hydrophobic acid (EfOMHPO) and transphilic acid (EfOMTPI) and Blavet River hydrophobic acid (BRHPO). The similarity between properties and reactivity with oxidants of these isolates and their corresponding bulk DOM matrix was already reported in previous studies (Benjamin, Croue, & Reiber, 1999; C. J. Hwang et al., 2001; Croué, 2004; Zheng & Croue, 2012). Each DOM was dissolved in a solution containing 1 mM NaCl (Fisher) and 1 mM $NaHCO_3$ (84 mg/L of $NaHCO_3$; Sigma), followed by filtration through a 0.22 µm membrane and stored at 4°C in the dark. BRHPO and EfOMTPI were also dissolved in 1 mM phosphate buffer for the carbonate-free experiments that investigated the role of the 1 mM $NaHCO_3$ buffer in rotavirus inactivation. The stock 10 mM phosphate solution was prepared by adding 76 mg monosodium phosphate (monohydrate, Fisher Scientific) and 2.5 g disodium phosphate (heptahydrate, Fisher Scientific) into 1 L of purified deionized (DI) water; once diluted, the pH

of the 1 mM phosphate solution was 7.9 ± 0.2. Total organic carbon content (TOC) measurements were done for solutions containing DOM isolates using a Shimadzu TOC analyzer. A 1 g/L of 3'-MAP stock solution was prepared in DI water and stored in the dark at 4°C. Sodium nitrate and sodium nitrite were prepared with DI water before each experiment.

3.3.2 Experimental setup for virus inactivation by simulated sunlight

Human and porcine rotavirus solutions in the presence of various photosensitizers were irradiated with solar simulator (Atlas Suntest® XLS+ photosimulator; Chicago, IL) that has the capability to irradiate at wavelengths ≥ 280 nm. The solar simulator xenon arc lamp was set at 400 $W \cdot m^{-2}$. For all experiments here, irradiance below 320 nm was reduced by a coated quartz filter with special window glass (Atlas, MTS) that was permanently installed within the solar simulator. To test rotavirus inactivation without UVB (wavelengths ≥ 320 nm), an additional filter (Newport, FSQ-WG320) with a 320 nm cut-off was positioned on each reactor during each experiment (refer to Figure 1 for the spectrum). For full spectrum irradiation tests, the 320 nm cut-off filter was not used. The spectra of the solar simulator with and without the UVB-cut off filter and natural sunlight were measured with a NIST-calibrated ILT950 spectrophotometer from International Light Technologies (Peabody, Massachusetts, USA) and are shown in Figure 5a.

All reactors (10-mL pyrex reactors) were covered on the outside with black vinyl electrical tape (Scotch, Super 33+, professional grade) to reduce reflected light. Except for the experiments in 1 mM phosphate buffer (pH 7.9 ± 0.2), the reactors for the inactivation tests consisted a total volume of 6-mL containing 1 mM $NaHCO_3$ buffer solution (84 mg/L $NaHCO_3$; pH 7.9 ± 0.2), known concentrations of photosensitizer (20 mg C/L), and an initial rotavirus

concentration of 10^4-10^5 FFU/mL. The reactors were placed within the solar simulator in a circulating water bath and stirred with Variomag electric stirrers at 130 rpm. A 200-µL sample aliquot was collected from each reactor at regular time intervals and stored at 4°C in the dark until processed, normally within 4 hours. Because the exogenous inactivation of rotavirus is temperature sensitive (Romero et al., 2011) and the inactivation kinetics differ for both rotavirus strains, experiments for human rotavirus were conducted at 25°C and for porcine rotavirus at 50°C, unless otherwise indicated. These temperatures allowed for measurable exogenous effects within 3 h, the desired length for experiments. A selected set of experiments were done at different temperatures: human rotavirus inactivation in the dark at varying temperatures in 1 mM $NaHCO_3$ buffer and porcine rotavirus in 20 mg C/L BRHPO or sensitizer-free 1 mM $NaHCO_3$ buffer at 25°C. A 1 mM $NaHCO_3$ (pH 7.9) buffer solution was used for most of the exogenous inactivation studies because it better reflects environmental conditions (Huang & Mabury, 2000). The concentration of carbonate species in natural surface waters has been measured in the range of 22 to 269 mg/L and carbonate species are also the main buffer of oceans, which have a pH value of around 8 (Huang & Mabury, 2000). Summaries of the raw data for human rotavirus (both stock 1 and stock 2) and porcine rotavirus inactivation experiments are found in Tables A3-A5 in the Appendix.

3.3.3 Measurements of phenol decay rates and steady-state concentrations of excited triplet state species

Phenol was used as a probe compound to help identify the radical responsible for the exogenous-induced inactivation of human rotavirus. Sorbic acid (*trans*, *trans*-hexadienoic acid) was used as a probe compound for excited triplet states of dissolved organic matter (Grebel, Pignatello, & Mitch, 2011). The decay of phenol (Gong, Lanzl, Cwiertny, & Walker, 2012;

Kohn & Nelson, 2007) and sorbic acid photoproducts (Grebel et al., 2011) were measured in irradiated solutions containing photosensitizers at 25°C. The 8-mL solutions contained 1 mM $NaHCO_3$ or 1 mM phosphate buffer, known concentrations of photosensitizers (20 mg C/L for all DOM solutions, 43 µM of $NaNO_2$, 590 µM of $NaNO_3$, and 15 or 30 mg/L of 3'-MAP) with initial phenol concentrations of 10 µM or varied initial concentrations of sorbic acid as described elsewhere (Grebel et al., 2011). The samples were analyzed by reverse-phase HPLC 1200 Series and an Eclipse XDB- C18 column in isocratic mode. For the sorbic acid method, the mobile phases were pumped at 1.2 mL/min and contained 85% 30 mM acetate buffer at pH 4.75 and 15% acetonitrile. Four isomer peaks were detected by diode array detector (DAD) at 254 nm and analyzed as described elsewhere (Rosado-Lausell et al., 2013b). For phenol, the HPLC mobile phase containing 60% methanol and 40% nanopure water was pumped at 1 mL/min and detected by DAD at 268 nm with reference wavelength at 600 nm. Phenol is commonly used as a OH radical probe (Gong et al., 2012; Kohn & Nelson, 2007). However, in solutions containing bicarbonate/carbonate ions, OH radicals are scavenged to produce carbonate radicals, which also lead to the decay of phenol (Burns et al., 2012; Busset, Mazellier, Sarakha, & De Laat, 2007). Therefore, the first-order decay constants, k_{exp} (h^{-1}), were reported instead of the measured steady-state OH radical concentrations. Summaries of the kinetics data for phenol decay and triplet state concentrations measurements are available in Table A6 and Table A7 in the Appendix.

3.3.4 Data analysis for simulated sunlight experiments

Linear regression analysis was used to calculate the –slope and correlation value R^2 of the $\ln(C/C_0)$ vs. time (h^{-1}) plot for both rotavirus and phenol experiments. For rotavirus, the first order inactivation rate constant (–slope) was reported as k_{obs} (h^{-1}), while for phenol the first order

decay rate constant (–slope) was reported as k_{exp} (h^{-1}). Linear regression was also used to asses if the $\ln(C/C_0)$ vs. time (h^{-1}) plot deviated from a slope of 0 ($p < 0.05$). Unless otherwise indicated, the mean and standard deviations were calculated from the rotavirus k_{obs} and phenol k_{exp} values obtained from 2-5 independent experiments (Tables A3 through A6 in the Appendix). Duplicate independent measurements for triplet state of 3'-MAP and DOM concentrations were conducted and a detailed experimental procedure is documented in Table A7 found in the Appendix. Tests for dark inactivation at various temperatures, quenching tests, and dark inactivation with H_2O_2 were conducted once, in parallel, and each sample of rotavirus collected was plated in duplicate (Tables A8 through A10 in the Appendix). Explanation for the choice of replicates, if N = 1, is provided in the SI (see Tables A7 through A10). Four to six samples were collected for each experiment and each sample was plated in duplicate for rotavirus, or analyzed once by the HPLC for the phenol decay measurements. OriginPro 8 SR1 (Northampton, MA, USA) linear regression tool was used to calculate the 95% confidence interval, R^2, and p-value of the linear regression line for the following relationships: human and porcine rotavirus k_{obs} values, human rotavirus k_{obs} and phenol k_{exp} values, and rotavirus k_{obs} and SUVA values. Two-tailed t-tests were also conducted to assess if given sets of human rotavirus k_{obs} values ($N \geq 3$) obtained in either 1 mM $NaHCO_3$ or 1 mM phosphate buffers in the presence of photosensitizers were statistically different ($p < 0.05$).

Unless otherwise indicated, all data were corrected for light screening to account for the irradiated samples with different absorbance spectra. Briefly, the light screening correction factor calculation was dependent on the absorbance values of DOM solutions, lamp irradiance output, and average depth throughout the experiment as described in detail elsewhere (Kohn & Nelson, 2007; Romero et al., 2011; Schwarzenbach, R. P.; Gschwend, P. M.; Imboden, 2002). The

absorbance of the photosensitizer solutions was obtained for the wavelengths from 280 nm to 700 nm (Figure A6 found in the Appendix). The wavelengths with non-zero absorbance were selected for correction because they were potentially able to undergo photolysis (Schwarzenbach, R. P.; Gschwend, P. M.; Imboden, 2002). For the lamp irradiance output, as measured by a NIST-calibrated spectrophotometer from 280 nm to 700 nm (Figure 1a), correction was conducted for all non-zero irradiance wavelengths. Assuming that all wavelengths are equal in energy, the correction factors were calculated for the wavelengths where the products of the irradiance and the absorbance of the photosenstizer were greater than zero. The product of the irradiance for solar simulator with the 320-cut off filter and natural sunlight and the absorbance of three photosensitizers are shown in Figure A6 (b-d) found in the Appendix.

3.4 Results and discussion

3.4.1 Thermal stability and its role in the exogenous inactivation of human and porcine rotaviruses

The thermal stability of human and porcine rotavirus was investigated by measuring the infectivity of the rotaviruses as a function of time in the 22-57°C range in the dark (Table A8). At 25°C, the dark k_{obs} values of both rotavirus strains did not deviate from a slope of zero ($p > 0.05$). At 40°C, the dark k_{obs} value for human rotavirus was ~7 times greater than porcine rotavirus at the same temperature. At higher temperatures, 50-57°C, the k_{obs} values were at least 20 times greater for human rotavirus than for porcine rotavirus (Table A8). These results showed that porcine rotavirus OSU had higher thermostability in the range of 40-57°C than human rotavirus Wa.

Protein studies have reported that single amino acid substitutions may alter a protein's thermostability (Imanaka, Shibazaki, & Takagi, 1986; Kristjánsson & Kinsella, 1991; Matthews, Nicholson, & Becktel, 1987). A comparison of the amino acid sequences found in GenBank for individual proteins of both human Wa and porcine OSU rotaviruses showed that four of the six structural proteins (VP1, VP2, VP3, and VP6) differ by as much as 7 percent in amino acid composition. The amino acid sequence composition of VP4 and VP7, the outermost proteins responsible for virus attachment and/or penetration into the host (Lopez & Arias, 2006), differed by 31 and 21 percent, respectively. Rotaviruses are classified based on two neutralizable outer capsid proteins, VP4 and VP7, where the VP7-specific types are termed G-types and VP4-specific types are termed P-types (Desselberger, 2000). Since VP4 and VP7 are coded by different RNA segments (Desselberger, 2000), the difference in amino acid sequence may lead to the different classifications for human Wa and porcine rotavirus OSU, G1P [8] and G5P [7], respectively. This difference may also be responsible for the observed thermostability. For example, the poliovirus 1 Brunhilde strain was twice as resistant to chlorine solution as the Mahoney strain despite the fact that the two strains differ in capsid protein sequences by just ~2 percent (Floyd, Sharp, & Johnson, 1979; Sharp & Leong, 1980; Wigginton & Kohn, 2012). The difference in amino acid composition between the two rotavirus strains may not only influence their susceptibility to heat inactivation, but may also affect their ability to become inactivated by other methods, including sunlight-induced exogenous inactivation.

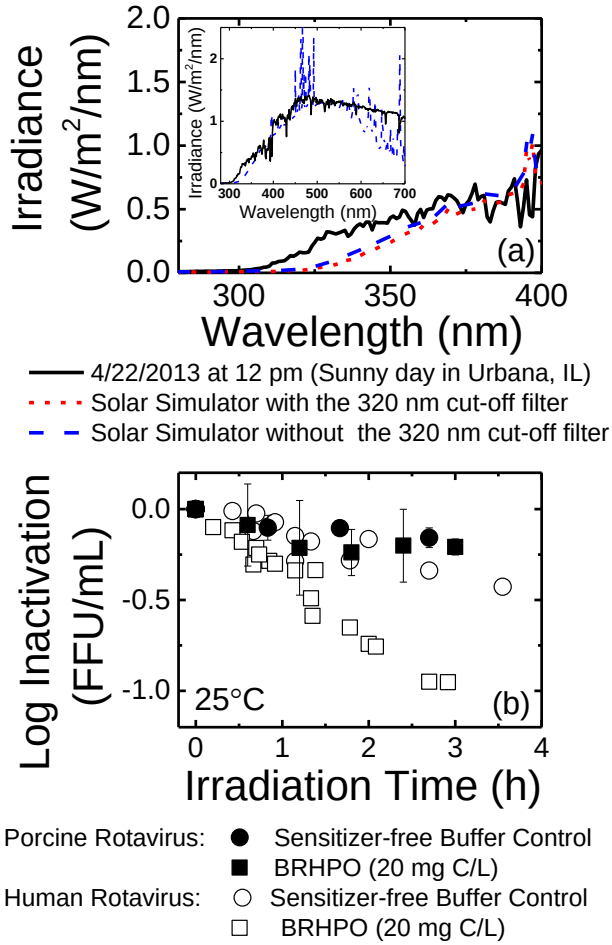

Figure 5. (a) Spectra of solar simulator with and without the UVB cut-off filter and natural sunlight and **(b)** inactivation kinetics of human and porcine rotavirus under simulated UVA and visible light irradiation at 25°C in 1 mM $NaHCO_3$ buffer (pH 7.9). For figure 1b, averages and standard deviations for inactivation experiments with porcine rotavirus (N = 3) were shown; error bars for the sensitizer-free buffer control are too small to be observed. All aggregated data obtained for human rotavirus inactivation conducted at different time were shown. Note that the human rotavirus k_{obs} values from each experiment are provided in Table A3 in the Appendix.

The inactivation kinetics of human and porcine rotavirus caused by UVA and visible light irradiation in solutions containing 1 mM $NaHCO_3$ buffer and 20 mg C/L of BRHPO at 25°C are shown in Figure 5b. The endogenous contribution was low (< 0.2-log_{10} reduction over a 2 h period) for both rotavirus strains at 25°C in the absence of BRHPO. The inactivation kinetics of porcine rotavirus in the presence or absence of BRHPO were not statistically different

($p = 0.87$, Figure 5b). This observation is consistent with a previous study(Romero et al., 2011) conducted with porcine rotavirus in a Suwannee River NOM (SRNOM) solution in 1 mM $NaHCO_3$ buffer at 25°C. Conversely, for human rotavirus at 25°C, the exogenous effect attributed by the presence of BRHPO was evident with a three-time increase in inactivation rate compared to that obtained in the sensitizer-free solution. While the exogenous effects were observed for human rotavirus at 25°C, these effects were observed at temperatures > 40°C for porcine rotavirus (Romero et al., 2011). Therefore, the tests for porcine rotavirus were conducted at 50°C. Although porcine k_{obs} values at 50°C were higher than human k_{obs} values at 25°C, the human and porcine k_{obs} values were linearly correlated ($R^2 = 0.92$; $p < 0.0001$, Figure 6a).

3.4.2 Roles of exogenous inactivation of rotavirus under full spectrum irradiation

As shown for other viruses (Love, Silverman, & Nelson, 2010; Silverman et al., 2013), including porcine rotavirus (Romero et al., 2011), UVB irradiation resulted in fast human rotavirus inactivation in the absence of exogenous photosensitizers in 1 mM $NaHCO_3$ at 25°C (Table A5 and Figure A7 in the Appendix). However, the presence of 20 mg C/L BRHPO at 25°C led to a 1.4-time increase in Stock 2 human rotavirus (k_{obs} of 8.6 ± 0.4 h^{-1}) values when compared to the sensitizer-free control (k_{obs} of 6.1 ± 0.7 h^{-1}) under full spectrum irradiation (Figure A7). Even when attenuation of solar UV was not accounted for, the k_{obs} values for solution containing BRHPO were still significantly higher than those obtained in the sensitizer-free solution ($N \geq 3$, t-test p-value = 0.028). Thus, for human rotavirus, because DOM can increase inactivation even under full spectrum irradiation, the exogenous mechanism is significant for human rotavirus. The substantial effects of the exogenous mechanism under full spectrum irradiation were recently reported for adenovirus type 2, MS2, and PRD1 (Silverman et al., 2013). For porcine rotavirus and poliovirus type 3, the exogenous contribution was

insignificant when compared to the endogenous inactivation under full spectrum irradiation at 26°C and 20°C, respectively (Romero et al., 2011; Silverman et al., 2013). These two rotavirus strains studied here are morphologically identical, but their capsid amino acid composition differ by up to 30%. This difference may suffice to make porcine rotavirus highly susceptible to endogenous inactivation, but resilient for exogenous inactivation at 25°C when compared to human rotavirus.

3.4.3 Roles of ROS on the exogenous-induced inactivation of human and porcine rotavirus

In this study, the presence of exogenous photosensitizers led to higher k_{obs} values for both human Wa and porcine OSU rotavirus when compared to the absence of photosensitizers (Figure 6a). Since the k_{obs} values of rotavirus in the sensitizer-free solution were significantly lower than those containing exogenous photosensitizers ($< 0.3\ h^{-1}$), it was concluded that the endogenous contribution was minimal for both rotavirus strains (Figure 2a) under UVA and visible light irradiation. For both rotavirus strains, the presence of 20 mg C/L of EfOMTPI resulted in relatively low k_{obs} ($< 0.5\ h^{-1}$), but in solutions with 20 mg C/L of EfOMHPO, BRHPO, or SWRHPO the k_{obs} values increased ($0.7\ h^{-1} < k_{obs} < 0.9\ h^{-1}$) relative to the sensitizer-free buffer control. To assess the specific roles of ROS produced by DOM solutions in the inactivation of both rotavirus strains, quenching tests were performed. The results of the quenching tests with L-histidine (50 mM) for $^1O_2$ and catalase (200 U/mL) for H_2O_2 are summarized in Table A9 in the Appendix. The ratios of the k_{obs} with and without the quencher were used to analyze the data. The ratios between the $k_{obs\_L\text{-}histidine}$ and k_{obs} (without the quencher) in the presence of the three DOM isolates (i.e., BRHPO, SWRHPO, EfOMHPO) solutions did not experimentally differ from 1 for both rotavirus strains. This observation suggests that $^1O_2$ was not the main reactive species causing the inactivation of the two rotavirus strains in agreement with results

previously reported for porcine rotavirus in solutions containing SRNOM and 50 mM L-Histidine at 50°C (Romero et al., 2011). The ratios between the $k_{obs\_catalase}$ and k_{obs} values in solutions containing the same DOM isolates were < 1 for both rotavirus strains, implying that H_2O_2 caused significant rotavirus inactivation during the sample irradiation. However, H_2O_2 concentrations up to 60 µM did not significantly lead to human rotavirus inactivation (Table A10). Similarly, H_2O_2 was shown to not directly cause porcine rotavirus inactivation(Romero et al., 2011) on the time scale of these experiments. Instead, the presence of H_2O_2 likely points to the significance of H_2O_2 intermediacy and/or pathway in the formation of OH radical in solutions containing DOM isolates (S. E. Page, Arnold, & McNeill, 2011; S. Page & Sander, 2012). Quenching tests were not conducted for EfOMTPI because the k_{obs} values for both human and porcine rotaviruses were too small for a meaningful statistical comparison between k_{obs} values with and without quenchers.

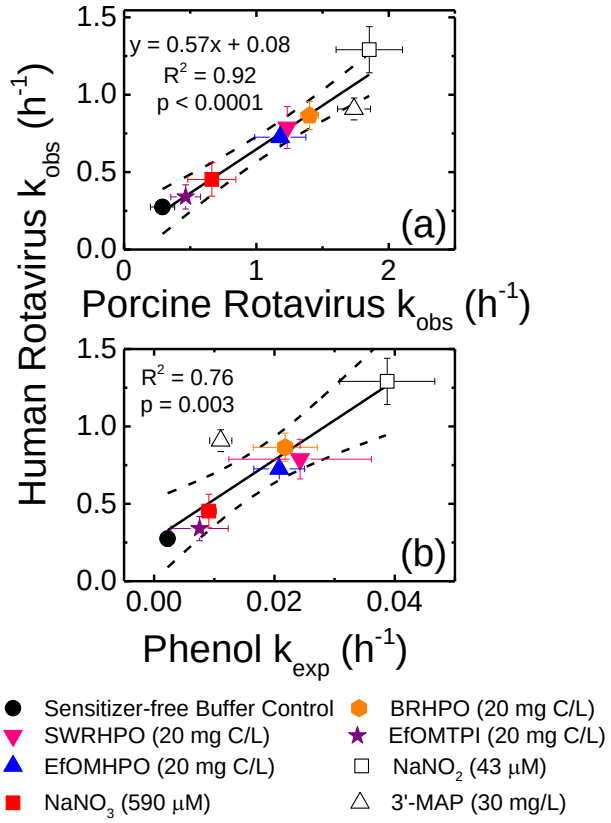

Figure 6. (a) Correlation between human rotavirus Wa and porcine rotavirus OSU inactivation rate constant values, k_{obs} (h^{-1}), and **(b)** human rotavirus k_{obs} values as a function of the phenol first-order decay rate constant, k_{exp} (h^{-1}). Unless otherwise indicated, all plots were corrected for light screening; all experiments were conducted in 1 mM $NaHCO_3$ buffer (pH 7.9) and at 25°C for human rotavirus and phenol; and conducted at 50°C for porcine rotavirus. Note that the rotavirus k_{obs} and phenol k_{exp} values from each experiment are provided in Tables A3-A7. For Figure 6a and 6b, the solid line indicates the linear regression line and the dashed lines indicate corresponding 95% confidence interval.

Other quenchers that are commonly used to assess the role of OH radicals or triplet state radicals include methanol (Georgi & Kopinke, 2005), azide (al Housari, Vione, Chiron, & Barbati, 2010), sodium formate (Kohn & Nelson, 2007), or sorbic acids (Grebel et al., 2011). Some of these quenchers are lethal to microorganisms (Burns et al., 2012). In this study, sorbate (quencher for triplet) and formate (quencher for OH radical) alone caused rotavirus inactivation (Romero et al., 2011). Because quenchers are used in excess concentrations (~mM) compared to the reactive species (fM) that upon irradiation, the quenchers' excited state species may cause

immediate inactivation of rotavirus. To avoid this quencher problem, the experiments with 3'-MAP were conducted to investigate the role of excited triple states. For OH radicals, experiments with nitrite, a dominant OH radical source, and DOM, a OH radical quencher, were conducted to assess the role of OH radical in rotavirus inactivation. See "contribution of excited triplet states" and "contribution of OH radical" sections below.

To further assess the role of other transient radicals on the exogenous inactivation of rotaviruses, the decay rate constants of phenol, k_{exp} (h^{-1}), were measured in solutions containing various photosensitizers and correlated ($R^2 = 0.76$, $p = 0.003$) with the corresponding human rotavirus k_{obs} values at 25°C (Figure 6b). Phenol is used as a OH radical probe (Gong et al., 2012; Kohn & Nelson, 2007). In solutions buffered with 1 mM $NaHCO_3$, carbonate radicals that are formed by scavenging OH radicals or through the triplet-excited state of DOM (Canonica et al., 2005) (only possible for DOM photosensitizers) may also contribute to the decay of phenol (Busset et al., 2007). The compound 3'-MAP has been used as a photosensitizer for excited triplet states (Canonica, Jans, Stemmler, & Hoigne, 1995), and in this study solutions with 30 mg/L of 3'-MAP showed low rates of phenol decay, although relatively high human rotavirus k_{obs} values (0.9 h^{-1}) were measured (Figure 6b). The implications of this finding are discussed next.

3.4.3.1 Contribution of excited triplet states

Measurements of the steady-state concentrations of excited triplet states are shown in Table A7 in the Appendix. The compound 3'-MAP is known to produce significant levels of excited triplet states (Canonica et al., 1995), and in this study the two highest concentrations of excited triplet states (1.8 and 4.9 fM) were measured in solutions containing 15 and 30 mg/L 3'-MAP, respectively. These 3'-MAP concentrations resulted in human rotavirus k_{obs} values of 0.5

and 0.9 h^{-1}, respectively. When correlated, 3'-MAP concentrations (mg/L) and human rotavirus k_{obs} values showed a positive non-linear trend even when human rotavirus k_{obs} values were not corrected for light screening ($R^2 = 0.98$, $p = 0.07$; Figure A8). This observation is consistent with the concentrations of excited triplet states produced by 3'-MAP that may cause human rotavirus inactivation. The measured concentrations of excited triplet states were the lowest for BRHPO and SWRHPO (20 mg C/L). However, the BRHPO and SWRHPO solutions resulted in higher human rotavirus k_{obs} values than in solutions containing 15 mg/L of 3'-MAP (0.9 and 0.8 h^{-1} vs. 0.5 h^{-1}). The phenol k_{exp} value observed in the 30 mg/L 3'-MAP solution was amongst the lowest measured for the set of photosensitizers, suggesting that compared to other reactive species produced by DOM isolates, triplet states of 3'-MAP caused lower decay of phenol. Thus given the positive correlation ($p < 0.05$) found between human rotavirus k_{obs} and phenol k_{exp} values for a variety of photosensitizers, other species besides excited triplet states causing phenol decay are likely also responsible for human rotavirus inactivation. The role of low concentrations of excited triplet states should not be ignored as these may synergistically contribute to the overall inactivation of human rotavirus, but these are likely not the major contributors to the observed inactivation of rotavirus.

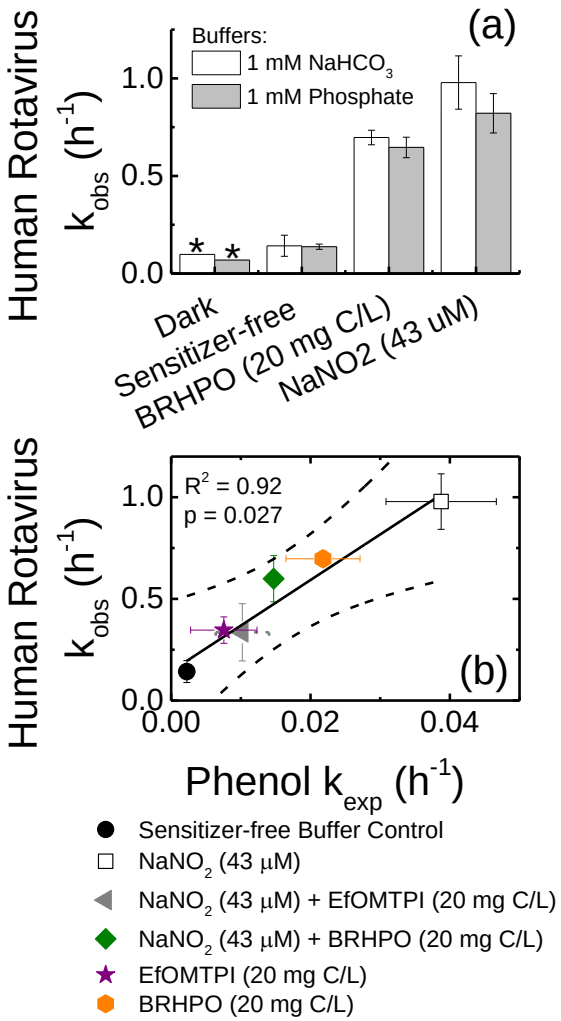

Figure 7. (a) Bar chart comparing the human rotavirus (Stock 2) k_{obs} values in 1 mM $NaHCO_3$ and 1 mM phosphate buffer at 25°C and pH 7.9 and **(b)** the correlation between human rotavirus (Stock 2) k_{obs} values as a function of phenol k_{exp} values obtained at 25°C in 1 mM $NaHCO_3$ buffer pH 7.9. For Figure 3a, the averages and standard deviations of the human rotavirus k_{obs} values ($N \geq 3$) were shown and the asterisks (*) denote that the linear regression plots for these conditions did not significantly deviate from a slope of 0 ($p > 0.05$). For Figure 7b, EfOMTPI (purple star) and BRHPO (orange hexagon) were not included in the linear regression and were included for comparison. The solid lines indicate the linear regression line and the dashed lines indicate the corresponding 95% confidence intervals. For Figure 7b, the other error bars are the standard deviations of at least two independent experiments.

3.4.3.2 Contribution of carbonate radical formed by bicarbonate buffer

To determine whether 1 mM bicarbonate buffer may contribute to human rotavirus inactivation, experiments were conducted in 1 mM $NaHCO_3$ and bicarbonate-free (1 mM phosphate buffer) buffers at pH 7.9. The mean and standard deviations ($N \geq 3$) for the sensitizer-free buffer control, BRHPO (20 mg C/L), and $NaNO_2$ (43 µM) in 1 mM $NaHCO_3$ and 1 mM phosphate buffers are shown in Figure 7a. The results of the t-test that compared the k_{obs} sets ($N \geq 3$) in each buffer for the same condition showed that the k_{obs} sets were not statistically different from each other ($p > 0.16$). In addition, the human rotavirus k_{obs} values and the phenol k_{exp} values in 1 mM phosphate buffer (absence of bicarbonates/carbonates) were also correlated ($R^2 = 0.87$, $p = 0.046$, Figure A9 in the Appendix). The absence of bicarbonate did not change the positive trend between human rotavirus k_{obs} and phenol k_{exp} values (Figure A9): higher phenol k_{exp} values (observed for BRHPO and $NaNO_2$) corresponded to higher human rotavirus k_{obs} values and lower phenol k_{exp} values (observed for EfOMTPI and the buffer control) corresponded to lower k_{obs} values. Thus, the role of the carbonate radical in the 1 mM $NaHCO_3$ solutions was not significant for the inactivation of human rotavirus.

3.4.3.3 Contribution of OH radical

To further understand the role of OH radicals produced through the photolysis of $NaNO_2$, an inorganic photosensitizer for OH radical formation (Mack & Bolton, 1999), phenol decay experiments and human rotavirus inactivation experiments were conducted in mixed solutions that contained $NaNO_2$ with BRHPO or EfOMTPI in 1 mM $NaHCO_3$ buffer (Figure 7b). OH radicals are efficiently consumed by DOM, which limits its steady-state concentration in waters illuminated by sunlight (al Housari et al., 2010). In solutions containing 1 mM $NaHCO_3$, $NaNO_2$ (43 µM), and BRHPO or EfOMTPI (20 mg C/L), the DOM scavenging effect of OH radicals was evident. Higher human rotavirus k_{obs} and phenol k_{exp} values were observed for $NaNO_2$ in

buffer alone than in solutions containing both $NaNO_2$ and DOM. In the presence of $NaNO_2$ and DOM, the human rotavirus k_{obs} values were similar to the k_{obs} values obtained in solutions containing the DOM (Figure 7b). It is likely that the high concentrations of DOM (20 mg/L) consumed the OH radicals arising from the photolysis of NO_2^- that would otherwise react with the virus.

In addition to nitrite, nitrate was investigated because it is also a known as an inorganic photosensitizer for OH radicals (Zepp, Hoigne, & Bader, 1987) and common in natural waters (Eddy & Williams, 1987). Whereas irradiation of $NaNO_3$ (590 µM) resulted in low k_{obs} of both rotavirus strains, irradiation of $NaNO_2$ (43 µM) resulted in high k_{obs} values (for human rotavirus: 0.5 ± 0.1 vs. 1.3 ± 0.2 h^{-1}; for porcine rotavirus: 0.7 ± 0.2 vs. 1.9 ± 0.3 h^{-1}). The lower rotavirus k_{obs} values observed in $NaNO_3$ solutions may arise from the reduced irradiance of our solar simulator for wavelengths < 320 nm (see spectra comparison, Fig. 5a). The absorbance peaks for NO_3^- and NO_2^- are at 302 and 352 nm, respectively (Mack & Bolton, 1999). Forty three µM of NO_2^- in 1 mM $NaHCO_3$ buffer is capable of causing significant rotavirus inactivation in solutions lacking DOM. NO_2^- is characterized by a higher UV absorbance and quantum yield for OH radical production than NO_3^- (Shankar, Nélieu, Kerhoas, & Einhorn, 2008). Although NO_2^- is not commonly found in natural waters, NO_2^- concentrations up to 66 µM have been measured in some river waters due to incomplete nitrification and denitrification cycles (Eddy & Williams, 1987). As suggested by our data and supported by others (Zepp et al., 1987), in natural waters, OH radical production through NO_2^- and NO_3^- photolysis is likely to be dominant in shallow, clear water bodies containing high ratios of NO_3^- / NO_2^- to DOM concentrations (Zepp et al., 1987). Because DOM attenuates UV light and it efficiently scavenges OH radicals, in natural waters with relatively high DOM and NO_3^- / NO_2^- concentrations, DOM is likely the prime

species determining the steady-state concentrations of OH radicals (Zepp et al., 1987) and rotavirus inactivation.

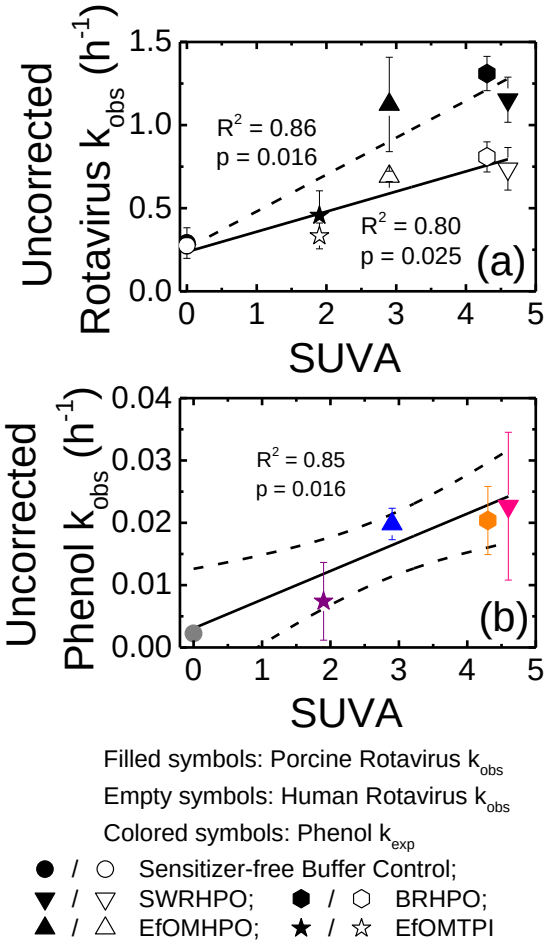

Figure 8. **(a)** Rotavirus kobs values and **(b)** phenol kexp values not corrected for light screening as a function of the specific UV254nm absorbance (SUVA; L·mg-1C·cm-1) of solutions containing DOM isolates and the buffer control in 1 mM NaHCO3 buffer (pH 7.9). For Figure 8a, the solid lines denote the linear regression line for the porcine and human rotavirus kobs values as a function of the SUVA values for five different solutions. For Figure 8b, the solid lines indicate the linear regression line and the dashed lines denote the 95% confidence intervals of the regression.

3.4.4 Role of the characteristics of DOM isolates on the exogenous inactivation of rotavirus

Specific UV absorbance (SUVA; $L \cdot mg^{-1}C \cdot cm^{-1}$) is defined as the UV absorbance of a water sample at 254 nm normalized for dissolved organic carbon (DOC) concentration (mg C/L). SUVA is a predictor of general chemical characteristics of DOC and is most commonly used for estimating the dissolved aromatic carbon content in water systems (Weishaar et al., 2003). As shown in Figure 4a, a significant correlation ($p < 0.05$) was observed between the uncorrected k_{obs} and SUVA values. Additionally, a statistically significant correlation ($p < 0.05$) between uncorrected phenol k_{exp} values and the SUVA values of solutions containing DOM isolates were observed (Figure 8b). Uncorrected values of k_{obs} were used for these correlations with SUVA to avoid the DOM confounding effect, as the correction factors applied to DOM-containing solutions are associated with the absorbance of the solutions. However, linear correlations using corrected values of k_{obs} and k_{exp} were also obtained for human and porcine rotavirus, and phenol decay (Figure A10 in the Appendix). The relationships between SUVA and oxidation reaction rate parameters for molecular ozone and OH radicals have been investigated previously (Westerhoff, Aiken, Amy, & Debroux, 1999). Positive correlations between SUVA and MS2 k_{obs} were also recently reported (Rosado-Lausell et al., 2013a). In this study, the correlations between SUVA and rotavirus k_{obs} and phenol k_{exp} values suggested that the aromaticity of solutions containing DOM isolates may influence their capacity to produce radicals during solar irradiation. Moreover, the hydrophilic fraction of DOM, EfOMTPI, had much lower reactivity compared to all three other hydrophobic fractions of DOM, including effluent wastewater (EfOMHPO) and river water DOM (SWRHPO and BRHPO). Because the hydrophobic fraction of DOM has higher aromaticity as reflected in the higher SUVA values, higher rotavirus k_{obs} values should correspond to samples with high aromaticity. The positive linear correlation

between rotavirus k_{obs} values and SUVA, shown in Figure 4, will be tested in future work with unpurified natural water samples.

3.5 Environmental relevance

This study showed that two strains of rotavirus had different resistance levels to sunlight-induced exogenous inactivation. Although both were inactivated by the exogenous mechanism, the inactivation kinetics for porcine rotavirus OSU were orders of magnitude slower than for human rotavirus Wa at 25°C. This observation is noteworthy because most inactivation studies are conducted with a single strain of a pathogenic group, and the results or trends in inactivation may not be representative of the other strains within the same genus. In nature, virus populations are genetically diverse (Tra My et al., 2011), and it is uncertain whether results obtained with a standard virus strain will apply to virus populations in natural environments globally. Rotavirus strains of different hosts have been shown to reassort, and the genetic diversity and evolution of rotavirus group A has been recently reviewed by Matthijssens and van Ranst (2012) (Matthijnssens & Van Ranst, 2012). To date, genome sequencing studies have shown evidence for reassortment of bovine and human rotaviruses (Afrad et al., 2013; Matsushima et al., 2012), and porcine and human rotavirus (Kim et al., 2012). Future studies could consider the varying responses of different pathogenic strains, possibly isolated from environmental samples, to disinfectants before recommending a treatment dose.

Excited triplet states have been shown to degrade antibiotics commonly found in the environment (Boreen, Arnold, & McNeill, 2005), but to date, little is known about the their contribution to pathogen inactivation. High concentrations of excited triplet states can lead to human rotavirus inactivation, and low concentrations may synergistically assist in the

exogenous-induced inactivation of rotavirus. However, excited triplet states are likely not the primary species causing rotavirus inactivation. OH radicals are the most reactive of the ROS and have been previously implicated with the inactivation of *Escherichia coli* (Cho, Chung, Choi, & Yoon, 2004) and MS2 (Nieto-Juarez, Pierzchła, Sienkiewicz, & Kohn, 2010). To our knowledge, this is the first study to provide evidence that the OH radical levels produced by UVA and visible light irradiation of natural DOM solutions can cause significant inactivation of human rotavirus. Advanced photo-oxidation and sunlight-mediated photo-oxidation with the capability of producing high OH concentrations may be capable of efficiently inactivating infectious pathogens such as rotaviruses.

3.6 Acknowledgement

We acknowledge the financial support of the Academic Excellence Alliance (AEA) program at King Abdullah University of Science and Technology (KAUST), NSF CAREER grant to T.H.N. (0954501), and NSF GRF DGE 07-15088 FLW to O.C.R. We thank Leonardo Gutierrez for helping with experiments, Dr. Joanna Shisler and Peter A. Maraccini for insightful discussion.

3.7 Literature cited

Afrad, M. H., Matthijnssens, J., Moni, S., Kabir, F., Ashrafi, A., Rahman, M. Z., … Rahman, M. (2013). Genetic characterization of a rare bovine-like human VP4 mono-reassortant G6P[8] rotavirus strain detected from an infant in Bangladesh. *Infect. Genet. Evol.*, *19*, 120–126. doi:10.1016/j.meegid.2013.06.030

Al Housari, F., Vione, D., Chiron, S., & Barbati, S. (2010). Reactive photoinduced species in estuarine waters. Characterization of hydroxyl radical, singlet oxygen and dissolved organic

matter triplet state in natural oxidation processes. *Photochem. Photobiol. Sci.*, *9*(1), 78–86. doi:10.1039/b9pp00030e

Arts, M. T., Robarts, R. D., Kasai, F., Waiser, M. J., Tumber, V. P., Plante, A. J., … de Lange, H. J. (2000). The attenuation of ultraviolet radiation in high dissolved organic carbon waters of wetlands and lakes on the northern Great Plains. *Limnol. Oceanogr.*, *45*(2), 292–299. doi:10.4319/lo.2000.45.2.0292

Benjamin, M. M., Croue, J. P., & Reiber, S. (1999). *Isolation, fractionation and characterization of natural organic matter in drinking water* (p. 324).

Boehm, A. B., Yamahara, K. M., Love, D. C., Peterson, B. M., McNeill, K., & Nelson, K. L. (2009). Covariation and photoinactivation of traditional and novel indicator organisms and human viruses at a sewage-impacted marine beach. *Environ. Sci. Technol.*, *43*(21), 8046–8052. doi:10.1021/es9015124

Boreen, A. L., Arnold, W. a, & McNeill, K. (2005). Triplet-sensitized photodegradation of sulfa drugs containing six-membered heterocyclic groups: identification of an SO2 extrusion photoproduct. *Environ. Sci. Technol.*, *39*(10), 3630–8. Retrieved from http://www.ncbi.nlm.nih.gov/pubmed/15952367

Burns, J. M., Cooper, W. J., Ferry, J. L., King, D. W., DiMento, B. P., McNeill, K., … Waite, T. D. (2012). Methods for reactive oxygen species (ROS) detection in aqueous environments. *Aquatic Sciences*, *74*(4), 683–734. doi:10.1007/s00027-012-0251-x

Busset, C., Mazellier, P., Sarakha, M., & De Laat, J. (2007). Photochemical generation of carbonate radicals and their reactivity with phenol. *J. Photochem. Photobiol., A*, *185*(2-3), 127–132. doi:10.1016/j.jphotochem.2006.04.045

C. J. Hwang, Krasner, S. W., Amy, G. L., Bruchet, A., Croue, J.-P., & Leenheer., J. L. (2001). *Polar NOM: Characterization, DBPs, Treatment*.

Canonica, S., Jans, U., Stemmler, K., & Hoigne, J. (1995). Transformation kinetics of phenols in water: Photosensitization by dissolved natural organic material and aromatic ketones. *Environ. Sci. Technol.*, *29*(7), 1822–1831. Retrieved from http://pubs.acs.org/doi/abs/10.1021/es00007a020

Canonica, S., Kohn, T., Mac, M., Real, F. J., Wirz, J., & von Gunten, U. (2005). Photosensitizer method to determine rate constants for the reaction of carbonate radical with organic compounds. *Environ. Sci. Technol.*, *39*(23), 9182–9188. Retrieved from http://www.ncbi.nlm.nih.gov/pubmed/16382940

Cho, M., Chung, H., Choi, W., & Yoon, J. (2004). Linear correlation between inactivation of E. coli and OH radical concentration in TiO2 photocatalytic disinfection. *Water Res.*, *38*(4), 1069–1077. doi:10.1016/j.watres.2003.10.029

Croué, J.-P. (2004). Isolation of humic and non-humic NOM fractions: structural characterization. *Environ. Monit. Assess.*, *92*(1-3), 193–207. Retrieved from http://www.ncbi.nlm.nih.gov/pubmed/15038544

Davies, C. M., Roser, D. J., Feitz, a J., & Ashbolt, N. J. (2009). Solar radiation disinfection of drinking water at temperate latitudes: inactivation rates for an optimised reactor configuration. *Water Res.*, *43*(3), 643–652. doi:10.1016/j.watres.2008.11.016

Davies-Colley, R. ., Donnison, A. ., Speed, D. ., Ross, C. ., & Nagels, J. . (1999). Inactivation of faecal indicator micro-organisms in waste stabilisation ponds: interactions of environmental factors with sunlight. *Water Res.*, *33*(5), 1220–1230. doi:10.1016/S0043-1354(98)00321-2

Desselberger, U. (2000). Rotaviruses: basic facts. In *Rotaviruses: Methods and Protocols* (Vol. 34, pp. 1–8). doi:10.1385/1-59259-078-0:1

Eddy, F., & Williams, E. (1987). Nitrite and freshwater fish. *Chem. Ecol.*, *3*(1), 1–38. Retrieved from http://www.tandfonline.com/doi/full/10.1080/02757548708070832

Floyd, R., Sharp, D., & Johnson, J. (1979). Inactivation by chlorine of single poliovirus particles in water. *Environ. Sci. Technol.*, *13*(4), 438–442. Retrieved from http://pubs.acs.org/doi/abs/10.1021/es60152a005

Georgi, A., & Kopinke, F.-D. (2005). Interaction of adsorption and catalytic reactions in water decontamination processes: Part I. Oxidation of organic contaminants with hydrogen peroxide catalyzed by activated carbon. *Appl. Catal. B-Environ.*, *58*(1-2), 9–18. Retrieved from http://dx.doi.org/10.1016/j.apcatb.2004.11.014.

Gerba, C. P., Rose, J. B., Haas, C. N., & Crabtree, K. D. (1996). Waterborne rotavirus: A risk assessment. *Water Res.*, *30*(12), 2929–2940. doi:10.1016/S0043-1354(96)00187-X

Gong, A. S., Lanzl, C. a, Cwiertny, D. M., & Walker, S. L. (2012). Lack of influence of extracellular polymeric substances (EPS) level on hydroxyl radical mediated disinfection of Escherichia coli. *Environ. Sci. Technol.*, *46*(1), 241–249. doi:10.1021/es202541r

Grebel, J. E., Pignatello, J. J., & Mitch, W. a. (2011). Sorbic acid as a quantitative probe for the formation, scavenging and steady-state concentrations of the triplet-excited state of organic compounds. *Water Res.*, *45*(19), 6535–6544. doi:10.1016/j.watres.2011.09.048

Griffin, D., & Donaldson, K. (2003). Pathogenic human viruses in coastal waters. *Clin. Microbiol. Rev.*, *16*(1), 129–143. doi:10.1128/CMR.16.1.129

He, X. Q., Cheng, L., Zhang, D. Y., Li, W., Xie, X. M., Ma, M., & Wang, Z. J. (2009). First molecular detection of group A rotaviruses in drinking water sources in Beijing, China. *Bull. Environ. Contam. Toxicol.*, *83*(1), 120–4. doi:10.1007/s00128-009-9708-6

Huang, J., & Mabury, S. (2000). Steady-state concentrations of carbonate radicals in field waters. *Environ. Toxicol. Chem.*, *19*(9), 2181–2188. Retrieved from http://onlinelibrary.wiley.com/doi/10.1002/etc.5620190906/full

Imanaka, T., Shibazaki, M., & Takagi, M. (1986). A new way of enhancing the thermostability of proteases. *Nature*, *324*(December), 695–697.

Joshi, P. C., & Keane, T. C. (2010). Investigation of riboflavin sensitized degradation of purine and pyrimidine derivatives of DNA and RNA under UVA and UVB. *Biochem Bioph Res Co*, *400*(4), 729–733. Retrieved from http://www.sciencedirect.com/science/article/pii/S0006291X10016591

Kim, H.-H., Matthijnssens, J., Kim, H.-J., Kwon, H.-J., Park, J.-G., Son, K.-Y., … Cho, K.-O. (2012). Full-length genomic analysis of porcine G9P[23] and G9P[7] rotavirus strains isolated from pigs with diarrhea in South Korea. *Infect. Genet. Evol.*, *12*(7), 1427–1435. doi:10.1016/j.meegid.2012.04.028

Kohn, T., & Nelson, K. L. (2007). Sunlight-mediated inactivation of MS2 coliphage via exogenous singlet oxygen produced by sensitizers in natural waters. *Environ. Sci. Technol.*, *41*(1), 192–197. Retrieved from http://www.ncbi.nlm.nih.gov/pubmed/17265947

Kristjánsson, M. M., & Kinsella, J. E. (1991). Protein and enzyme stability: structural, thermodynamic, and experimental aspects. *Adv. Food Nutr. Res.*, *35*, 237–316. Retrieved from http://www.ncbi.nlm.nih.gov/pubmed/1930884

Li, D., Gu, a Z., Zeng, S.-Y., Yang, W., He, M., & Shi, H.-C. (2011). Monitoring and evaluation of infectious rotaviruses in various wastewater effluents and receiving waters revealed correlation and seasonal pattern of occurrences. *J. Appl. Microbiol.*, *110*(5), 1129–37. doi:10.1111/j.1365-2672.2011.04954.x

Li, D., Gu, A. Z., He, M., Shi, H.-C., & Yang, W. (2009). UV inactivation and resistance of rotavirus evaluated by integrated cell culture and real-time RT-PCR assay. *Water Research*, *43*(13), 3261–9. doi:10.1016/j.watres.2009.03.044

Lopez, S., & Arias, C. F. (2006). Early steps in rotavirus cell entry. In P. Roy (Ed.), *Reoviruses: Entry, Assembly and Morphogenesis* (1st ed., pp. 39–66). Berlin, Germanay: Springer-Verlag Berlin Heidelberg. doi:10.1007/3-540-30773-7_2

Love, D. C., Silverman, A., & Nelson, K. L. (2010). Human virus and bacteriophage inactivation in clear water by simulated sunlight compared to bacteriophage inactivation at a southern California beach. *Environ. Sci. Technol.*, *44*(18), 6965–6970. doi:10.1021/es1001924

Mack, J., & Bolton, J. (1999). Photochemistry of nitrite and nitrate in aqueous solution: a review. *J. Photochem. Photobiol., A*, *128*(1-3), 1–13. Retrieved from http://www.sciencedirect.com/science/article/pii/S1010603099001550

Marshall, G. S. (2009). Rotavirus disease and prevention through vaccination. *Pediatr. Infect. Dis. J.*, *28*(4), 351–362. doi:10.1097/INF.0b013e318199494a

Matsushima, Y., Nakajima, E., Nguyen, T. A., Shimizu, H., Kano, A., Ishimaru, Y., … Ushijima, H. (2012). Genome Sequence of an Unusual Human G10P[8] Rotavirus Detected in Vietnam. *J. Virol.*, *86*(18), 10236–7. doi:10.1128/JVI.01588-12

Matthews, B. W., Nicholson, H., & Becktel, W. J. (1987). Enhanced protein thermostability from site-directed mutations that decrease the entropy of unfolding. *PNAS*, *84*(19), 6663–6667. Retrieved from http://www.pubmedcentral.nih.gov/articlerender.fcgi?artid=299143&tool=pmcentrez&rendertype=abstract

Matthijnssens, J., & Van Ranst, M. (2012). Genotype constellation and evolution of group A rotaviruses infecting humans. *Curr. Opin. Virol.*, *2*(4), 426–433. doi:10.1016/j.coviro.2012.04.007

Nieto-Juarez, J. I., Pierzchła, K., Sienkiewicz, A., & Kohn, T. (2010). Inactivation of MS2 coliphage in Fenton and Fenton-like systems: role of transition metals, hydrogen peroxide and sunlight. *Environ. Sci. Technol.*, *44*(9), 3351–3356. doi:10.1021/es903739f

Page, S. E., Arnold, W. a, & McNeill, K. (2011). Assessing the contribution of free hydroxyl radical in organic matter-sensitized photohydroxylation reactions. *Environ. Sci. Technol.*, *45*(7), 2818–2825. doi:10.1021/es2000694

Page, S., & Sander, M. (2012). Hydroxyl radical formation upon oxidation of reduced humic acids by oxygen in the dark. *Environ. Sci. Technol.*, *46*(3), 1590–1597. Retrieved from http://pubs.acs.org/doi/abs/10.1021/es203836f

Romero, O. C., Straub, A. P., Kohn, T., & Nguyen, T. H. (2011). Role of temperature and Suwannee River natural organic matter on inactivation kinetics of rotavirus and bacteriophage MS2 by solar irradiation. *Environmental Science & Technology*, *45*(24), 10385–10393. doi:10.1021/es202067f

Rosado-Lausell, S. L., Wang, H., Gutiérrez, L., Romero-Maraccini, O. C., Niu, X.-Z., Gin, K. Y. H., … Nguyen, T. H. (2013a). Roles of singlet oxygen and triplet excited state of dissolved organic matter formed by different organic matters in bacteriophage MS2 inactivation. *Water Research*, *47*, 1–11. doi:10.1016/j.watres.2013.05.018

Rosado-Lausell, S. L., Wang, H., Gutiérrez, L., Romero-Maraccini, O. C., Niu, X.-Z., Gin, K. Y. H., … Nguyen, T. H. (2013b). Roles of singlet oxygen and triplet excited state of dissolved organic matter formed by different organic matters in bacteriophage MS2 inactivation. *Water Research*, *47*(14), 4869–4879. doi:10.1016/j.watres.2013.05.018

Sanchez-Padilla, E., Grais, R. F., Guerin, P. J., Steele, A. D., Burny, M.-E., & Luquero, F. J. (2009). Burden of disease and circulating serotypes of rotavirus infection in sub-Saharan Africa: systematic review and meta-analysis. *Lancet Infect. Dis.*, *9*(9), 567–76. doi:10.1016/S1473-3099(09)70179-3

Schwarzenbach, R. P.; Gschwend, P. M.; Imboden, D. M. (2002). Chapter 15: Direct Photolysis. In *Environmental Organic Chemistry* (2nd ed., pp. 611–640). New York, NY: John Wiley & Sons.

Shankar, M. V, Nélieu, S., Kerhoas, L., & Einhorn, J. (2008). Natural sunlight NO(3)(-)/NO(2)(-)-induced photo-degradation of phenylurea herbicides in water. *Chemosphere*, *71*(8), 1461–1468. doi:10.1016/j.chemosphere.2007.12.003

Sharp, D., & Leong, J. (1980). Inactivation of poliovirus I (Brunhilde) single particles by chlorine in water. *Appl. Environ. Microbiol.*, *40*(2), 381–385. Retrieved from http://aem.asm.org/content/40/2/381.short

Silverman, A. I., Peterson, B. M., Boehm, A. B., McNeill, K., & Nelson, K. L. (2013). Sunlight inactivation of human viruses and bacteriophages in coastal waters containing natural photosensitizers. *Environ. Sci. Technol.*, *47*(4), 1870–1878. doi:10.1021/es3036913

Strakhovskaya, M. G., Shumarina, A. O., Fraikin, G. Y., & Rubin, A. B. (1999). Endogenous porphyrin accumulation and photosensitization in the yeast Saccharomyces cerevisiae in the presence of 2,2′-dipyridyl. *J. Photochem. Photobiol., B*, *49*(1), 18–22. Retrieved from http://www.sciencedirect.com/science/article/pii/S1011134498002152

Tra My, P. V., Rabaa, M. a, Vinh, H., Holmes, E. C., Hoang, N. V. M., Vinh, N. T., … Baker, S. (2011). The emergence of rotavirus G12 and the prevalence of enteric viruses in hospitalized pediatric diarrheal patients in southern Vietnam. *Am. J. Trop. Med. Hyg.*, *85*(4), 768–775. doi:10.4269/ajtmh.2011.11-0364

Van Zyl, W. B., Page, N. a, Grabow, W. O. K., Steele, a D., & Taylor, M. B. (2006). Molecular epidemiology of group A rotaviruses in water sources and selected raw vegetables in southern Africa. *Appl. Environ. Microbiol.*, *72*(7), 4554–60. doi:10.1128/AEM.02119-05

Viau, E. J., Goodwin, K. D., Yamahara, K. M., Layton, B. A., Sassoubre, L. M., Burns, S. L., … Boehm, A. B. (2011). Bacterial pathogens in Hawaiian coastal streams—Associations with fecal indicators, land cover, and water quality. *Water Res.*, *45*(11), 3279–3290. Retrieved from http://www.sciencedirect.com/science/article/pii/S0043135411001448

Weishaar, J. L., Aiken, G. R., Bergamaschi, B. a, Fram, M. S., Fujii, R., & Mopper, K. (2003). Evaluation of specific ultraviolet absorbance as an indicator of the chemical composition and reactivity of dissolved organic carbon. *Environ. Sci. Technol.*, *37*(20), 4702–4708. Retrieved from http://www.ncbi.nlm.nih.gov/pubmed/14594381

Westerhoff, P., Aiken, G., Amy, G., & Debroux, J. (1999). Relationships between the structure of natural organic matter and its reactivity towards molecular ozone and hydroxyl radicals. *Water Research*, *33*(10), 2265–2276. doi:10.1016/S0043-1354(98)00447-3

Wigginton, K. R., & Kohn, T. (2012). Virus disinfection mechanisms: the role of virus composition, structure, and function. *Curr. Opin. Virol.*, *2*(1), 84–89. doi:10.1016/j.coviro.2011.11.003

Zepp, R., Hoigne, J., & Bader, H. (1987). Nitrate-induced photooxidation of trace organic chemicals in water. *Environ. Sci. Technol., 21*(5), 443–450. Retrieved from http://pubs.acs.org/doi/abs/10.1021/es00159a004

Zheng, X., & Croue, J. P. (2012). Contribution of different effluent organic matter fractions to membrane fouling in ultrafiltration of treated domestic wastewater. *J. Water Reuse Desalin.*, *2*(4), 204–209.

CHAPTER 4

ASPECTS OF HUMAN ROTAVIRUS INACTIVATION MECHANISMS AS EXAMINED BY QUANTITATIVE PCR: THE ROLES OF SOLAR AND THERMAL TREATMENTS[3]

4.1 Abstract

Rotavirus is the leading cause of diarrheal diseases in children under the age of five. Infectious rotavirus particles often are resistant to disinfection by conventional wastewater treatment. Moreover, these virions can persist in water. Solar and heat treatments inactivate rotavirus, but it is unknown how these treatments inactivate the virus on a molecular level. The goal of this study was to identify positive correlations between disinfection of virus and inhibition of portions of the rotavirus lifecycle to identify the mechanisms of solar or heat inactivation of virus. Several portions of the virus life cycle were examined after heat or solar treatment of rotavirus: virus-host cell interactions; integrity of the rotavirus NSP3 gene; viral RNA synthesis. We observed that only rotavirus RNA synthesis decreased at the same rate as rotavirus infectivity when virions were subjected to heat disinfection, suggesting that heat treatment disinfected rotaviruses primarily by targeting viral transcription functions. When using solar disinfection, the decrease of rotavirus infectivity and RNA synthesis were linearly correlated, but the rotavirus RNA synthesis rates did not decrease at the same rates as rotavirus infectivity. We conclude that both solar and heat inactivation of viruses was attributed to a defect in viral RNA synthesis.

[3] Romero-Maraccini, O. C.; Shisler, L.J.; Nguyen, T. H. Aspects of human rotavirus inactivation mechanisms as examined by quantitative PCR: the roles of solar irradiation and temperature. *Manuscript submitted.*

4.2 Introduction

Rotavirus is the leading cause of diarrhea hospitalizations for children under five years of age, and is responsible for the deaths of an estimated 453,000 children each year (Parashar et al., 2013). Rotavirus is transmitted via several routes including, the fecal–oral route or by ingestion of contaminated water and food (Gerba, Rose, Haas, & Crabtree, 1996; Marshall, 2009). A previous study found that rotaviruses in domestic sewage can remain infectious after undergoing typical wastewater treatment, and wastewater discharges contaminated with rotaviruses were shown to spread and contaminate receiving waters, including rivers (D Li et al., 2011). Thus, the successful disinfection of rotaviruses has the potential to reduce or prevent rotavirus-induced morbidity and mortality.

Rotavirus can be inactivated effectively by solar disinfection (Romero, Straub, Kohn, & Nguyen, 2011; Romero-Maraccini et al., 2013), and disinfection is attributed to both solar UV/visible light irradiation and to the increase in water temperature (Wegelin, M.; Canonica, S.; Mechsner, K.; Fleischmann, F.P.; Metzler, 1994). High energy solar UVB with wavelengths from 280 nm to 320 nm can quickly inactivate both porcine and human rotavirus at 14-42ºC (Romero et al., 2011; Romero-Maraccini et al., 2013). While it is expected that solar UVB directly damage the rotavirus genome, it is not known what step in the life cycle of rotavirus is disrupted by solar UVB irradiation. When natural organic matter (NOM) solution was exposed to solar UVA and visible light, NOM acted as sensitizer to form reactive oxygen species, including singlet oxygen and hydroxyl radicals. Previous studies showed that if this solution also contained rotavirus, hydroxyl radicals caused human rotavirus inactivation at 25ºC and porcine rotavirus inactivation at 55ºC (Romero et al., 2011; Romero-Maraccini et al., 2013). The difference in stability of porcine rotavirus and human rotavirus also showed in light-free

experiments (5). At 57 °C in the dark, human rotavirus was completely inactivated within minutes, while porcine rotavirus is stable at temperature up to 40 ºC (Romero-Maraccini et al., 2013). To date, no publications identify how solar or heat inactivation affects rotavirus on a molecular level. We argue that the identification of these molecular mechanisms will be the basis for the rational design for new or improvement of current technologies to detect and control rotaviruses in water. Here, we evaluated how solar or heat incubation affected individual steps of the well-characterized rotavirus lifecycle. Quantitative reverse transcription PCR (qRT-PCR) was used to assess the rates at which untreated versus heat- or solar-treated rotavirus either associated with their host cell, or induced viral RNA synthesis in host cells. We also investigated the integrity of the NSP3 viral gene before and after solar and heat treatments. Results from each biological assay were compared to the rate at which human rotavirus infectivity was lost upon solar and heat treatments, as measured by a classical focus forming unit assay. A schematic summarizing the approaches taken to investigate the molecular mechanism of human rotavirus inactivation upon solar or heat treatments is shown in Figure A11 found in the Appendix.

4.3 Methods and materials

4.3.1 Human rotavirus propagation, purification, and cell lines

Detailed protocols for human rotavirus Wa propagation and purification have been described elsewhere (Romero-Maraccini et al., 2013). Briefly, human rotavirus Wa [American Type Culture Collection (ATCC) #VR-2018] was treated with trypsin (10 µg/ml, 30 min at 37 °C, Sigma) and incubated with monkey kidney cellular monolayers (MA104; ATCC #CRL-2378.1). Once cytopathic effects were observed, infected cells and supernatant were collected and subjected to freeze/thaw cycles thrice. Next, samples were centrifuged at 1000 x g for 10 minutes at 20°C and rotavirus-containing supernatants were collected and filtered through a

filtration membrane (Thermo Scientific, Nalgene) of 0.45 μm pore size. The filtrate was concentrated using an ultrafiltration membrane (polymer polyvinylidene fluoride; Koch Membrane) of a 100 kDa pore-size. Samples were enumerated using a focus forming unit assay and quantified as focus forming units (FFUs)/mL (Romero et al., 2011). The final rotavirus stock concentration was 10^6 FFU/mL.

4.3.2 Disinfection treatment of rotaviruses

Inactivation experiments were conducted with 9×10^4 FFU/mL virus stock in 50 μl of virus solution containing 1 mM $NaHCO_3$ buffer. For each disinfection experiment, two 50 μl samples of virus were used for each treatment and/or time point (Figure 1). At least 3-4 treatment time points were collected per experiment, and all experiments were performed in duplicate. Each independent experiment included duplicate untreated rotavirus samples and MEM lacking rotaviruses as positive and negative controls, respectively.

4.3.2.1 Solar treatment

A solar simulator (Atlas Suntest XLS+ photosimulator; Chicago, IL) was used for all solar disinfection experiments. The solar simulator was equipped with a coated quartz filter with special window glass (Atlas, MTS) that was permanently installed to reduce the irradiance of wavelengths below 320 nm. The solar simulator setting used for experiments was 400 $W \cdot m^{-2}$. Additional filters that block the irradiance of wavelengths below 280 nm (FSQ-WG280; Newport Corp., Franklin, MA) or 320 nm (FSQ-WG320) were used to distinguish between full spectrum or UVA and visible light irradiation, respectively [spectra shown in reference (Romero-Maraccini et al., 2013)]. Full spectrum irradiation tests were performed to primarily investigate the direct and endogenous mechanisms, whereas UVA and visible light irradiation tests were conducted to assess the exogenous effects. The filters with the 280 or 320 nm

wavelength cut-off were placed over the wells of a 96-well plate containing the 50 µl samples. The 96-well plate containing the samples was incubated in a water bath set to 20 °C for the duration of the experiment. Sample evaporation over the course of the experiments was < 5%.

Four different conditions were used for solar treatments of rotaviruses: full spectrum irradiation of solutions containing 20 mg C/L of the organic sensitizer (full spectrum + sensitizer), full spectrum irradiation of a sensitizer-free buffer solution (full spectrum), UVA and visible light irradiation of solutions containing 20 mg C/L of the organic sensitizer (UVA+vis + sensitizer), and UVA and visible light irradiation of a sensitizer-free buffer solution (UVA+vis). The model organic sensitizer used in this study was the Suwannee River natural organic matter that is commercially available from the International Humic Substances Society. The organic sensitizer was dissolved in 1 mM $NaHCO_3$ buffer and stirred overnight in the dark, followed by filtration through a 0.22 µm pore-size membrane (cellulose acetate, VWR) prior to storing at 4°C in the dark. Total organic carbon (mg C/L) was measured using a TOC-V analyzer (Shimadzu), and a concentration of 20 mg C/L was used for the experiments containing the organic sensitizer.

4.3.2.2 Heat treatment

For all treatments, inactivation experiments were conducted with 9×10^4 FFU/mL virus stock in 50 µl of virus solution containing 1 mM $NaHCO_3$ buffer. Virus aliquots were placed in a 200-µL plastic tube and incubated in a 57 °C water bath for treatment times as indicated.

4.3.3 Infectivity assays

The infectivity assay was performed as described previously (Romero et al., 2011; Romero-Maraccini et al., 2013). Briefly, after each disinfection treatment, each virus sample was incubated with 10 µg/ml trypsin from porcine pancreas (Sigma-Aldrich) for 30 min at 37 °C. Next, samples were added to confluent MA104 cell monolayers grown in 24-well plates with

Minimum Essential Medium (MEM; Gibco) at 37 °C in a 5% CO_2 incubator. Cells and viruses were incubated for 30 min in an incubator with 5% CO_2 set to 37 °C. Subsequently, cellular monolayers were washed twice with MEM and incubated 37 °C for 15-18 h. At 15-18 hours post-infection (hpi) the focus forming unit assay was used to quantify rotavirus infectivity rates (Romero et al., 2011). Infectivity rates were expressed as $k_{infectivity}$ and were obtained from the first-order kinetics plot $\ln(FFU_t/FFU_0)$ versus treatment time (h), where FFU_t refers to the focus forming units measured for the treated virus samples and FFU_0 for non-treated virus samples.

4.3.4 Measurement of rotavirus NSP3 RNA levels

Reverse transcription quantitative PCR (qRT-PCR) was used to quantify rotavirus NSP3 gene segments in either purified virions or cells inoculated with viruses. For both assays, 3×10^4 FFU/ml was used. For both assays, total RNA was extracted from purified virions or from virus-inoculated cell using the using the E.Z.N.A Total RNA Kit I (Omega Bio-Tek) following manufacturer's instructions. The total RNA was eluted with 30 µl of molecular grade water and the samples were stored at -80 °C. The RNA samples underwent no more than two freeze/thaw cycles. Extracted RNA was quantified using a Qubit 2.0 fluorometer (Life Technologies) and the Qubit RNA BR Assay kit (Life Technologies) for all RNA samples except for samples in which the integrity of the rotavirus genome was evaluated.

The rotavirus NSP3 gene accounts for 0.7% of total rotavirus genome. End point RT-PCR reactions were prepared using iTaq Universal SYBR Green One-Step Kit (Bio-Rad, Hercules, CA) in a MiniOpticon RT-PCR system (Bio-Rad). A total reaction volume of 10 µL was prepared consisting of 3 µL of RNA template, 1x one-step SYBR® Green reaction mix, 1x iScript RT enzyme mix, 300 nM of each forward (JVKF) and reverse primers (JVKR) obtained from Jothikumar et al. and Mattioli et al. (Jothikumar, Kang, & Hill, 2009; Mattioli, Pickering,

Gilsdorf, Davis, & Boehm, 2013) (refer to Table A11 in the Appendix). Cycling parameters consisted of a 10 minute reverse transcription step at 50°C, followed by a 1 minute denaturation step at 95°C and then 35 cycles of 95°C for 10 seconds, 54°C for 15 seconds, and 60 °C for 30 seconds. Each RNA sample was assayed twice with qRT-PCR. Intact rotavirus samples were used to establish a calibration curve where six 10-fold dilutions were used in every qRT-PCR run. A sample without RNA template was also included in every qRT-PCR run as a negative control. For each rotavirus sample (except for the samples where RNA concentration was too low), obtained copy numbers were normalized by the RNA concentration (ng/µl).

4.3.5 NSP3 RNA levels in treated and untreated purified virions

When assaying purified virions for NSP3 gene integrity, 50 µl of treated or untreated rotavirus samples were incubated with 350-µl of the lysis buffer included in the E.Z.N.A Total RNA Kit I. Then, the total RNA extraction was conducted as recommended by the manufacture. Three µl of extracted RNA were analysed by qRT-PCR to quantify the number of NSP3 segment copies in the treated samples (qRT-PCR_t) and non-treated samples (qRT-PCR_0). Finally, the rate of change in genome integrity, k_{damage}, was calculated from the negative slope of the ln(RT-PCR_t/ qRT-PCR_0) versus treatment time (h) plot.

4.3.6 NSP3 RNA qRT-PCR to detect virus-host cell interactions

The effect of disinfection on virus binding to host cells was evaluated by quantifying NSP3 RNA as follows. Untreated or treated rotaviruses were incubated with 10 µg/ml of trypsin for 30 min at 37 °C. The rotavirus samples were diluted with MEM to a final volume of 150 µl. Next virus-containing samples were inoculated onto confluent MA104 cells grown in 24-well plates. Monolayers were incubated at 4°C for 1 h with occasional rocking, and then cells were washed three times with 500 µl of ice-cold PBS to remove unbound rotaviruses. Next, cell

monolayers were lysed with 350 µl of the lysis buffer included in the E.Z.N.A Total RNA Kit I, followed by extraction of the total cellular and viral RNA as stated above. Three microliters of the extracted RNA were used in the qRT-PCR program to quantify the rotavirus NSP3 segments in the treated (qRT-PCR_t) and non-treated rotavirus samples (qRT-PCR_0) associated with MA104 cells. The rate of change in binding ability, $k_{observed\_binding}$, was calculated from the negative slope of the ln(qRT-PCR_t/ qRT-PCR_0) versus treatment time (h) plot. A calibration curve of the initial human rotavirus concentrations used and the obtained bound NSP3 segment copies is shown in Figure A12 in the Appendix.

This $k_{observed\_binding}$ rate was corrected to obtain the true change in binding rate, $k'_{binding}$, as follows: $k'_{binding} = k_{observed\_binding} - k_{damage}$. For some treatments, multiple linear regression tests demonstrated that the kinetics of the changes in genome integrity (control) were not statistically different from the kinetics of the changes in binding ($p > 0.05$). For the treatments where these kinetic plots were not statistically different, $k'_{binding}$ rate constant was set to zero.

4.3.7 NSP3 RNA qRT-PCR to detect rotavirus RNA synthesis

Untreated (qRT-PCR_0) or treated (qRT-PCR_t) viruses were incubated with cellular MA104 monolayers. At 15-18 hpi, monolayers were washed once with PBS, and then incubated with 350 µl of the E.Z.N.A lysis buffer. Total RNA was extracted and three microliters of extracted RNA were used for qRT-PCR analysis. The rate of change in rotavirus RNA synthesis, $k_{observed\_synthesis}$, was calculated from the negative slope of the ln(qRT-PCR_t/ qRT-PCR_0) versus treatment time (h) plot. The true rate of change in viral RNA synthesis, $k'_{synthesis}$, was corrected as follows: $k'_{synthesis} = k_{observed-synthesis} - k_{damage} - k'_{binding}$.

The raw data for the rotavirus RNA measurements for each treatment are shown in the Appendix along with a summary of the data used for the analysis (see Figure A14 and Table A12). No loss of signal was measured in dark controls incubated at room temperature for any of the rotavirus RNA measurement assays (shown in Figure A14 panel D).

4.4 Data analysis

The negative slopes, first-order decay rate constants, and their standard errors were calculated from the $\ln(FFU_t/FFU_0)$ or $\ln(qRT\text{-}PCR_t/qRT\text{-}PCR_0)$ vs. time (h) plots of data aggregated from at least duplicate experiments. To account for the changes of the NSP3 gene segment signal due to treatment alone or changes in binding, the $k_{observed\_binding}$ and $k_{observed\_synthesis}$ rate constants were corrected by subtracting the k_{damage} and $k'_{binding}$ rates, respectively. The law of error propagation for simple average errors was used to propagate the standard error to the corrected rate constants. Linear regression and multiple linear regression tests were used to asses if the slope of the lines were statistically different from a slope of 0 or if two lines were statistically different from each other, respectively. P values < 0.05 were considered significant.

4.5 Results

4.5.1 Human rotavirus infectivity upon heat or solar treatment.

The inactivation kinetics $[\log_{10}(FFU_t/FFU_0)]$ vs. treatment time (h^{-1}) for human rotavirus with simulated sunlight irradiation or heat (57°C) in the dark are shown in Figure 9. The first-order decay rate constants obtained from the negative slope of the $\ln(FFU_t/FFU_0)$ vs. treatment time (h^{-1}) plots were also calculated, reported as $k_{infectivity}$ rate constants, and are summarized in Table A12. Consistent with our previous findings (Romero-Maraccini et al., 2013), heat treatment resulted in the highest inactivation kinetics ($k_{infectivity}$ ± standard error, 57.4 ± 11.6 h^{-1}). Treatment by full spectrum light irradiation of solutions containing or lacking the sensitizer (24.0

± 3.0 h^{-1} and 12.8 ± 0.59 h^{-1}, respectively) resulted in the next highest $k_{infectivity}$ rates. The inactivation kinetics for solutions irradiated with UVA and visible light with (5.91 ± 0.26 h^{-1}) and without (2.56 ± 0.19 h^{-1}) the organic sensitizer were lower than for the full spectrum irradiation conditions. Importantly, multiple linear regression tests comparing the inactivation kinetic plots with one another showed that the inactivation kinetics plot for each treatment were statistically different from one another, with p values < 0.01 for all treatment comparisons. In summary, heat and full spectrum irradiation were the most effective treatments against human rotavirus.

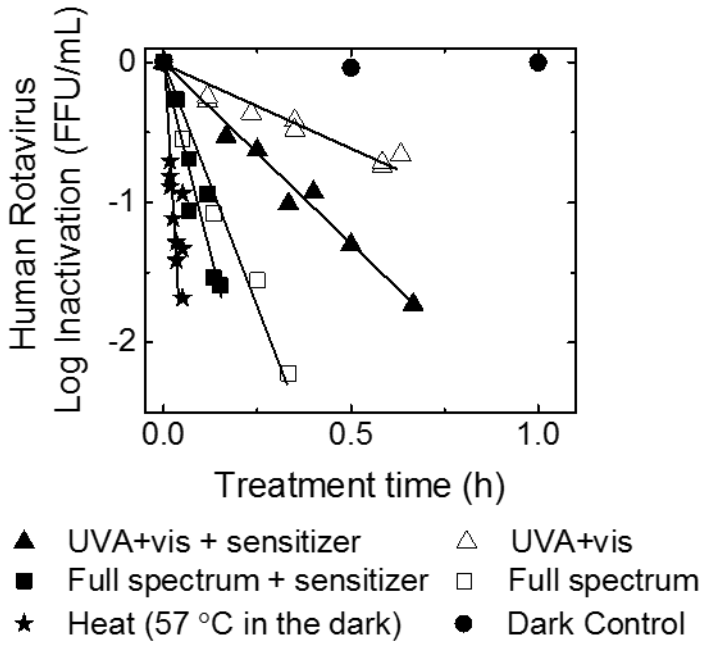

Figure 9. Rotavirus infectivity after solar and heat treatments. The infectivity data from at least two independent experiments were aggregated and plotted here as $\log_{10}$ (FFU_t/FFU_0) vs. treatment time (h). Inactivation experiments were conducted in solutions containing 1 mM $NaHCO_3$ buffer (pH 8), 0 or 20 mg C/L of an organic sensitizer, and an initial rotavirus concentration of 9×10^4 FFU/ml. Samples of treated or untreated rotaviruses were inoculated onto MA104 cell monolayers. At 15-18h post-infection, cells were fixed and immunostained, and FFUs were quantified using an inverted microscope.

4.5.2 Detecting NSP3 gene integrity by qPCR

If the NSP3 genome segment of rotavirus could be amplified by qPCR, then we interpreted this to mean that the genome was not damaged by heat or solar treatment to the extent that it could not interact with NSP3-specific primers. The rate of change of the qPCR signal generated by amplifying the NSP3 segment after heat or solar treatments was calculated from the negative slope of the $\ln(qRT\text{-}PCR_t / qRT\text{-}PCR_0)$ versus treatment time (h), and the negative slope was designated as the rate of change k_{damage} (Figure 10).

While both UVB and UVA fractions of sunlight cause nucleic acid damage by inducing primarily pyrimidine dimers, UVB causes more extensive damage than UVA irradiation (Schuch & Menck, 2010). Our results with rotavirus inactivation reflected a same trend: higher NSP3 segment decay rates ($k_{damage} \pm$ standard error; $\geq 0.69 \pm 0.12\ h^{-1}$) occurred when viruses were treated with full spectrum versus UVA and visible light ($\leq 0.41 \pm 0.04\ h^{-1}$). The decay rates remained similar in the presence or absence of the organic sensitizer (Figure 10), suggesting that direct and endogenous damage caused by UV irradiation had a greater effect on the genome integrity than the damage resulting from the exogenous mechanism. It should be noted that similar results are reported when disinfecting human adenovirus type 2 (Bosshard, Armand, Hamelin, & Kohn, 2013).

Results showed that heat treatment of rotaviruses caused a significant decay in infectivity (Figure 9), but did not induce extensive genome damage (Figure 10 and Figure A14). The kinetic plot for the NSP3 segment signal did not significantly change over time (linear regression $p > 0.05$). These results are in agreement with the known higher resistance of viral nucleic acids to heat treatment (Dan Li et al., 2010).

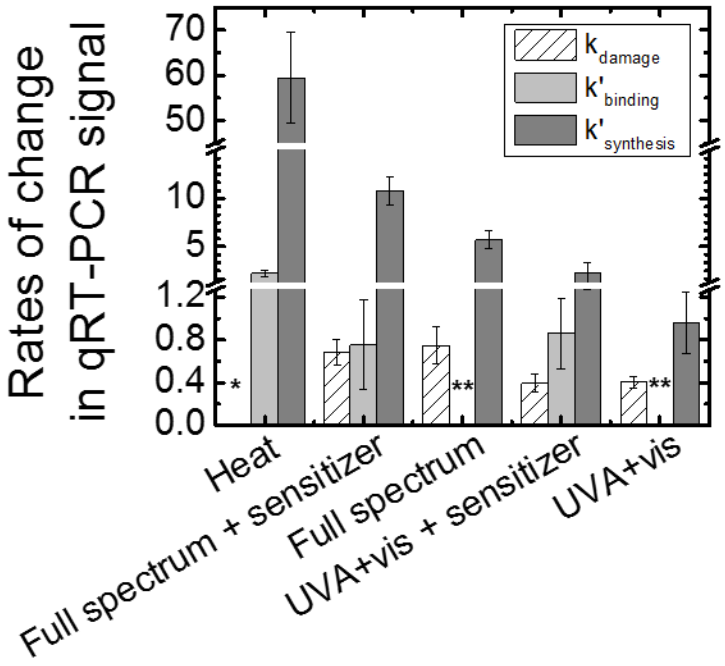

Figure 10. Rate of change of the PCR amplification of the NSP3 gene (k_{damage}), true rate of change in binding of virus to host cells ($k'_{binding}$), and true rate of change in viral NSP3 synthesis ($k'_{synthesis}$) when viruses were exposed to the indicated treatments. Data from at least two separate experiments were aggregated and plotted as ln(qRT-PCR$_t$/qRT-PCR$_0$) vs. treatment time (h) and the negative slope and the standard error were calculated from linear regression tests. The calculated negative slopes are represented here as the rates of change and the standard errors are the error bars. The $k'_{binding}$ and $k'_{synthesis}$ rates were corrected to account for the rate of change in the PCR target region signal as a consequence of treatment alone and binding. The asterisk (*) denotes that the slope of the linear regression for the k_{damage} data set did not deviate from 0 ($p > 0.05$). The two asterisks (**) denote that no true rate of change in binding ability was determined based on multiple linear regression tests that compared the slopes of the PCR signal kinetics from genome integrity and binding data ($p > 0.05$). Y-axis breaks are from 1.27-1.28 and 15-45.

4.5.3 Detecting changes in rotavirus binding ability after heat and solar treatments

Next, we assessed the rate at which treated and untreated human rotaviruses associated with their host cells. Viruses were incubated with MA104 cells at 4°C, conditions known to allow virus-host interactions but prevent virus internalization. Cellular monolayers were washed to remove unbound virus particles. qRT-PCR quantification of rotavirus particles was possible because each rotavirus particle contains a single NSP3 segment. In support of this, the Appendix Figure A12 showed a binding calibration curve conducted for varying untreated rotavirus

concentrations. The number of viruses bound to MA104 cells was directly dependent on the number of viruses present in the infecting solution.

We only observed extensive binding inhibition for viruses treated with heat and solar treatments containing the organic sensitizer (Figure 10). Heat treatment of rotavirus resulted in the highest $k'_{binding}$ rate, suggesting heat treatment caused the highest inhibition of rotavirus binding to its host receptors; therefore, rotaviruses were not able to complete their life cycle. The next highest $k'_{binding}$ rates were obtained for solar treatments containing the organic sensitizer. In contrast, solar treatments lacking organic sensitizer did not induce extensive changes in the ability of rotavirus to bind to its host; that is, based on multiple linear regression tests, the negative slopes from the linear plots of the qRT-PCR signal obtained for the genome integrity and binding assays were not significantly different (p value > 0.05). Thus, only damages initiated by heat and the solar-mediated exogenous mechanism contributed to a reduction in rotavirus binding to host cells, likely as a consequence of binding protein damage.

Overall, the magnitudes of the human rotavirus $k_{infectivity}$ and $k'_{binding}$ rate constants were significantly different for all treatments (see Table A12). For instance, for heat treatment, the $k_{infectivity}$ rate was $57.4 \pm 11.6\ h^{-1}$ and the $k'_{binding}$ rate was $2.22 \pm 0.29\ h^{-1}$. Because the change in binding rates did not decrease at the same rate as rotavirus infectivity for all treatments tested, we concluded that binding inhibition was not the principle cause of virus inactivation. Therefore, assessment of other rotavirus life cycle functions need to be considered for these treatments.

4.5.4 Rotavirus RNA synthesis

We developed an assay that quantified the rate at which viral RNA synthesis occurred in cells inoculated with untreated or treated viruses. In this case, the rate of viral RNA synthesis was assessed by quantifying NSP3 gene levels in infected cells by qRT-PCR. When cells were

inoculated with untreated rotavirus, there was a 20-fold increase in NSP3 amplicons at 15-18 hpi (Figure A13 in the Appendix). The rate of change in rotavirus RNA synthesis, $k_{observed\_synthesis,}$ for each treatment was calculated from the slope of the linear plots of the normalized NSP3 target region copies harvested 15-18 hpi [ln ($qRT\text{-}PCR_t/qRT\text{-}PCR_0$)] as function of treatment time (h). The $k_{observed\_synthesis}$ rates were corrected for changes in PCR signal stemming from the genome integrity and binding assays. The true rates of change in rotavirus RNA synthesis were reported as $k'_{synthesis}$ values and are shown in Figure 10 for all treatments tested.

Overall, viral RNA synthesis decayed at a similar rate as rotavirus infectivity (Figures 9-11A). For example, the $k'_{synthesis}$ and $k'_{infectivity}$ rates were the highest for heat treatment and lowest for the UVA and visible light irradiation treatment. The $k'_{synthesis}$ and $k_{infectivity}$ values obtained for the solar treatments were significantly correlated ($p = 0.002$), suggesting that solar-mediated damages significantly inhibited rotavirus RNA synthesis, which prevented the synthesis of mature rotaviruses. However, the slope of the linear correlation for the $k'_{synthesis}$ as a function of $k_{infectivity}$ was less than 1 (0.46; see Figure 11A), indicating that the inhibition of viral RNA synthesis by solar treatments was not the sole mechanism of virus inactivation. Thus, solar treatment uses more than one mechanism to inactivate rotaviruses.

Unlike solar treatments, heat treatment of rotavirus resulted in a $k'_{synthesis}$ value similar in magnitude to the $k_{infectivity}$ value (Figure 11A). The $k'_{synthesis}$ and $k_{infectivity}$ values calculated for heat treatment were $59.4 \pm 9.81\ h^{-1}$ and $57.4 \pm 11.6\ h^{-1}$, respectively. These rate constants were similar even when accounting for the $k'_{binding}$ and k_{damage} values. Thus, heat treatment inactivates rotaviruses by preventing viral RNA replication.

4.5.5 Implications of measuring rotavirus RNA levels as an approach to quantify infectious rotaviruses

The uncorrected viral RNA synthesis rates of change, $k_{observed\_synthesis}$ comprise the decay in PCR signal arising from damages in rotavirus genome, binding to host cells, and RNA synthesis upon treatment. The $k_{observed\_synthesis}$ approach is known as the integrated cell culture qRT-PCR (ICC-qRT-PCR) method and is commonly used in lieu of conventional cell culture assays to test virus infectivity (Blackmer & Reynolds, 2000; Dan Li, Gu, He, Shi, & Yang, 2009; Reynolds, Gerba, & Pepper, 1996). Here, heat treatment of rotavirus resulted in very similar $k_{observed\_synthesis}$ and $k_{infectivity}$ values 61.6 ± 9.75 h^{-1} and 57.4 ± 11.6 h^{-1}, respectively, indicating that heat treatment induced damage to viral components responsible for transcription functions (Figure 11B). To observe an aggregated effect of the solar treatments, the $k_{observed\_synthesis}$ rates were plotted as a function of $k_{infectivity}$ rates (Figure 11B). The results of this linear correlation showed that the slope was less than one (0.50), indicating the occurrence of damage to rotavirus transcription functions. However, inhibition of rotavirus transcription is not the only mechanism in which solar treatments damage rotavirus. Thus, the infectivity data obtained from the $k_{observed\_synthesis}$ or the ICC-qRT-PCR method may not correctly represent the infectivity data obtained from cell culture infectivity assays.

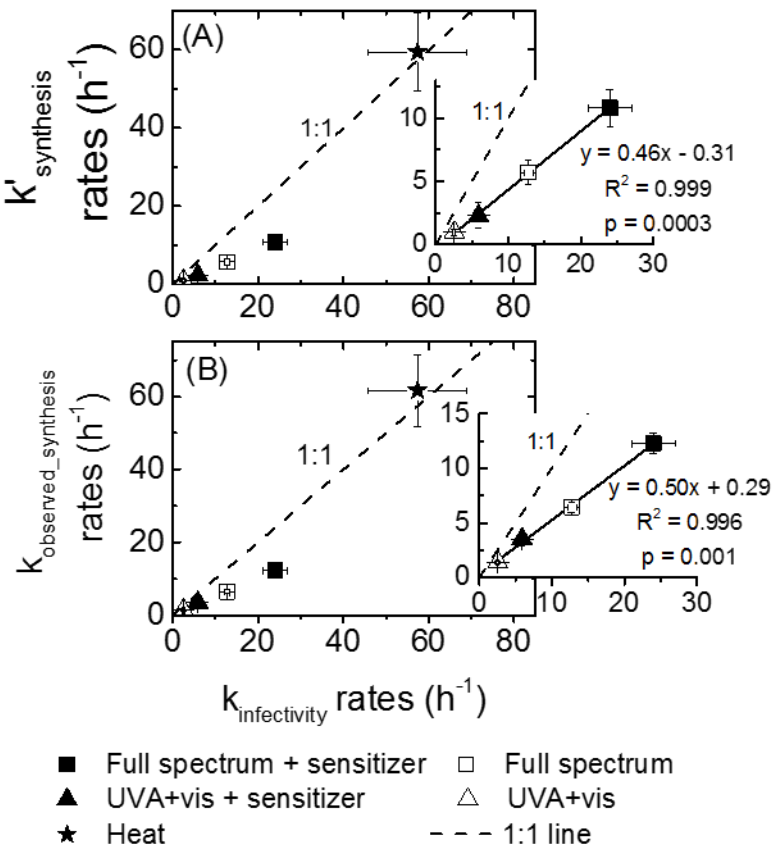

Figure 11. (A) True rates of change ($k'_{synthesis}$) and (B) uncorrected rates of change ($k_{observed\_synthesis}$) in viral RNA synthesis in infected cells with rotaviruses treated by heat or simulated sunlight irradiation as a function of infectivity decay rates ($k_{infectivity}$). Data from at least two separate experiments were aggregated and plotted as ln(qRT-PCR$_t$ or FFU$_t$/qRT-PCR$_0$ or FFU$_0$) vs. treatment time (h) and the negative slope and the standard error were calculated from linear regression tests. For each treatment, the calculated negative slopes are represented here as the rates of change in viral RNA synthesis and the standard errors are the error bars. The insets show the significant linear correlations ($p < 0.01$) between the (A) $k'_{synthesis}$ and $k_{infectivity}$ and (B) $k_{observed\_synthesis}$ and $k_{infectivity}$ for solar treatments. Heat treatment data were not used in the linear regression analysis because their trend was different from the solar treatment data.

4.6 Discussion

We developed different assays to quantify rotavirus NSP3 RNA as a means to assess genome integrity, virus binding to the host cell, or viral RNA synthesis in cells inoculated with rotaviruses that were treated with simulated sunlight or heat. Under the assumption that the decay rates of each individual rotavirus life cycle portions should add up to the overall

inactivation decay rates, the extent to which solar and heat treatments caused specific viral damages was evaluated. Specifically, we found that the mechanisms responsible for rotavirus inactivation were largely or entirely linked to the decay of viral RNA synthesis (Figure 12). As a corollary, virus-host cell interactions and the integrity of the virus genome were not substantially affected by heat or solar treatment of rotaviruses.

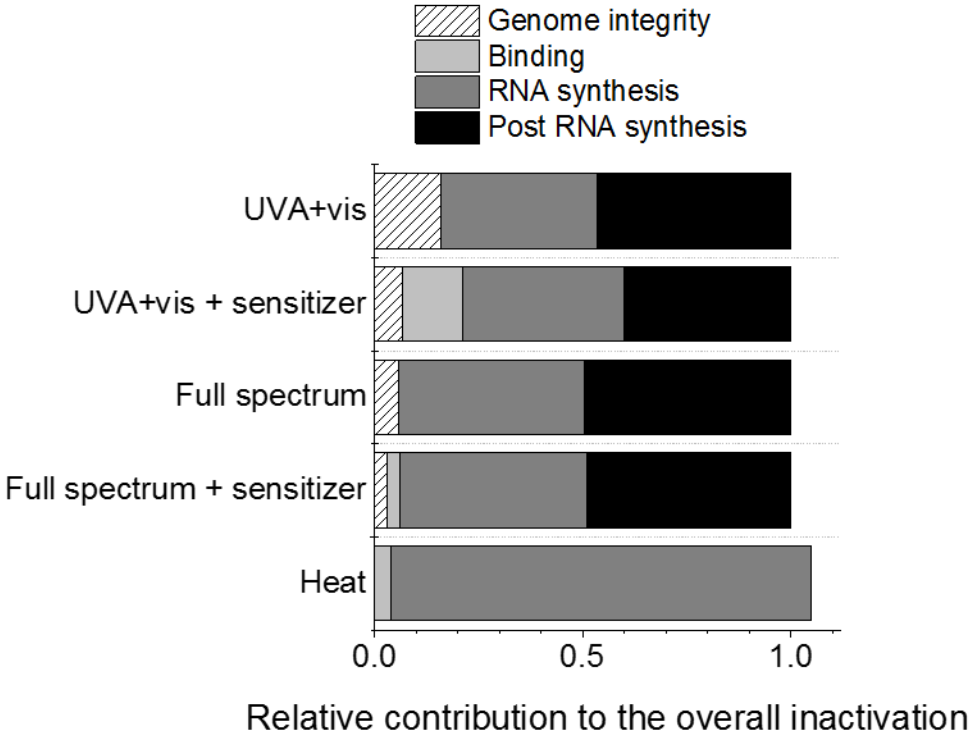

Figure 12. The relative contribution of individual life cycle steps investigated to the overall rotavirus inactivation by solar and heat treatments. This figure was generated under the assumption that the rates of decay of individual life cycle portions are cumulative and that these add up to the infectivity decay rates: $\sum_{individual} k = k_{infectivity}$.

A comparison of the $k_{infectivity}$ (59.4 ± 9.81 h^{-1}) and $k'_{synthesis}$ (57.4 ± 11.6 h^{-1}) rates obtained upon heat treatment suggested that rotavirus inactivation was entirely associated with the decay of viral RNA synthesis. Inhibition of viral RNA synthesis could stem from a damaged genome or other viral structures involved in rotavirus transcription functions. However, because no extensive changes in genome integrity were measured (Figure 10), we argue that genome

damage was likely not the principle cause leading to viral RNA synthesis inhibition and subsequent inactivation. It should be noted that others reported that heat treatment had a negligible effect on the integrity of portions of a virus genome (Dan Li et al., 2010; Pecson, Martin, & Kohn, 2009; Wigginton, Pecson, Bosshard, Kohn, & Sigstam, 2012). Instead, we argue that the decay in viral RNA synthesis was likely triggered by damage to proteins involved in viral RNA synthesis functions, as protein conformations have been associated with the heat treatment of viruses (Nelson et al., 2008; Wigginton et al., 2012). Of the five treatments investigated here, the $k'_{binding}$ value was the highest for the heat-treated rotavirus samples (Figure 10), though the relative contribution of binding inhibition to the overall heat inactivation was practically negligible (Figure 12). Yet, binding inhibition is indicative of structural protein damage, and at large, structural proteins are involved in the early rotavirus life cycle steps including binding, entry, and viroplasm formation (20–25). For example, structural proteins VP4 and VP7 are entirely responsible for binding and entry into the host cells (Díaz-Salinas & Romero, 2013; Lopez & Arias, 2006; Martínez, López, Arias, & Isa, 2013). Since binding was compromised, it is evident that protein damage occurred, and that rotavirus entry into the host was also likely inhibited (Lopez & Arias, 2006). Based on our analysis, we concluded that heat treatment primarily damaged viral components involved in the early portions of the rotavirus life cycle including viral RNA transcription.

For all solar treatments, the $k'_{synthesis}$ rate constants correlated positively with the $k_{infectivity}$ rate constants ($p = 0.002$). However, the $k'_{synthesis}$ rate constants only accounted for nearly half of the $k_{infectivity}$ rates, implying that other factors not included in the $k'_{synthesis}$ were equally responsible for the observed rotavirus inactivation upon solar treatments (Figure 11A). Genome damage was evident based on the k_{damage} rate constants ($> 0.40 \pm 0.06\ h^{-1}$) obtained for all solar

treatments, regardless of the light source or presence and absence of the organic sensitizer (Figure 10). The contribution of the changes in genome integrity to the overall inactivation for each solar treatment varied, with the decay in genome integrity contributing the most to the inactivation caused by sensitizer-free UVA and visible light irradiation treatment and least to the inactivation caused by the sensitizer-containing solutions irradiated with full spectrum light (Figure 12). Damaged genome can hinder genome transcription and other post transcription functions such as protein translation and genome replication. Hence, evidence of genomic impairment such as that shown by the k_{damage} values may explain why the rate of decay in viral RNA synthesis cannot completely explain the rate of decay in rotavirus infectivity for all solar treatments.

Upon solar treatment, a decay in binding to host cells was only apparent for the conditions containing the organic sensitizer, although the relative contribution of binding inhibition rates to the overall decay rates in infectivity was higher for UVA and visible light irradiation than for full spectrum irradiation (Figures 10 and 12). The requirement of the organic sensitizer for the occurrence of extensive binding inhibition suggested that the radicals produced through the exogenous mechanisms damaged the rotavirus proteins VP4 and VP7, which are responsible for attachment and entry (Díaz-Salinas & Romero, 2013; Lopez & Arias, 2006; Martínez et al., 2013). A reduction in viral binding ability and higher protein damage were reported previously as a consequence of photo-induced damages triggered through the exogenous mechanism. During the solar treatment of MS2 bacteriophage and adenovirus type 2, binding and protein damages, respectively, were significant in solutions containing a sensitizer (Bosshard et al., 2013; Wigginton et al., 2012). Here, the rotavirus $k'_{synthesis}$ and $k'_{infectivity}$ rates were higher in the organic sensitizer-containing solutions than in the sensitizer-free solutions,

suggesting that the exogenous damages were reflected in both the infectivity and viral RNA synthesis decay rates. Based on our data, we conclude that rotavirus inactivation by solar irradiation in the presence of the organic sensitizer likely stems from genome and binding protein damage that resulted from a combination of the direct, endogenous and exogenous mechanisms. In the absence of the organic sensitizer, solar treatments appeared to induce primarily genome damage through the endogenous and direct mechanisms, which explains the relatively lower $k_{infectivity}$ and $k'_{synthesis}$ rates.

Of the life cycle portions investigated here, inhibition of viral RNA synthesis served as a better measure of rotavirus inactivation for all treatments. The measurement of changes in viral functions that can be directly associated with inactivation is essential in determining which components are the principle targets of a treatment. Often the detection and quantification of isolated protein or genome damages cannot be directly linked to virus inactivation (Bosshard et al., 2013; Eischeid, Meyer, & Linden, 2009; Pecson et al., 2009). An approach that combines virus functionality and specific virus structures is needed to identify the specific targets for solar and heat treatments. To our knowledge, this study is the first to investigate and correlate human rotavirus Wa inactivation by heat and solar treatments with the loss of viral RNA synthesis function. The results from the $k_{observed\_synthesis}$ assay, also known as the integrated cell culture qPCR (ICC-qPCR) assay, can serve to indicate virus infectivity. This approach takes advantage of the sensitive, rapid, and reliable detection features of qRT-PCR to quantify viral RNA synthesis. In this study, the loss of viral RNA synthesis assay and the FFU assay captured a 3-log and 2-log unit decay, respectively (Figures 9 and A14), although the concentrations for the FFU assay were three times higher. Although commonly used (Blackmer & Reynolds, 2000; Dan Li et al., 2009; Reynolds et al., 1996), the ICC-qRT-PCR method is not well understood.

Based on the data presented here, we provide further insights for the use of the ICC-qRT-PCR as an infectivity assay.

We showed that for heat treatment of rotavirus the $k_{observed\_synthesis}$ values and $k_{infectivity}$ values were statistically equivalent ($p > 0.05$). Yet, upon solar treatments the $k_{observed\_synthesis}$ values were two-times lower than the $k_{infectivity}$ values (Figure 11B). Based on these results, we found that the type of rotavirus treatment influenced the results obtained with the ICC-qRT-PCR assay. Unlike heat treatment of rotavirus, solar treatments damage virus components responsible for post-transcription functions, likely protein translation and genome replication, that cannot be captured by the ICC-qRT-PCR assay. These findings provide potential explanations for the inconsistencies reported between cell culture and ICC-qRT-PCR inactivation data. For example, data obtained with the ICC-qRT-PCR method showed that a much higher UV dose was needed to achieve a 3-log rotavirus reduction than the previously reported with data determined by a cell culture assay (Dan Li et al., 2009). In a study by Blackmer, et al. (2000), the contact time for chlorine disinfection of poliovirus was found to be about five times greater when employing the ICC-qRT-PCR assay than when employing a conventional cell culture assay (Blackmer & Reynolds, 2000). Inactivation data obtained with the ICC-qRT-PCR assay could overestimate the treatment dose needed to achieve a specific log viral reduction resulting in unnecessarily high treatment costs. We argue that understanding the mechanisms of inactivation is crucial for each disinfection treatment and virus before dose treatment recommendations are made with data obtained with the ICC-qRT-PCR assay.

In conclusion, we provided loss of function data of human rotavirus Wa after heat and solar treatments. Investigating the rates of change in binding and viral RNA synthesis functions provided further insight into the rotavirus components that are targets for solar and heat

treatments. In general, heat treatment targeted rotavirus components that influenced viral RNA synthesis, likely structural proteins responsible for entry and other transcription functions. For solar treatments, rotavirus infectivity was caused by inhibition of viral RNA synthesis and other later portions of the rotavirus life cycle. Apart from an improved understanding of the inactivation mechanism for rotaviruses, our findings have implications for the use of the integrated cell culture and qRT-PCR assay employed as an infectivity assay for a number of human viruses. We showed that inactivation kinetics obtained with the ICC-qRT-PCR assay may be different from the inactivation kinetics obtained with a cell culture assay and that this difference is influenced by the treatment used.

4.7 Acknowledgments

We acknowledge the financial support of the NSF CAREER grant to T.H.N. (0954501), and NSF GRF DGE 07-15088 FLW to O.C.R. We thank Hanting Wang for helping with experiments and Peter A. Maraccini for insightful discussions.

4.8 Literature cited

Arias, C. F., Isa, P., Guerrero, C. a, Méndez, E., Zárate, S., López, T., … López, S. (2002). Molecular biology of rotavirus cell entry. *Archives of Medical Research*, *33*(4), 356–61. Retrieved from http://www.ncbi.nlm.nih.gov/pubmed/12234525

Blackmer, F., & Reynolds, K. (2000). Use of integrated cell culture-PCR to evaluate the effectiveness of poliovirus inactivation by chlorine. *Appl. Environ. Microbiol.*, *66*(5), 2267–2269. doi:10.1128/AEM.66.5.2267-2268.2000.Updated

Bosshard, F., Armand, F., Hamelin, R., & Kohn, T. (2013). Mechanisms of human adenovirus inactivation by sunlight and UVC light as examined by quantitative PCR and quantitative proteomics. *Appl. Environ. Microbiol.*, *79*(4), 1325–1332. doi:10.1128/AEM.03457-12

Díaz-Salinas, M., & Romero, P. (2013). The spike protein VP4 defines the endocytic pathway used by rotavirus to enter MA104 cells. *J. Virol.*, *87*(3), 1658–1663. Retrieved from http://jvi.asm.org/content/87/3/1658.short

Eischeid, A. C., Meyer, J. N., & Linden, K. G. (2009). UV disinfection of adenoviruses: molecular indications of DNA damage efficiency. *Appl. Environ. Microbiol.*, *75*(1), 23–8. doi:10.1128/AEM.02199-08

Gerba, C. P., Rose, J. B., Haas, C. N., & Crabtree, K. D. (1996). Waterborne rotavirus: A risk assessment. *Water Res.*, *30*(12), 2929–2940. doi:10.1016/S0043-1354(96)00187-X

Greenberg, H. B., & Estes, M. K. (2009). Rotaviruses: from pathogenesis to vaccination. *Gastroenterology*, *136*(6), 1939–51. doi:10.1053/j.gastro.2009.02.076

Guglielmi, K. M., McDonald, S. M., & Patton, J. T. (2010). Mechanism of intraparticle synthesis of the rotavirus double-stranded RNA genome. *J. Biol. Chem.*, *285*(24), 18123–8. doi:10.1074/jbc.R110.117671

Gutiérrez, M., Isa, P., Sánchez-San Martin, C., Pérez-Vargas, J., Espinosa, R., Arias, C. F., & López, S. (2010). Different rotavirus strains enter MA104 cells through different endocytic pathways: the role of clathrin-mediated endocytosis. *J. Virol.*, *84*(18), 9161–9. doi:10.1128/JVI.00731-10

Jothikumar, N., Kang, G., & Hill, V. R. (2009). Broadly reactive TaqMan assay for real-time RT-PCR detection of rotavirus in clinical and environmental samples. *Journal of Virological Methods*, *155*(2), 126–31. doi:10.1016/j.jviromet.2008.09.025

Li, D., Gu, a Z., Zeng, S.-Y., Yang, W., He, M., & Shi, H.-C. (2011). Monitoring and evaluation of infectious rotaviruses in various wastewater effluents and receiving waters revealed correlation and seasonal pattern of occurrences. *J. Appl. Microbiol.*, *110*(5), 1129–37. doi:10.1111/j.1365-2672.2011.04954.x

Li, D., Gu, A. Z., He, M., Shi, H.-C., & Yang, W. (2009). UV inactivation and resistance of rotavirus evaluated by integrated cell culture and real-time RT-PCR assay. *Water Research*, *43*(13), 3261–9. doi:10.1016/j.watres.2009.03.044

Li, D., Gu, A. Z., Yang, W., He, M., Hu, X.-H., & Shi, H.-C. (2010). An integrated cell culture and reverse transcription quantitative PCR assay for detection of infectious rotaviruses in environmental waters. *Journal of Microbiological Methods*, *82*(1), 59–63. doi:10.1016/j.mimet.2010.04.003

Lopez, S., & Arias, C. F. (2006). Early steps in rotavirus cell entry. In P. Roy (Ed.), *Reoviruses: Entry, Assembly and Morphogenesis* (1st ed., pp. 39–66). Berlin, Germanay: Springer-Verlag Berlin Heidelberg. doi:10.1007/3-540-30773-7_2

Marshall, G. S. (2009). Rotavirus disease and prevention through vaccination. *Pediatr. Infect. Dis. J.*, *28*(4), 351–362. doi:10.1097/INF.0b013e318199494a

Martínez, M., López, S., Arias, C., & Isa, P. (2013). Gangliosides have a functional role during rotavirus cell entry. *J. Virol.*, *87*(2), 1115–1122. Retrieved from http://jvi.asm.org/content/87/2/1115.short

Mattioli, M. C., Pickering, A. J., Gilsdorf, R. J., Davis, J., & Boehm, A. B. (2013). Hands and water as vectors of diarrheal pathogens in Bagamoyo, Tanzania. *Environ. Sci. Technol.*, *47*(7), 355–363. doi:10.1021/es303878d

Nelson, C. D. S., Minkkinen, E., Bergkvist, M., Hoelzer, K., Fisher, M., Bothner, B., & Parrish, C. R. (2008). Detecting small changes and additional peptides in the canine parvovirus capsid structure. *Journal of Virology*, *82*(21), 10397–407. doi:10.1128/JVI.00972-08

Parashar, U., Steele, D., Neuzil, K., Quadros, C. De, Tharmaphornpilas, P., Serhan, F., … Glass, R. (2013). Progress with rotavirus vaccines: summary of the Tenth International Rotavirus Symposium. *Expert Review of Vaccines*, *12*(2), 113–117. doi:10.1586/erv.12.148

Pecson, B. M., Martin, L. V., & Kohn, T. (2009). Quantitative PCR for determining the infectivity of bacteriophage MS2 upon inactivation by heat, UV-B radiation, and singlet

oxygen: advantages and limitations of an enzymatic treatment to reduce false-positive results. *Appl. Environ. Microbiol.*, *75*(17), 5544–54. doi:10.1128/AEM.00425-09

Pesavento, J. B., Crawford, S. E., Estes, M. K., & Prasad, B. V. V. (2006). Rotavirus proteins: structure and assembly. *Curr. Top. Microbiol. Immunol.*, *309*, 189–219. Retrieved from http://www.ncbi.nlm.nih.gov/pubmed/16913048

Reynolds, K., Gerba, C., & Pepper, I. (1996). Detection of infectious enteroviruses by an integrated cell culture-PCR procedure. *Applied and Environmental Microbiology*, *62*(4), 1424–1427. Retrieved from http://aem.asm.org/content/62/4/1424.short

Romero, O. C., Straub, A. P., Kohn, T., & Nguyen, T. H. (2011). Role of temperature and Suwannee River natural organic matter on inactivation kinetics of rotavirus and bacteriophage MS2 by solar irradiation. *Environmental Science & Technology*, *45*(24), 10385–10393. doi:10.1021/es202067f

Romero-Maraccini, O. C., Sadik, J., Rosado-Lausell, S. L., Pugh, C. R., Niu, X.-Z., Croue, J.-P., & Nguyen, T. H. (2013). Sunlight-Induced Inactivation of Human Wa and Porcine OSU Rotaviruses in the Presence of Exogenous Photosensitizers. *Environmental Science & Technology*, *47*(19), 11004–11012. Retrieved from http://pubs.acs.org/doi/abs/10.1021/es402285u

Schuch, A. P., & Menck, C. F. M. (2010). The genotoxic effects of DNA lesions induced by artificial UV-radiation and sunlight. *J. Photochem. Photobiol., B*, *99*(3), 111–116. doi:10.1016/j.jphotobiol.2010.03.004

Trask, S. D., Ogden, K. M., & Patton, J. T. (2012). Interactions among capsid proteins orchestrate rotavirus particle functions. *Current Opinion in Virology*, *2*(4), 373–9. doi:10.1016/j.coviro.2012.04.005

Wegelin, M.; Canonica, S.; Mechsner, K.; Fleischmann, F.P.; Metzler, A. (1994). Solar water disinfection: scope of hte process and analysis of radiation experiments. *J Water SRT-Aqua*, *43*(3), 154–169.

Wigginton, K. R., Pecson, B. M., Bosshard, F., Kohn, T., & Sigstam, T. (2012). Virus inactivation mechanisms: impact of disinfectants on virus function and structural integrity. *Environ. Sci. Technol.*, *46*(21), 12069–12078. doi:10.1021/es3029473

CHAPTER 5

CONCLUSION AND FUTURE RESEARCH

We provided a comprehensive solar inactivation study of rotavirus. This study investigated the solar inactivation mechanisms of two rotavirus strains: human Wa and porcine OSU strains. The endogenous and exogenous inactivation mechanisms upon solar treatment were investigated as a function of different fractions of light, temperature, and type of photosensitizers. Additionally, we investigated the molecular mechanisms of human rotavirus inactivation by solar and thermal treatments. Table 1 below summarizes the research questions addressed in this study.

Table 1. Summary of research questions

Research Questions	Experiments Conducted	Summary of Results
Can porcine rotavirus OSU become inactivated by solar irradiation? If so, under what conditions?	1) MS2 and porcine rotavirus OSU inactivation with varying SRNOM concentrations and different fractions of simulated light 2) ROS measurements	1) Full spectrum irradiation was highly effective against porcine rotavirus 2) UVA-visible light irradiation was only effective at high temperatures for porcine rotavirus 3) OH radicals were linked to porcine rotavirus inactivation
What are the roles different photosensitizers on porcine rotavirus inactivation?	1) Porcine rotavirus inactivation experiments with UVA and visible light irradiation in different photosensitizer solutions	1) Not all photosensitizers were equal. Those inductive of OH radicals appeared to result in higher kobs values
Do human rotavirus Wa and porcine rotavirus OSU differ when treated with heat and sunlight?	Inactivation experiments with both strains: 1) in the dark at different temperatures 2) with UVA and visible light irradiation of solutions containing different photosensitizers	1) Porcine rotavirus has higher thermostability than human rotavirus 2) Both rotavirus strains were likely inactivated by the same radicals since the kobs values for all photosensitizers correlated

Table 1 (continued)

What are the radicals leading to rotavirus inactivation?	1) Indirect measurements of OH radicals, singlet oxygen, triplet state species, and carbonate radicals formed by the irradiation of different photosensitizers	1) OH radicals and triplet state species are the most likely responsible for rotavirus inactivation
Why does rotavirus become inactivated by sunlight and heat treatments?	1) Using qRT-PCR molecular assays, several aspects of rotavirus inactivation were investigated for solar and heat treatments	1) Inactivation was attributed to a defect in viral RNA synthesis

The effects of the different fractions of light, temperature, and photosensitizers are summarized in Table 2. The most environmentally relevant findings of this study were:

- Although structurally identical, the two human and porcine rotavirus strains had different responses to solar and thermal treatments.
- Porcine rotavirus had higher thermostability (retained infectivity at much higher temperatures for longer periods of time) than human rotavirus.
- Regardless of the presence or absence of NOM, the endogenous mechanism caused by full spectrum irradiation was the most effective against both rotavirus strains.
- For full spectrum irradiation, the presence of DOM lowered the inactivation kinetics of porcine rotavirus but increased the inactivation kinetics of human rotavirus.
- For UVA and visible light irradiation, porcine rotavirus appeared to be stable even in the presence of photosensitizers (exogenous mechanism) for temperatures up to 40°C. For the same condition, human rotavirus was susceptible to the exogenous mechanism 25°C.
- Rotavirus inactivation was linked to genome damage by solar irradiation, regardless of the sunlight fraction, while thermal treatment caused primarily protein damage.

- The presence of organic matter augmented rotavirus inactivation by causing protein damage, likely targeted by the indirectly-produced radicals.

Table 2. Effects of physical parameters on the inactivation kinetics of the two rotavirus strains as compared to the sensitizer-free buffer control

Condition at 25°C (unless otherwise indicated)	Physical Parameter	Human Rotavirus Wa	Porcine Rotavirus OSU
Dark	Sensitizer-free Buffer control	$p > 0.05$	$p > 0.05$
	Dissolved organic matter (20 mg C/L; not corrected for light screening)	$p > 0.05$	$p > 0.05$
	At 50°C with or without DOM (20 mg C/L; not corrected for light screening)	**(+)** $k_{obs} = 6.8\ h^{-1}$	**(+)** $k_{obs} = 0.28\ h^{-1}$
UVA + visible light irradiation	Sensitizer-free Buffer control	$k_{obs} = 0.25\ h^{-1}$	$k_{obs} = 0.30\ h^{-1}$
	Dissolved organic matter (20 mg C/L; not corrected for light screening)	**(+)** $k_{obs} = 0.8\ h^{-1}$	**(○)** $k_{obs} = 0.40\ h^{-1}$
	At 50°C with DOM (20 mg C/L; not corrected for light screening)	Not available	**(+)** $k_{obs} = 0.55\ h^{-1}$
Full spectrum irradiation	Sensitizer-free Buffer control	$k_{obs} = 6.0\ h^{-1}$	$k_{obs} = 9.3\ h^{-1}$
	DOM (20 mg C/L; not corrected for light screening)	**(+)** $k_{obs} = 8.0\ h^{-1}$	**(–)** $k_{obs} = 4.6\ h^{-1}$
	At 40°C with DOM (20 mg C/L; not corrected for light screening)	Not available	**(–)** $k_{obs} = 5.7\ h^{-1}$

Notation: $p > 0.05$ implies that the linear regression test for the kinetic plot did not deviate from a slope of 0 ($p > 0.05$); **(+)**/ **(–)** denote that there was a statistically significant increase/decrease, respectively, in the rate when compared to the sensitizer-free buffer control for that condition; **(○)** denotes that there was no statistical difference between the condition and the control.

These findings shed light into the inactivation mechanisms of rotaviruses that can be targeted by newly developed water treatment technologies. For example, to improve SODIS, plastic or other materials that do not attenuate UVB photons will result in faster rotavirus inactivation. Currently, plastic bottles such soda bottles, block most of the UVB light and thus greatly reduce the potential for rotavirus inactivation. If UVB is blocked and photosensitizers are not present, the recommended 4-log inactivation of rotavirus for SODIS treatment would occur after exposure to sunlight for three full days (instead of the recommended 6 h if sunny) (Graf et al., 2010). UVB is heavily attenuated in wastewaters; therefore wastewater treatment technologies should rely on the UVA and visible light effects. For wastewater treatment, the synergistic effects of high temperature > 40°C and sunlight can greatly reduce the time needed for 4-log rotavirus removal, however partial mixing will be required. The presence of sensitizers that produced OH radicals or triplet state species is recommended for effective rotavirus inactivation. In this study, the aromatic content of the waters as measured by the specific UV_{254} nm absorbance (SUVA) served as an indicator for the photosensitizers' ability to generate these radicals.

Our study focused on the mechanistic aspects of rotavirus inactivation by natural photosensitizer, different light fractions, and temperature. Understanding the photochemical and microbiological mechanisms leading to rotavirus inactivation will help in the development of robust drinking water and wastewater treatment systems. However, in the environment, there are several processes that greatly vary from the conditions investigated here. Several key aspects have not been investigated here and remain of interest for future research.

1. Sunlight intensity and emitted photons for different fraction of light vary throughout time. Our study focused on a fixed light source where full spectrum or UVA and visible light

intensity remained constant throughout experiments. It remains unclear how changes in intensity and fractions of light affect inactivation. A comprehensive study of the effects of natural sunlight at different times during a day and during various seasons is needed to validate results obtained in the laboratory.

2. Photosensitizers present in natural water such as wastewater were not tested. To improve our understanding of the natural occurring photochemical processes, we must investigate solar inactivation of rotaviruses in unpurified natural water samples, such as unpurified wastewater samples.

3. Other rotavirus strains should be tested. The two rotavirus strains investigated here showed that their susceptibility to solar and thermal treatments were different. Thus, in the natural environment it is difficult to predict how other virus strains will respond to solar or thermal treatments. A solar inactivation study with a large diversity of rotaviruses, including some naturally circulating strains, is needed to better understand the solar inactivation mechanisms of rotaviruses and better predict how these will respond to sunlight and temperature fluctuations in the environment.

Overall, our study contributes to a more complete picture of rotavirus inactivation by solar and thermal treatments. Figure 13 below summarizes the main contributions of this comprehensive study. We showed that rotaviruses were effectively inactivated upon solar irradiation, especially with full spectrum irradiation that contains UVB light. When the UVB fraction of sunlight was blocked, rotavirus inactivation greatly decreased when compared to full spectrum irradiation. However, the irradiation of natural organic matter triggered a photochemical production of radicals that, although low in concentration, indirectly inactivated rotavirus. These photo-chemically produced radicals were likely hydroxyl radicals and excited

triplet state species. Our molecular work showed that rotavirus inactivation was linked to genome damage by solar irradiation, regardless of the sunlight fraction, while thermal treatment caused primarily protein damage. Finally, our results demonstrate that new water treatment technologies should focus on increasing protein or genome damage through UVB irradiation or protein oxidation.

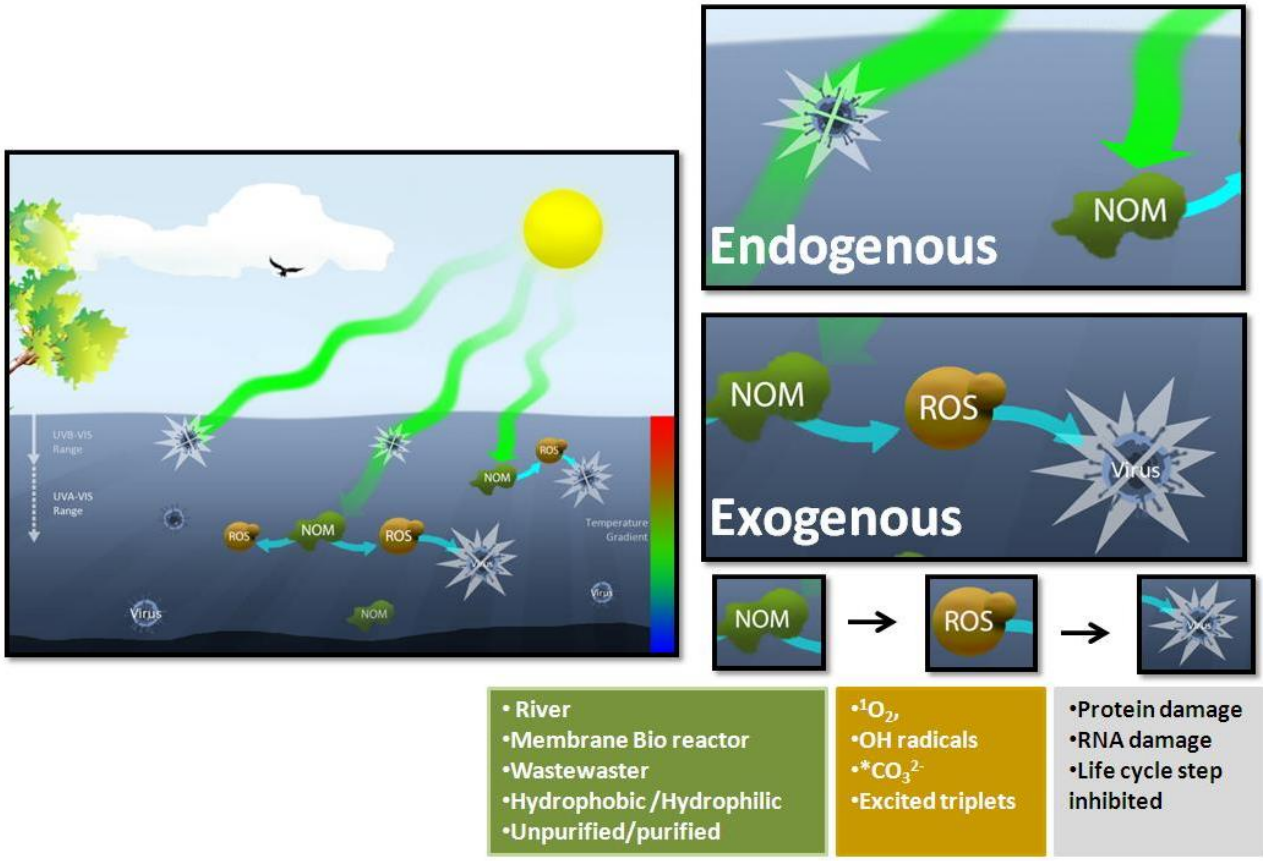

Figure 13. Diagram depicting sunlight inactivation mechanisms presumed to take place in sunlit surface waters. Depending on NOM concentrations, UVB through visible light photons can penetrate the top centimeters of a water column, thus inducing both endogenous and exogenous inactivation. UVA and visible light photons can reach deeper into a water column than UVB, and can primarily induce exogenous inactivation. The exogenous inactivation is highly dependent on the NOM or sensitizer's photoreactivity for producing ROS capable of causing viral damage. OH radicals and triple states spices are likely the main photochemically produced radicals leading to rotavirus inactivation. Upon solar treatment, damage to proteins and nucleic acid was observed.

5.1 Literature cited

Graf, J., Zebaze Togouet, S., Kemka, N., Niyitegeka, D., Meierhofer, R., & Gangoue Pieboji, J. (2010). Health gains from solar water disinfection (SODIS): evaluation of a water quality intervention in Yaoundé, Cameroon. *J. Water Health*, *8*(4), 779–96. doi:10.2166/wh.2010.003

APPENDIX

SUPPLEMENTAL TABLES AND FIGURES

A.1 Chapter 2

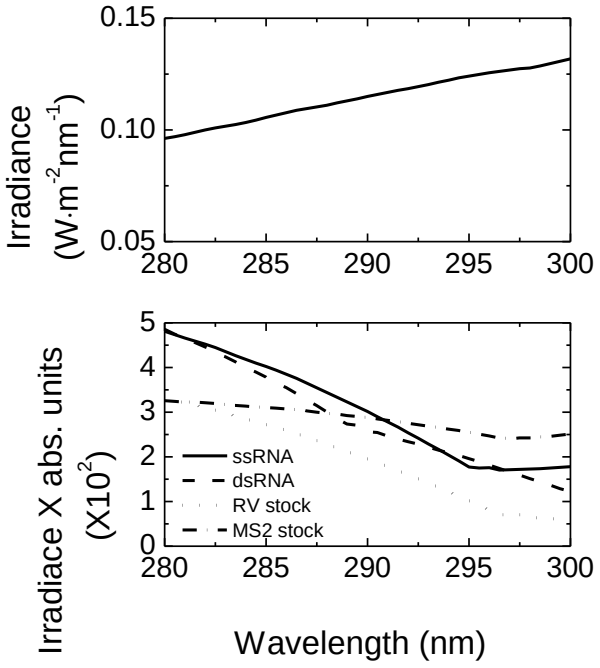

Figure A1. Irradiance spectrum of the solar simulator without the Newport 320 nm cut-off filter from 280 – 300 nm (**a**) and the product of irradiance and absorbance units of the single stranded RNA, double stranded RNA, pure rotavirus stock, and pure MS2 stock (**b**). As shown here, the product of the irradiance of the lamp and the absorbance units was highest at 280 nm for all four cases.

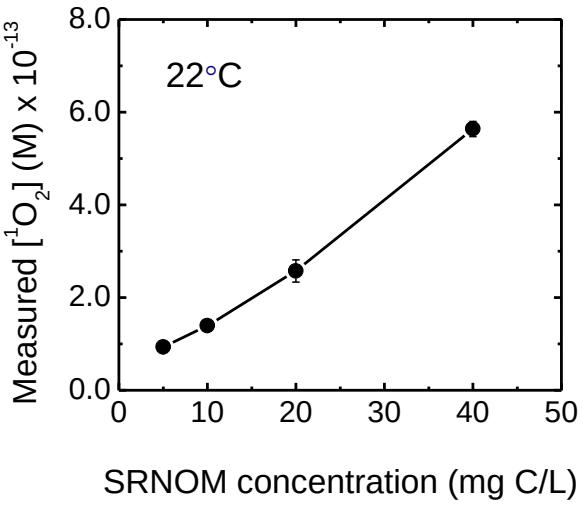

Figure A2: The measured singlet oxygen ($^1O_2$) concentration (M) as a function of SRNOM (mg C/L) in 1 mM sodium bicarbonate buffer. Furfuryl alcohol (C_0 = 40 µM) was used as probe for $^1O_2$. The data were corrected for light screening (280-400 nm) and the error bars denote 95% confidence intervals.

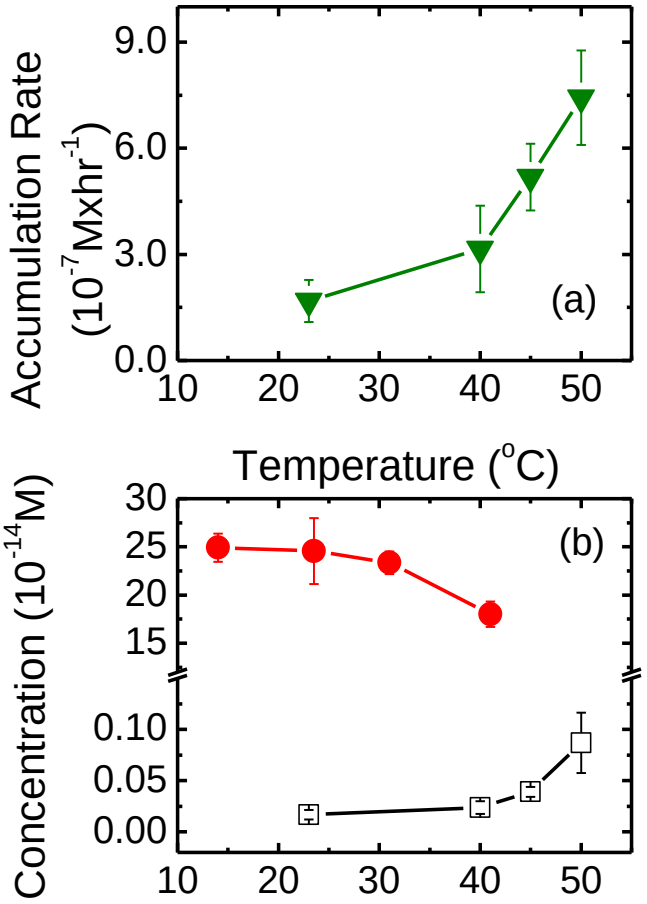

Figure A3: (**a**) Hydrogen peroxide accumulation rate (M / hr) as a function of temperature (°C) in 1 mM sodium bicarbonate buffer containing of 20 mg C/L of SRNOM and (**b**) the apparent singlet oxygen ($^1O_2$; filled circles) and hydroxyl radical (·OH; open squares) concentrations (M). Furfuryl alcohol (C_0 = 40 µM) and phenol (C_0 = 10 µM) were used as probes for $^1O_2$ and ·OH, respectively. Error bars indicate 95% confidence intervals.

Table A1a. Summary of MS2 bacteriophage inactivation by solar simulator in the presence of SRNOM

Condition		Dark (0 and 20 mg C/L SRNOM)	UVA-vis + 0 mg C/L of SRNOM	UVA-vis + 10 mg C/L of SRNOM	UVA-vis + 20 mg C/L of SRNOM	UVA-vis + 20 mg C/L of SRNOM	Full spectrum + 0 mg C/L of SRNOM	Full spectrum + 20 mg C/L of SRNOM
14 °C	k_{obs}	nd	0.20	--	0.70	--	3.3	4.0
	STDEV*		0.08	--	0.09	--	0.55	0.85
	R^2 range		0.55-0.97	--	0.98	--	0.99	0.97-0.99
	n**	1	2	--	1	--	1	2
22 ± 1 °C	k_{obs}	nd	0.26	0.48	0.88	2.04	3.5	4.23
	STDEV*		0.19	0.03	0.21	0.08	0.35	0.23
	R^2 range		0.97-0.99	0.97-0.99	0.98-0.99	0.99-1	0.99-1	0.98-0.99
	n**	2	4	2	3	2	2	2
33± 1 °C	k_{obs}	nd	0.22	--	1.16	--	3.34	4.49
	STDEV*		0.03	--	0.14	--	0.37	1.1
	R^2 range		0.99	--	0.99	--	0.99	0.98
	n**	1	1	--	1	--	1	1
42 ±1 °C	k_{obs}	nd	0.26	--	1.6	--	3.9	5.0
	STDEV*		0.14	--	0.30	--	0.3	0.36
	R^2 range		0.97-0.99	--	0.99-1	--	0.99-1	0.95-0.99
	n**	2	3	--	3	--	2	2
50 °C	k_{obs}	0.5	1.26		3.0			
	STDEV*	0.2	0.21		0.24			
	R^2 range	0.99	0.96		0.97			
	n**	1	1		1			

Table A1a (continued)
nd-denotes an inactivation kinetic plot whose slope did not differ from a slope of zero ($p > 0.05$).
*STDEV is the standard deviation and applies only to conditions where $n > 1$. Wherever $n = 1$, the 95% confidence interval was reported.
**n denotes the number of experiments, each with one replicate. We conducted MS2 inactivation experiments with two different MS2 stocks. The trend for most conditions was replicated. In the manuscript figures, we only showed and discussed data from a single MS2 stock.

Table A1b. Summary of Rotavirus inactivation by solar simulator in the presence of SRNOM

Condition		Dark 0 and 20 mg C/L SRNOM	UVA-vis + 0 mg C/L of SRNOM	UVA-vis + 0 mg C/L of SRNOM in D_2O	UVA-vis + 20 mg C/L of SRNOM	UVA-vis + 20 mg C/L of SRNOM in D_2O	Full spectrum + 0 mg C/L of SRNOM	Full spectrum + 20 mg C/L of SRNOM
14 °C	k_{obs}	Nd	0.3	--	0.33	--	7.8	7.31
	STDEV*		0.1	--	0.11	--	0.2	1.4
	R^2 range		0.95	--	0.98	--	0.95-0.99	0.99
	n**	1	1	--	1	--	3	2
23 -26 °C	k_{obs}	Nd	0.30	0.29	0.4	0.26	9.25	8.58
	STDEV*		0.23	0.02	0.17	0.02	1.12	3
	R^2 range		0.94-0.99	0.95-0.96	0.98-0.99	0.98-0.99	0.98-0.99	.98-0.99
	n**	2	5	2	5	2	4	4
34 °C	k_{obs}	nd	0.27	--	0.30	--	10	8.63
	STDEV*		0.16	--	0.09	--	2.57	4.5
	R^2 range		0.98-0.99	--	0.96	--	0.96	0.99
	n**	1	2	--	1	--	1	2
42±1 °C	k_{obs}	nd	0.29	--	0.55	--	11.4	9.42
	STDEV*		0.25	--	0.08	--	0.12	3.3
	R^2 range		0.99	--	0.99	--	0.99-1	0.97-0.99
	n**	2	2	--	2	--	2	3
50 °C	k_{obs}	0.33	0.5	--	1.43	1.56		
	STDEV*	0.08	0.17	--	0.20	0.16		
	R^2 range	0.96-0.99	0.94-0.99	--	0.97-0.99	0.97-0.99		
	n**	2	2	--	5	2		

nd-denotes an inactivation kinetic plot whose slope did not differ from a slope of zero ($p > 0.05$).

*STDEV is the standard deviation and applies only to conditions where $n > 1$. Wherever $n = 1$, the corresponding 95% confidence interval was reported.

**n denotes the number of experiments, each with one replicate. Most rotavirus inactivation conditions were replicated in separate experiments with distinct rotavirus stocks. Although undesirable, different rotavirus stocks were needed due to low rotavirus yield. However, as noted in the table, the rotavirus inactivation trend was consistent. In the manuscript, we only showed and discussed data from a single rotavirus stock.

Table A1c. Rotavirus quenching test

Condition	**50 °C**			
	k_{obs}	**std*** **	**R^2 range**	**n****
UVA-vis + 20 mg/L as DOC + 50 mM L-Histidine	1.74	0.24	0.98	2
UVA-vis + 20 mg/L as DOC + 200 U/mL Catalase	0.67	0.11	0.92-0.99	3
Dark: 6 uM H_2O_2	0.23	0.18	0.96	1
Dark: 60 uM H_2O_2	0.41	0.32	0.95	1
Dark: 600 uM H_2O_2	5.48	3.06	0.97	1

Table A2. Rotavirus inactivation rates with quenching tests at 50 °C

Condition Tested	k_{obs} (hr^{-1})	95% Confidence Interval
Dark -0/20 mg C/L of SRNOM	0.5	0.2
0 mg C/L of SRNOM	0.5	0.2
20 mg C/L of SRNOM	1.5	0.3
20 mg C/L of SRNOM + D_2O	1.5	0.2
20 mg C/L of SRNOM + 50 mM L-Histidine	1.6	0.2
20 mg C/L of SRNOM + 200 U/mL Catalase	0.7	0.3

A.2 Chapter 3

Chemicals and Reagents. The following chemicals were of the purest grade available from commercial sources and were used as received: phenol (99+% Acros Organics); Sodium nitrite (98.5% Acros Organics); Sodium nitrate (99+%, Acros Organics); 3'-methoxyacetophenone (3'-MAP; 98%, Acros); Sorbic acid (*trans, trans*-hexadienoic acid, t, t-HDA, 99% Acros Organics). Quenching agents*:* L-Histidine (98% Acros Organics) and catalase from bovine liver (Aldrich) were also used as received. HPLC reagents: methanol (99.9% HPLC grade: Sigma), acetonitrile (99.9 % HPLC grade; Sigma), formic acid (98% Fluka) were also used as received. Solutions were prepared with deionized water purified with Barnstead nanopure water system.

Propagation and Concentration of the Model Viruses. Porcine rotavirus OSU (ATCC #VR-892) and human rotavirus Wa (ATCC #VR-2018) were obtained from the American Type Culture Collection (ATCC). Both strains were propagated in monkey kidney cell lines (MA104; ATCC #CRL-2378.1) after treatment with 10 µg/mL trypsin from porcine pancreas (Sigma Aldrich) for 30 min and incubation in Minimum Essential Media (MEM; Gibco) containing 0.5 µg/mL of trypsin as described in detail elsewhere (Arnold, Patton, & McDonald, 2009). Briefly, the rotavirus was then purified through three-time sequential freezing at -80°C and thawing, followed by centrifugation at 1000 g for 10 minutes at 20°C to remove cell debris. Thereafter, rotavirus was filtered through a filtration membrane (Thermo Scientific, Nalgene) of pore size 0.45 µm to remove cell debris. Lastly, the 0.45 µm membrane permeate was concentrated on an ultrafiltration membrane (polymer polyvinylidene fluoride; Koch Membrane) of 100 kDa and rotavirus was retained in the retentate of the 100 kDa filtration unit. The final rotavirus stock concentration ranged between 10^5-10^6 focus forming units (FFU) per mL. Rotavirus stocks were stored in the

dark at 4°C. Samples were enumerated through an immunochemical infectivity assay and quantified as focus forming units per mL (FFU/mL) as described in detail in our previous publication (Romero, Straub, Kohn, & Nguyen, 2011). Two different stocks (Stock 1 and Stock 2) of human rotaviruses were used for the experiments reported here. The two stocks followed the same inactivation trend with different photosensitizers as shown in Figure A5 in the Appendix. Unless otherwise stated, all human rotavirus inactivation tests were conducted with Stock 1.

Cell Growth and Infectivity Assay. The rotavirus focus forming assay and enumeration procedures were described in more detail elsewhere (Rolsma, Gelberg, & Kuhlenschmidt, 1994; Romero et al., 2011). Briefly, a MA-104 cell line was maintained and utilized throughout the duration of the experiments. Cells were grown in Minimal Essential Medium (Harry Eagle's MEM; Gibco) containing 5% fetal bovine serum (FBS; Invitrogen) and 1X Antibiotic-Antimycotic (100X; Invitrogen). MA104 were maintained in an incubator with 5% CO_2 at 37°C until confluence was achieved. Confluent 96-well tissue culture plates (FD Falcon, Fisher) were inoculated with diluted samples from the reactor experiments. Trypsin was added to each sample at a concentration of 10 µg/ml for 30 min prior to infection to activate the virus binding site.(Arnold et al., 2009) Confluent wells were rinsed twice with sterile phosphate buffer. A diluted sample aliquot of 50µL was added to a confluent and washed well and incubated at 37°C for 30 minutes. Each diluted sample was plated in duplicate. Following incubation, the wells were rinsed twice with non-complete MEM and incubated at 37°C for 18 hours. Focus forming unit method was performed on the well plates after incubation. Rotavirus infection occurring in the MA-104 cells was quantified using light microscopy.

Quenching Tests & Dark Hydrogen Peroxide (H_2O_2) Inactivation Tests. Quenching tests were conducted to suppress the steady state concentrations of singlet oxygen ($^1O_2$) and H_2O_2 in the irradiated solutions containing DOM isolates. L-histidine was used for $^1O_2$ and catalase for H_2O_2 at concentrations of 50 mM and 200 U/mL, respectively. For the dark inactivation tests with H_2O_2, commercially available H_2O_2 (30%, Fisher) was used.

SUVA Determination. SUVA values were determined for DOM solutions prepared from lyophilized soluble (i.e.,filtered through 0.45 µm membrane) DOM isolates. SUVA values are the results of the division of the UV absorbance measured at 254 nm and the TOC (DOC) content of the solutions prepared. Low ionic strength buffer used in our work has no impact on the UV absorbance of DOM solution and, as a consequence, on SUVA. Analyses conducted on 0.45 µm filtered solution showed that lyophilised DOM fractions are fully soluble when prepared at near neutral pH buffer. SUVA values are more generally expressed as $cm^{-1}.L.mg^{-1}$ (unit used in our paper) and traditionally ranged from 2 (low SUVA) to 5 (high SUVA). Thus, the SUVA values were expressed in linear scale.

Figure A4. Rationale for the experiments conducted in this study

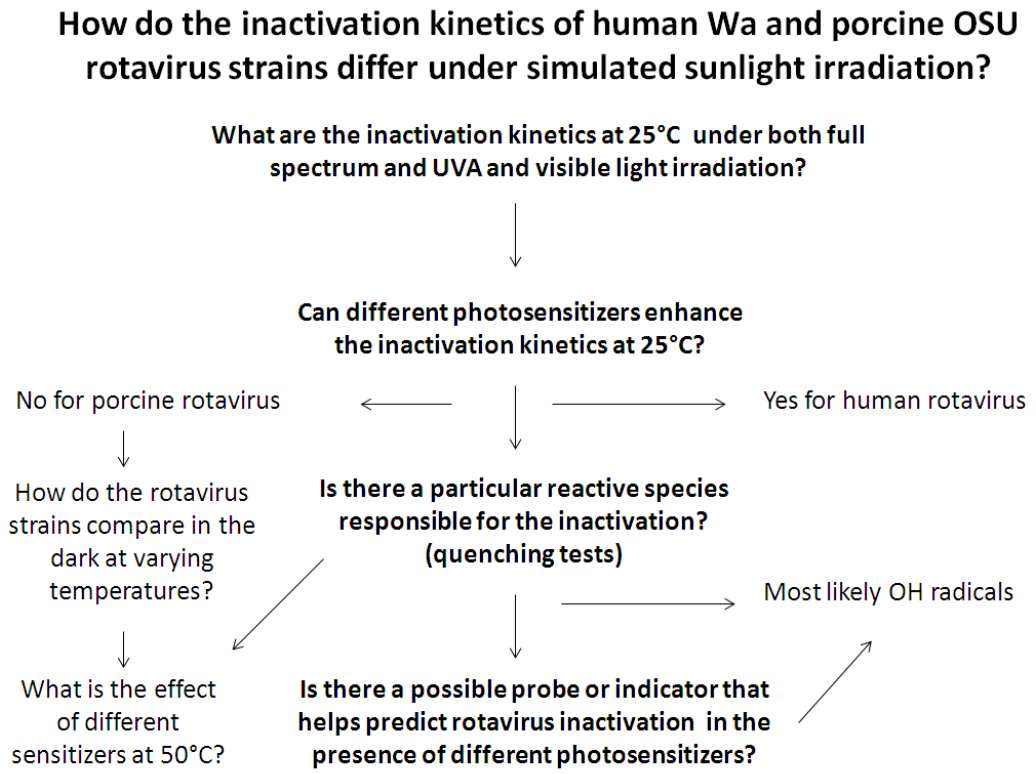

Experiments conducted to address the question
1. Human and porcine rotavirus inactivation tests at 25°C irradiated with UVA and visible light 2. Human rotavirus inactivation with full spectrum irradiation
3. Human and porcine rotavirus inactivation tests at 25°C irradiated with UVA and visible light in the presence of BRHPO 4. Dark inactivation experiments at varying temperatures for both rotavirus strains 5. Human rotavirus inactivation by full spectrum in the presence of BRHPO
6. Human and porcine rotavirus inactivation with different photosensitizers at 25°C and 50°C, respectively 7. Quenching tests 8. Role of $NaNO_2$ in solutions containing DOM
9. Phenol decay measurements in different photosensitizers at 25°C and correlation with human rotavirus inactivation 10. Excited triplet state measurements 11. SUVA measurements for the DOM isolates and correlations with rotavirus inactivation

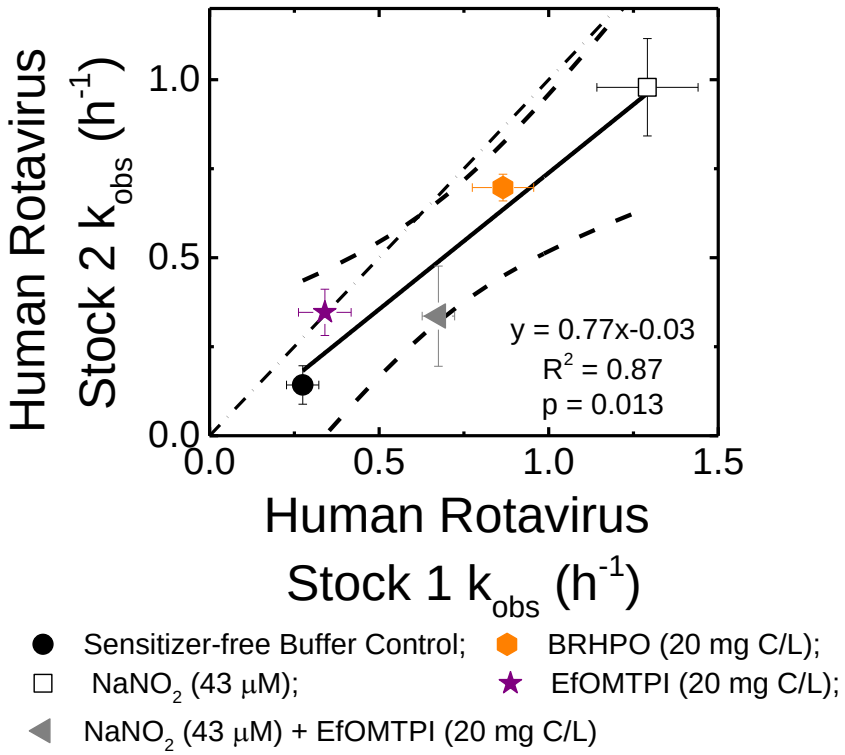

Figure A5. Comparison of the human rotavirus k_{obs} values for Stock 1 and Stock 2 in the presence of various photosensitizers at 25°C in 1 mM $NaHCO_3$ buffer. Stock 2 appears to be slightly less resistant (0.77X) to solar-induced exogenous inactivation than Stock 1. However, the inactivation trend remains the same for both human rotavirus stocks. The dash dotted (-·-) line of slope = 1 is included for comparison to the linear regression line.

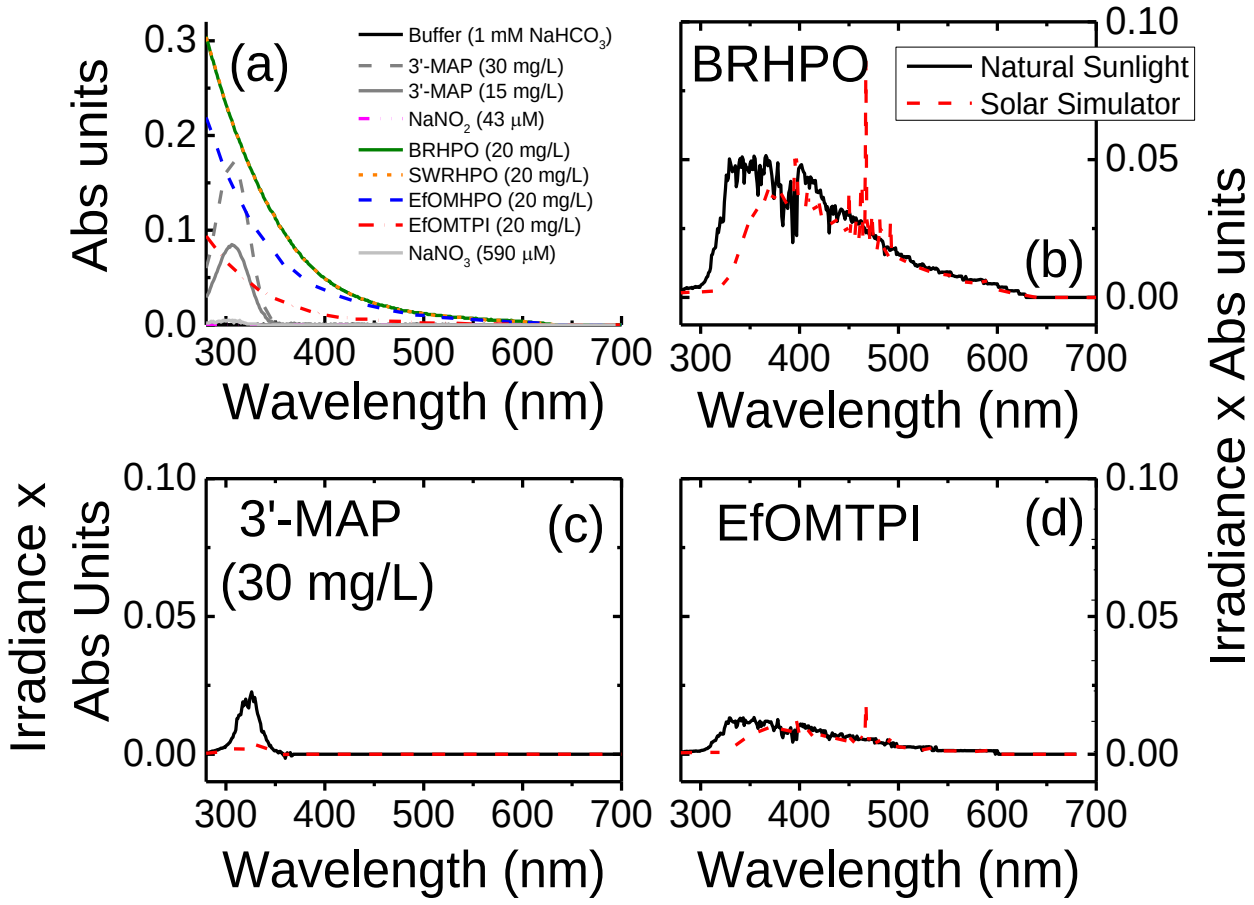

Figure A6. **(a)** The absorbance spectra of the photosensitizers used in this study and the plots showing the product of the irradiance and the absorbance of **(b)** 20 mg C/L BRHPO, **(c)** 30 mg/L 3'-MAP and **(d)** 20 mg C/L EfOMTPI for each wavelength from 280 to 700 nm. The irradiance values ($W/m^2/nm$) were measured for natural sunlight or for the filtered (320 nm cut-off) solar simulator and the spectra are shown in Figure 1a.

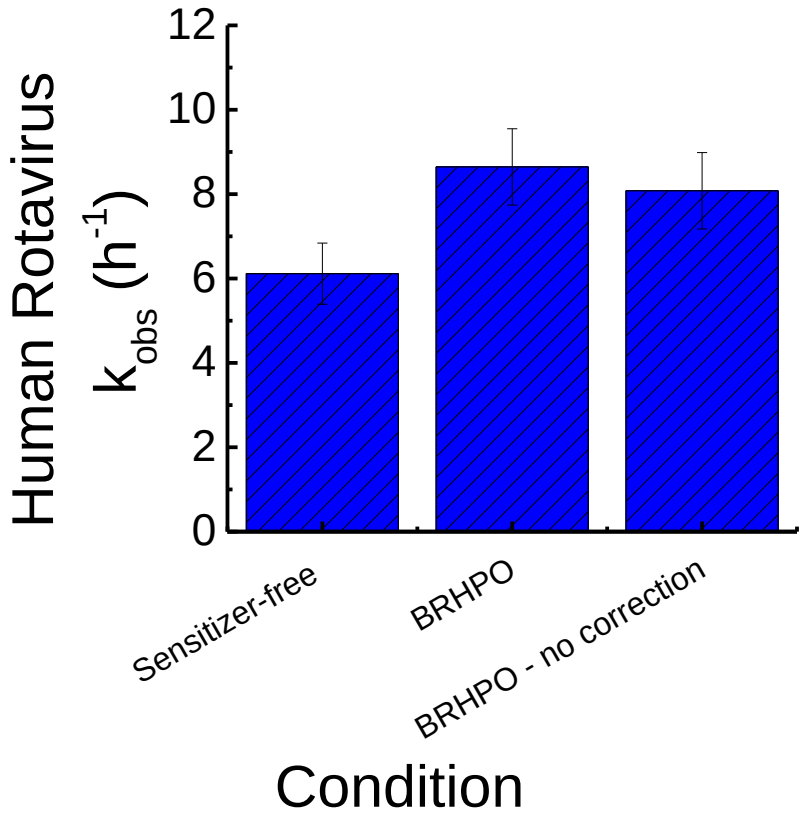

Figure A7. Human rotavirus k_{obs} (Stock 2) values (h^{-1}) obtained under full spectrum irradiation at 25°C in 1 mM $NaHCO_3$ buffer in the presence of absence of 20 mg C/L BRHPO. The bars denoted the averages and corresponding standard deviations ($N \geq 3$) of the human rotavirus k_{obs} values obtained after linear regression analysis.

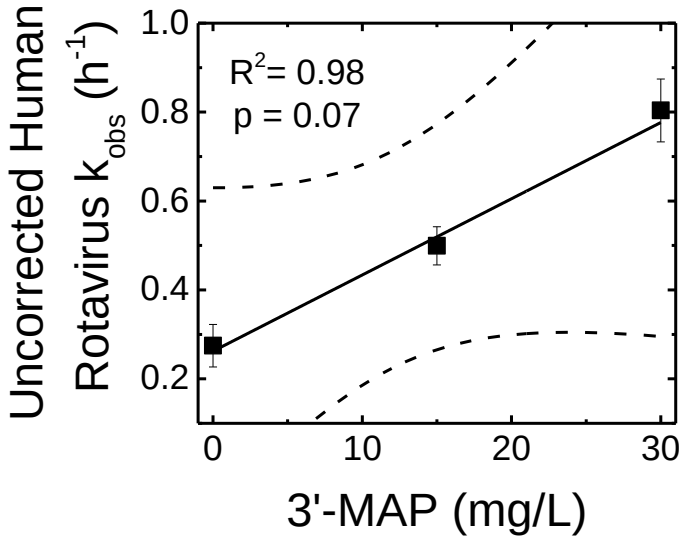

Figure A8. Uncorrected human rotavirus k_{obs} values as a function of 3'-MAP concentrations (mg/L) obtained at 25°C in 1 mM $NaHCO_3$ buffer (pH 7.9). The solid lines in the integrated figure indicate the linear regression line and the dashed lines indicate the 95% confidence intervals of the regression.

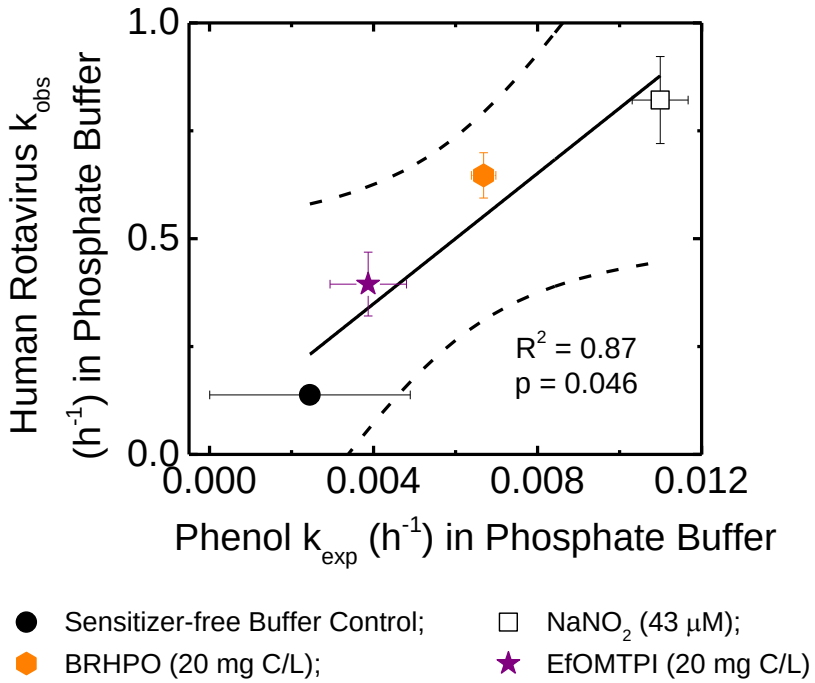

Figure A9. Human rotavirus (Stock 2) k_{obs} values as a function of the phenol k_{exp} (h^{-1}) obtained in bicarbonate-free (1 mM phosphate) buffer at 25°C and pH 7.9. The solid lines indicate the linear regression line and the dashed lines indicate the 95% confidence intervals of the regression.

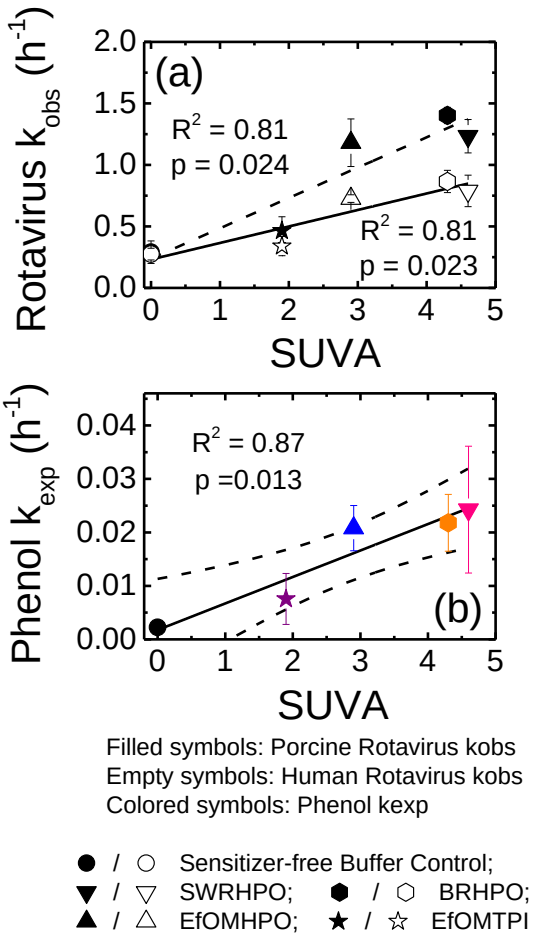

Figure A10. (a) Rotavirus k_{obs} values and **(b)** phenol k_{exp} values corrected for light screening as a function of the specific UV_{254nm} absorbance (SUVA) of solutions containing DOM isolates and the buffer control in 1 mM $NaHCO_3$ buffer (pH 7.9). For Figure A10a, the solid lines denote the linear regression line for the porcine and human rotavirus k_{obs} values as a function of the SUVA values for five different solutions. For Figure A10b, the solid lines indicate the linear regression line and the dashed lines denote the 95% confidence intervals of the regression.

Table A3. Summary of inactivation kinetic data for human rotavirus Wa (Stock 1) obtained at 25°C

Photosensitizer[a]	Number of uncorrected human rotavirus replicates reported as uncorrected k_{obs} values (h^{-1})[b]					Average uncorrected k_{obs} values (h^{-1})	Correction factor	Corrected k_{obs} value (h^{-1})	STDEV	R^2 range
	1	2	3	4	5					
Sensitizer-Free Buffer Control	0.31	0.22	0.29			0.27		0.27	0.05	0.96-0.99
BRHPO (20 mg C/L)	0.84	0.66	0.87	0.83	0.84	0.81	1.07	0.87	0.09	0.97-0.99
SWRHPO (20 mg C/L)	0.80	0.83	0.79	0.51	0.77	0.74	1.07	0.79	0.13	0.94-0.99
EfOMTPI (20 mg C/L)	0.25	0.36	0.40			0.33	1.02	0.34	0.08	0.91-0.95
EfOMHPO (20 mg C/L)	0.72	0.72	0.66	0.67		0.69	1.05	0.73	0.03	0.93-99
$NaNO_2$ (43 µM)	1.38	1.03	1.35	1.32	1.37	1.29		1.29	0.15	0.94-0.99
$NaNO_3$ (590 µM)	0.55	0.41	0.32	0.53		0.45		0.45	0.11	0.87-0.99
3'MAP (30 mg/L)	0.77	0.75	0.88			0.80	1.13	0.91	0.07	0.89-0.97
3'MAP (15 mg/L)	0.52	0.53	0.45			0.50	1.06	0.53	0.04	0.89-0.98
EfOMTPI (20 mg C/L) + $NaNO_2$ (43 µM)	0.64	0.71				0.67	1.02	0.68	0.05	0.68-0.95

[a] Unless otherwise indicated, all experiments were conducted in 1 mM $NaHCO_3$ buffer and irradiated with UVA and visible light.

[b] Each k_{obs} value is the slope of the $\ln(N/N_{initial})$ vs. time (h^{-1}) plot from an independent experiment. For each experiment, at least four time points were collected, plated in duplicate, and averaged to generate the $\ln(N/N_{initial})$ vs. time (h^{-1}) plot. Linear regression was used to calculate the slope ($-k_{obs}$ value) and the corresponding R^2 value.

Note: at least one independent dark control experiments was conducted for each buffer solution and the following conditions: sensitizer-free buffer control, 20 mg C/L of DOM, 30 mg/L 3'-MAP, 590 µM $NaNO_3$, and BRHPO (20 mg C/L) with $NaNO_2$ (43 µM). The dark inactivation plots did not deviate from a slope of 0 ($p > 0.05$).

Table A4. Summary of inactivation kinetic data for human rotavirus Wa (Stock 2) obtained at 25°C

Photosensitizer[a]	Number of uncorrected human rotavirus replicates reported as uncorrected k_{obs} values (h^{-1})[b]					Average uncorrected k_{obs} values (h^{-1})	Correction factor	Corrected k_{obs} value (h^{-1})	STDEV	R^2 range
	1	2	3	4	5					
Sensitizer-Free Buffer Control	0.17	0.08	0.17			0.14		0.14	0.05	0.90-0.95
BRHPO (20 mg C/L)	0.69	0.64	0.62			0.65	1.07	0.70	0.04	0.96-0.98
$NaNO_2$ (43 µM)	0.86	1.07	1.12	0.87		1.29		1.29	0.15	0.94-0.99
EfOMTPI (20 mg C/L) + $NaNO_2$ (43 µM)	0.23	0.32	0.53			0.33	1.02	0.34	0.14	0.84-0.97
BRHPO (20 mg C/L) + $NaNO_2$ (43 µM)	0.50	0.51	0.73			0.56	1.07	0.60	0.11	0.81-0.99
EfOMTPI (20 mg C/L)	0.29	0.28				0.34	1.02	0.35	0.06	0.95-0.98
Sensitizer-Free Buffer Control[c]	0.13	0.15	0.13	0.15		0.14		0.14	0.01	0.77-0.96
BRHPO (20 mg C/L)[c]	0.54	0.64	0.65	0.58		0.60	1.07	0.65	0.05	0.93-0.99
$NaNO_2$ (43 µM)[c]	0.74	0.93	0.78			0.82		0.82	0.10	0.91-0.98
EfOMTPI (20 mg C/L)[c]	0.39	0.39				0.39	1.02	0.39	0.00	0.95-0.97
Sensitizer-Free Buffer Control[d]	6.31	6.73	5.31			6.11		6.11	0.73	0.84-0.92
BRHPO (20 mg C/L)[d]	8.39	8.12	8.98	6.83		8.08	1.07	8.64	0.44	0.93-0.99

[a] Unless otherwise indicated, all experiments were conducted in 1 mM $NaHCO_3$ buffer and irradiated with UVA and visible light.

[b] Each k_{obs} value is the slope of the $\ln(N/N_{initial})$ vs. time (h^{-1}) plot from an independent experiment. For each experiment, at least four time points were collected, plated in duplicate, and averaged to generate the $\ln(N/N_{initial})$ vs. time (h^{-1}) plot. Linear regression was used to calculate the slope ($-k_{obs}$ value) and the corresponding R^2 value.

[c] These experiments were conducted in 1mM phosphate buffer and irradiated with UVA and visible light

[d] These experiments were conducted in 1 mM $NaHCO_3$ buffer and irradiated with full spectrum irradiation

Note: at least one independent dark control experiments was conducted for each buffer solution and the following conditions: sensitizer-free buffer control, 20 mg C/L of DOM, and BRHPO (20 mg C/L) with $NaNO_2$ (43 µM). The inactivation plots did not deviate from a slope of 0 ($p > 0.05$).

Table A5. Summary of inactivation kinetic data for porcine rotavirus OSU

Photosensitizer[a]	Number of uncorrected human rotavirus replicates reported as uncorrected k_{obs} values (h^{-1})[b]					Average uncorrected k_{obs} values (h^{-1})	Correction factor	Corrected k_{obs} value (h^{-1})	STDEV	R^2 range
	1	2	3	4	5					
Sensitizer-Free Buffer Control	0.42	0.29	0.27	0.16	0.31	0.29		0.29	0.09	0.86-0.99
BRHPO (20 mg C/L)	1.24	1.37	1.32			1.31	1.07	1.40	0.07	0.95-0.96
SWRHPO (20 mg C/L)	1.31	1.01	1.07	1.21		1.15	1.07	1.23	0.14	0.90-0.99
EfOMTPI (20 mg C/L)	0.50	0.36	0.57	0.34	0.52	0.46	1.02	0.47	0.11	0.95-0.99
EfOMHPO (20 mg C/L)	0.90	1.24	1.23			1.12	1.05	1.18	0.19	0.90-0.99
$NaNO_2$ (43 µM)	1.75	1.55	1.84	1.82	2.31	1.85		1.85	0.25	0.88-0.99
$NaNO_3$ (590 µM)	0.86	0.47	0.76	0.56		0.66		0.66	0.18	0.91-0.99
3'MAP (30 mg/L)	1.45	1.68	1.48			1.54	1.13	1.74	0.12	0.95-0.98
Sensitizer-Free Buffer Control[c]	0.12	0.11	0.15			0.13		0.13	0.02	0.86-0.99
BRHPO (20 mg C/L)[c]	0.14	0.09	0.28			0.17	1.07	0.18	0.10	0.62-0.78

[a] Unless otherwise indicated, all experiments were conducted at 50°C in 1 mM $NaHCO_3$ buffer and irradiated with UVA and visible light.

[b] Each k_{obs} value is the slope of the $\ln(N/N_{initial})$ vs. time (h^{-1}) plot from an independent experiment. For each experiment, at least four time points were collected, plated in duplicate, and averaged to generate the $\ln(N/N_{initial})$ vs. time (h^{-1}) plot. Linear regression was used to calculate the slope ($-k_{obs}$ value) and the corresponding R^2 value.

[c] These conditions were conducted at 25°C in 1 mM $NaHCO_3$ buffer and irradiated with UVA and visible light

Note: two independent dark control experiments were conducted for each buffer solution and the following conditions: sensitizer-free buffer control, 20 mg C/L of DOM, 30 mg/L 3'-MAP, 590 µM $NaNO_3$, and BRHPO (20 mg C/L) with $NaNO_2$ (43 µM). The inactivation plots did not deviate from a slope of 0 ($p > 0.05$).

Table A6. Summary of phenol decay rate constants (k_{exp}) obtained at 25°C

Photosensitizer[a]	Number of uncorrected phenol replicates reported as uncorrected k_{exp} values ($x10^{-2}$)[b]					Average uncorrected k_{exp} (h^{-1}) values ($x10^{-2}$)	Correction factor	Corrected k_{exp} (h^{-1}) value ($x10^{-2}$)	STDEV ($x10^{-2}$)	R^2 range
	1	2	3	4	5					
Sensitizer-Free Buffer Control	0.28	0.20	0.29	0.29	0.18	0.22		0.22	0.04	0.63-0.99
BRHPO (20 mg C/L)	2.27	2.68	1.59	1.61		2.04	1.07	2.18	0.53	0.76-0.99
SWRHPO (20 mg C/L)	3.64	1.60	1.57			2.27	1.07	2.43	1.19	0.90-0.96
EfOMTPI (20 mg C/L)	0.48	1.29	0.46			0.74	1.02	0.76	0.48	0.80-0.94
EfOMHPO (20 mg C/L)	2.28	1.68				1.98	1.05	2.08	0.42	0.90-0.99
$NaNO_2$ (43 µM)	4.79	3.45	3.39			3.88		3.88	0.79	0.88-0.99
$NaNO_3$ (590 µM)	0.77	1.02	0.94			0.91		0.91	0.12	0.94-0.99
3'MAP (30 mg/L)	0.85	1.11				0.98	1.13	1.11	0.18	0.91-0.97
EfOMTPI (20 mg C/L) + $NaNO_2$ (43 µM)	1.27	0.73				1.00	1.02	1.02	0.38	0.85-0.99
BRHPO (20 mg C/L) + $NaNO_2$ (43 µM)	1.62	1.13				1.38	1.07	1.47	0.51	0.90-0.92
Sensitizer-Free Buffer Control[c]	0.07	0.42				0.25		0.25	0.24	0.60-0.70
BRHPO (20 mg C/L)[c]	0.60	0.65				0.63	1.07	0.67	0.03	0.80-0.98
EfOMTPI (20 mg C/L)[c]	0.31	0.45				0.38	1.02	0.39	0.09	0.96-0.99
$NaNO_2$ (43 µM)[c]	1.15	1.05				1.1		1.1	0.07	0.97-0.98

[a] Unless otherwise indicated, all experiments were conducted in 1 mM $NaHCO_3$ buffer and irradiated with UVA and visible light.

[b] Each k_{obs} value is the slope of the $\ln(N/N_{initial})$ vs. time (h^{-1}) plot from an independent experiment. For each experiment, at least four time points were collected, analyzed by the HPLC, and averaged to generate the $\ln(N/N_{initial})$ vs. time (h^{-1}) plot. . Linear regression was used to calculate the slope ($-k_{obs}$ value) and the corresponding R^2 value.

[c] These conditions were conducted in 1mM phosphate buffer

Note: at least one independent dark control experiment was conducted for each buffer containing buffer only, BRHPO (20 mg C/L), EfOMTPI (20 mg C/L), $NaNO_2$ (43 µM), 30 mg/L 3'MAP, and DOM+$NaNO_2$ (conditions shown above). The dark inactivation plots did not deviate from a slope of 0 ($p > 0.05$).

Table A7. Summary of excited triplet state concentrations.

Photosensitizer	Excited triplet state concentrations (fM) Set 1	Excited triplet state concentrations (fM) Set 2	Average excited triplet state concentrations (fM)
3'-MAP (30 mg/L)	5.29	4.4	4.87
3'-MAP (15 mg/L)	1.69[a]	1.83[a]	1.76
EfOMHPO (20 mg C/L)	0.47[a]	0.42[a]	0.45
EfOMTPI (20 mg C/L)	0.42[a]	0.37[a]	0.39
BRHPO (20 mg C/L)	0.23[a]	0.24	0.23
SWRHPO (20 mg C/L)	0.16[a]	0.14[a]	0.15

[a] Excited state triplet concentrations were previously reported in Rosado-Lausell *et al.* (2013).(Rosado-Lausell et al., 2013)

Steady-state concentrations of excited triplet states of dissolved organic matter were measured using sorbic acid (trans, trans-hexadienoic acid, t, t-HDA) as a chemical probe, as described elsewhere.(Grebel, Pignatello, & Mitch, 2011) Briefly, the 8-mL reactors contained 20 mg C/L of sensitizers in 1 mM $NaHCO_3$ at pH 7.9 ± 0.2, and were spiked with 5 different concentrations ranging from 100 µM to 1000 µM of sorbic acid. A non-irradiated reactor containing 200 µM of t, t-HDA was also prepared and sampled to confirm that no other degradation pathway was responsible for the decay of the probe. Two sets of experiments were conducted for 21 to 24 hours and sampled every 5 to 6 hours. Photo-products of sorbic acid after reacting with triplet states were analyzed using the HPLC and four isomer peaks were identified (trans-trans, trans-cis, cis-trans, and cis-cis species). The molar absorption coefficients provided by Grebel *et al.* (2011) were used to calculate the concentrations of the isomers produced. The cis-trans isomer concentrations were used to calculate the triplet removal rates by the probe, which were subsequently applied to calculate excited triplet formations and the steady-state concentrations of the triplet states produced upon irradiation.

Table A8. Human and porcine inactivation rate constants obtained in dark experiments as a function of temperature

Temperature (°C)	Human k_{obs} (h^{-1}) ± 95% CI	R^2	Porcine k_{obs} (h^{-1}) ± 95% CI	R^2
25*	0.01 ± 0.1	0.17	0.05 ± 0.26	0.10
40	0.51 ± 0.4	0.93	0.07 ± 0.04	0.88
50	6.80 ± 4.7	0.95	0.28 ± 0.15	0.99
57	51.5 ± 7.8	0.98	2.54 ± 0.60	0.96

*****Inactivation kinetic plots do not statistically differ from a slope of 0. Linear regression p-values for human and porcine rotavirus inactivation kinetics at 25°C were 0.58 and 0.60, respectively.

These experiments were conducted once for porcine rotavirus because these experiments had been conducted before for our previous publication and the results were replicated.(Romero et al., 2011) For human rotavirus, the dark experiments were conducted in parallel and the k_{obs} values were very different at each temperature. Therefore, the trend was easily observed. For human rotavirus, the k_{obs} value at 50°C was replicated, but for consistency, only the experiments conducted in parallel were reported. Experiments that were conducted in parallel were also plated in parallel on the same confluent plate resulting in less variability. The irradiation experiments had to be replicated because most of the conditions could not be conducted in parallel or plated on the same confluent plate.

Table A9. Effects of quenching on human and porcine rotavirus inactivation kinetics

Condition*	Human Rotavirus ratios		Porcine Rotavirus ratios	
	$k_{obs\text{-}Lhistidine}/k_{obs}$	$k_{obs\text{-}catalase}/k_{obs}$	$k_{obs\text{-}Lhistidine}/k_{obs}$	$k_{obs\text{-}catalase}/k_{obs}$
BRHPO	1.1	0.72	1.0	0.20
SWRHPO	1.0	0.70	1.1	0.49
EfOMHPO	0.97	0.54	1.1	0.26

*For each DOM condition, the DOC concentration was 20 mg C/L.

For each DOM, the tests with and without the quencher were conducted in parallel. Experiments that were conducted in parallel were also plated in parallel on the same confluent plate and leaving less room for variability. For porcine rotavirus, the trend was replicated in our previous publication.(Romero et al., 2011)

Table A10. Human Rotavirus Inactivation in the dark at 25°C with [H_2O_2] in 1 mM $NaHCO_3$

[H_2O_2] µM	k_{obs}	R^2	95% CI	p value
6		0.06		0.38*
60		0.2		0.63*
600	0.32	0.84	0.11	0.03
1000	0.26	0.96	0.07	0.02

*Denote linear regression plots that did not deviate from a slope of 0 ($p > 0.05$).

These experiments were conducted in parallel. In our previous study(Romero et al., 2011) we showed that irradiation of 20 mg C/L at 50°C did not accumulate [H_2O_2] higher than 6 µM. The purpose of this experiment was to assess whether or not [H_2O_2] of 6 µM inactivated human rotavirus at 25°C in 1 mM $NaHCO_3$. Our results showed that a H_2O_2 concentration of up to 60 µM did not increase the inactivation kinetics of human rotavirus. The other [H_2O_2] concentrations were tested to identify what concentration range led to human rotavirus inactivation. These tests showed that very high [H_2O_2] (600 µM) is needed for human rotavirus inactivation. These tests were conducted in parallel, which results in less variability.

A.2.1 Literature cited for Chapter 2 Appendix

Arnold, M., Patton, J. T., & McDonald, S. M. (2009). Culturing, storage, and quantification of rotaviruses. *Curr. Protoc. Microbiol.*, *15*, Unit 15C.3. doi:10.1002/9780471729259.mc15c03s15

Grebel, J. E., Pignatello, J. J., & Mitch, W. a. (2011). Sorbic acid as a quantitative probe for the formation, scavenging and steady-state concentrations of the triplet-excited state of organic compounds. *Water Res.*, *45*(19), 6535–6544. doi:10.1016/j.watres.2011.09.048

Rolsma, M. D., Gelberg, H. B., & Kuhlenschmidt, M. S. (1994). Assay for evaluation of rotavirus-cell interactions: identification of an enterocyte ganglioside fraction that mediates group A porcine rotavirus recognition. *J. Virol.*, *68*(1), 258–68. Retrieved from http://www.pubmedcentral.nih.gov/articlerender.fcgi?artid=236285&tool=pmcentrez&rendertype=abstract

Romero, O. C., Straub, A. P., Kohn, T., & Nguyen, T. H. (2011). Role of temperature and Suwannee River natural organic matter on inactivation kinetics of rotavirus and bacteriophage MS2 by solar irradiation. *Environmental Science & Technology*, *45*(24), 10385–10393. doi:10.1021/es202067f

Rosado-Lausell, S. L., Wang, H., Gutiérrez, L., Romero-Maraccini, O. C., Niu, X.-Z., Gin, K. Y. H., … Nguyen, T. H. (2013). Roles of singlet oxygen and triplet excited state of dissolved organic matter formed by different organic matters in bacteriophage MS2 inactivation. *Water Research*, *47*(14), 4869–4879. doi:10.1016/j.watres.2013.05.018

A.3 Chapter 4

Figure A11. Summary of the rotavirus replication cycle and our experimental approaches for investigating the inactivation mechanisms

Rotavirus replication cycle	Replication steps investigated	Our experimental approach
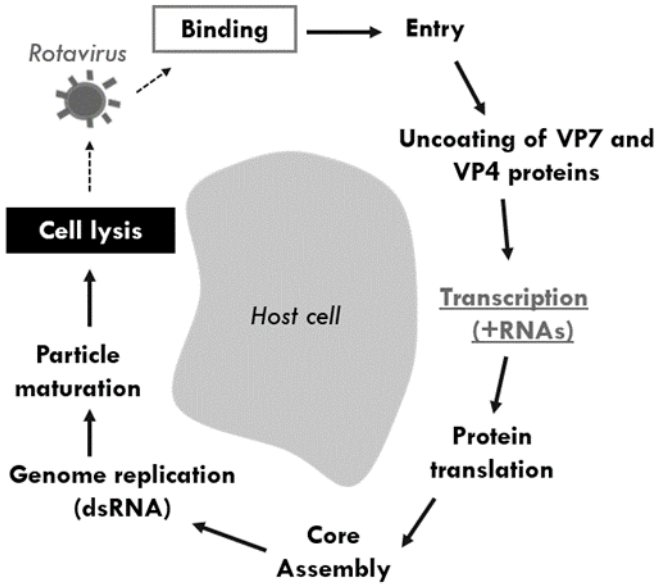	***Genome integrity*** of rotavirus genome	1. Quantified the loss of the PCR target region signal immediately upon treatment
	Binding of rotavirus onto MA104 host receptors	1. Treated rotaviruses were plated onto MA104 cells at 4°C for 1 h 2. Unbound rotaviruses were washed 3X with PBS, cells lysed, total RNA extracted, and rotavirus NSP3 primers used for quantification using qRT-PCR
	RNA synthesis of the rotavirus NSP3 segment	1. Treated rotaviruses were plated onto MA104 cells at 37°C for 30 min. 2. Unbound rotaviruses were washed 3X with PBS and incubated for 15-18 h, cells lysed, total RNA extracted, and rotavirus NSP3 primers used for quantification using qRT-PCR.
	Cell lysis of rotavirus and completion of the replication cycle	1. Quantified using an immunochemical infectivity assay for rotavirus.

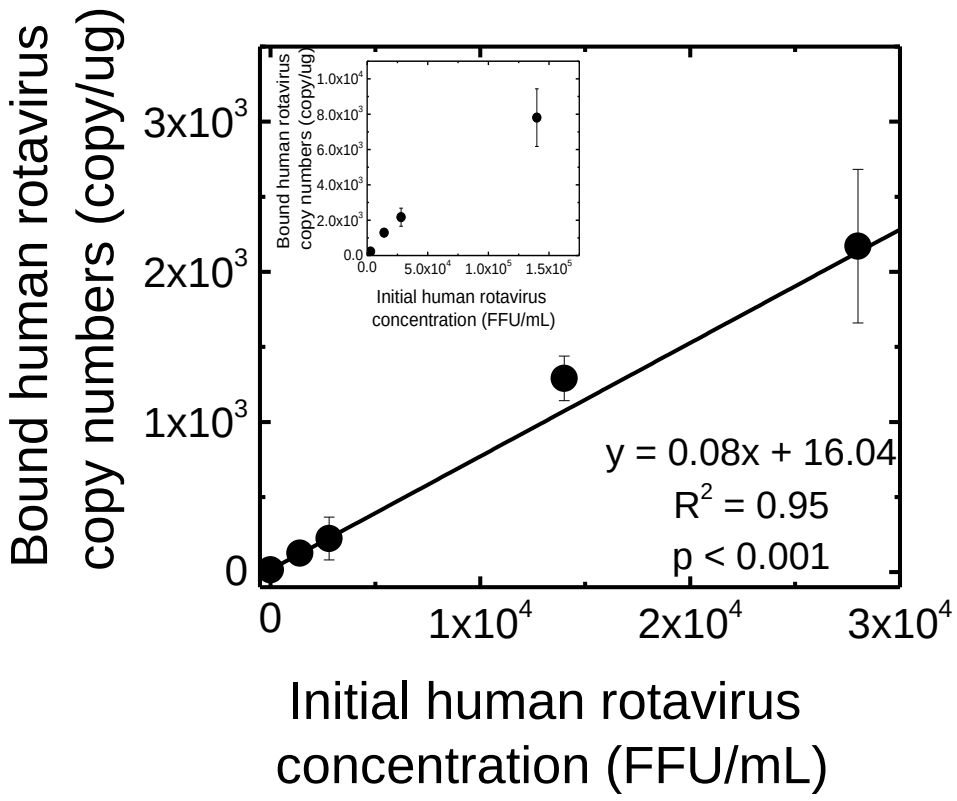

Figure A12. A calibration curve with 6 different human rotavirus concentrations was generated and the correlation was good ($R^2 = 0.95$). The error bars denote the range of duplicate samples tested. Based on this calibration curve and excellent reproducibility of copy numbers, we chose to work with low rotavirus concentrations (3×10^4 FFU/mL). Note the initial rotavirus concentration was much higher than the copy numbers obtained, suggesting that not all viruses were able to attach to cellular receptors. In fact, based on the data from this calibration curve, only ~8% of the rotavirus particles were able to bind to the cells.

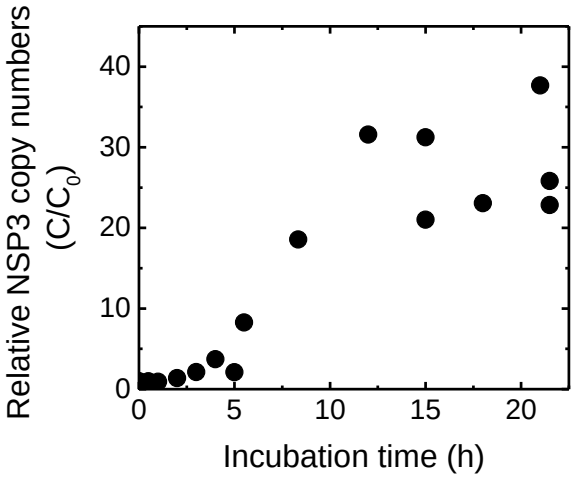

Figure A13. Relative NSP3 target region generated in infected MA104 cells 15-18 hpi with rotavirus concentration of 3×10^4 FFU/mL. Each point represents a single time point. To reduce variability, each set of experiments (i.e. viral RNA synthesis assay for heat treatment) was carried out on the same plate, where MA104 cells were seeded at the same time and contained approximately the same number of cells ($2\text{-}5 \times 10^6$ cells/ml).

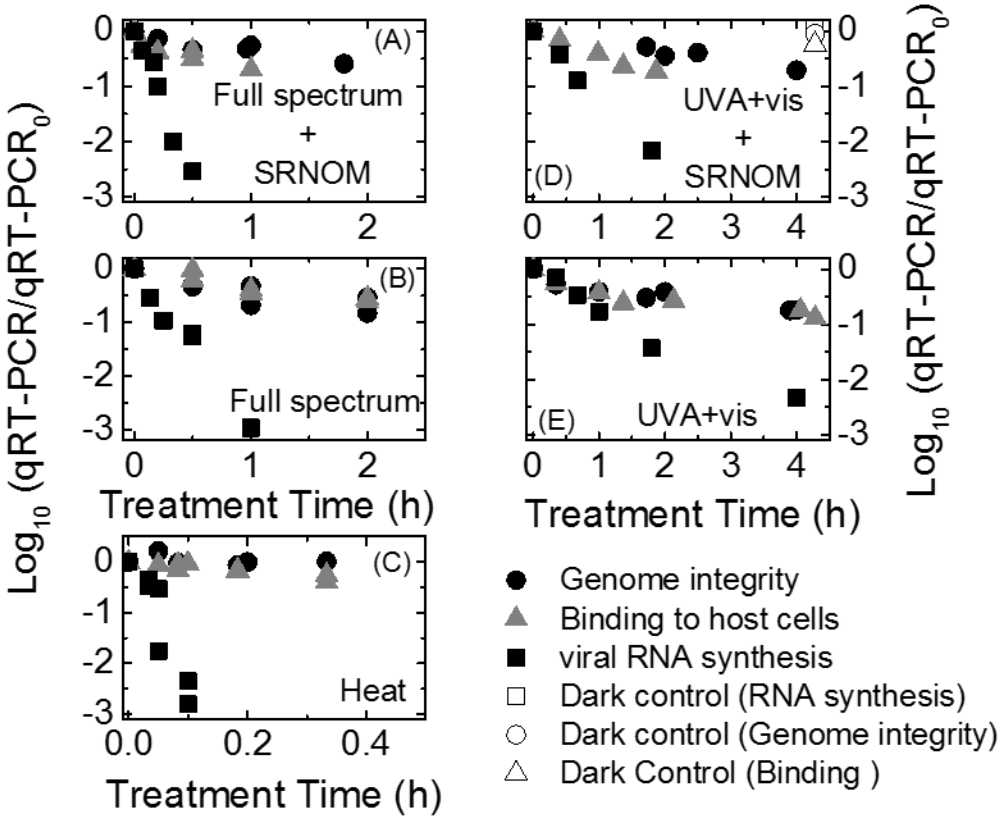

Figure A14. Uncorrected linear plots of the qRT-PCR signal changes (log qRT-PCR$_t$/qRT-PCR$_0$) over time for each assay and treatment (A-E). One set of duplicate experiments were conducted in the dark for each assay and is shown in panel D. Note that the time of each experiment varied depending on the treatment: shorter times were needed for heat treatment and longer times for UVA+vis light irradiation.

Table A11. Primer Details

Gene	Primer Name	Primers (5’ to 3’ direction)	Final Primer Conc.	Product Size	Annealing Temp	Reference
NSP3	JVKF	CAGTGGTTGATGCTCAAGAT	0.3 µM	131 bp	54°C	Jothikumar, *et al.* 2009 (11)
	JVKR	TCATTGTAATCATATTGAATACCCA				Mattioli *et al.* 2013 (10)

Table A12. Summary of the decay rate constants and statistical parameters for each assay and treatment investigated

Decay rate constants	Parameters	57°C (Dark)	UVA-vis	UVA-vis + SRNOM	Full spectrum	Full spectrum + SRNOM
Damage (k_{damage})	k_{damage} (h^{-1}) ± standard error	0.44 ± 0.73[a]	0.40 ± 0.06	0.41 ± 0.04	0.74 ± 0.18	0.69 ± 0.12
	R^2	0.06	0.89	0.97	0.75	0.87
	P value	0.58	0.0002	0.0004	0.005	0.002
Binding ($k_{observed\_binding}$)	$k_{observed\_binding}$ (h^{-1}) ± standard error	2.22 ± 0.29	0.43 ± 0.07	0.95 ± 0.04	0.69 ± 0.11	1.44 ± 0.30
	R^2	0.86	0.85	0.99	0.88	0.82
	P value	< 0.0001	0.0004	<0.0001	0.0006	0.005
Entry + Replication ($k_{observed\_entry+replication}$)	$k_{observed\_penetration+replication}$ (h^{-1}) ± standard error	61.6 ± 9.75	1.39 ± 0.11	2.79 ± 0.09	6.44 ± 0.49	12.3 ± 0.92
	R^2	0.87	0.97	0.99	0.97	0.97
	P value	0.0007	< 0.0001	< 0.0001	< 0.0001	< 0.0001
Corrected binding ($k'_{binding}$)	$k'_{binding}$ (h^{-1}) ± standard error	2.22 ± 0.29	0.02 ± 0.12[b]	0.55 ± 0.08	-0.05 ± 0.2[b]	0.75 ± 0.42
Corrected entry + replication ($k'_{entry+replication}$)	$k'_{penetration+replication}$ (h^{-1}) ± standard error	59.4 ± 10.0	0.96 ± 0.29	1.84 ± 0.20	5.69 ± 0.94	10.8 ± 1.46
Inactivation ($k_{infectivity}$)	$k_{infectivity}$ (h^{-1}) ± standard error	57.4 ± 11.6	2.56 ± 0.19	5.91 ± 0.26	12.8 ± 0.59	24.0 ± 3.0
	R^2	0.73	0.95	0.99	0.99	0.92
	P value	0.0007	< 0.0001	< 0.0001	< 0.0001	0.0002

[a]Denotes that the ($qRT\text{-}PCR_0/qRT\text{-}PCR_t$) or ($FFU_0/FFU_t$) vs. time (h) linear plot was not statistically different from a slope of 0 (linear regression test $p > 0.05$).

[b]Denotes that there was no significant difference between the linear plots vs. time obtained for the damage and binding assays (multiple linear regression tests $p > 0.05$).